

**The role of non-canonical NF- $\kappa$ B for liver  
homeostasis, chronic liver injury and  
hepatocarcinogenesis**

by

Christin Elßner, M.Sc.

Dissertation

submitted to the Combined Faculty of Natural Sciences and Mathematics  
of the Ruperto Carola University Heidelberg, Germany  
for the degree of

Doctor of Natural Sciences

# **Dissertation**

submitted to the  
Combined Faculty of Natural Sciences and Mathematics  
of the Ruperto Carola University Heidelberg, Germany  
for the degree of

Doctor of Natural Sciences

presented by

Christin Elßner, M. Sc. in Biochemistry and Molecular Biology

born in Berlin-Friedrichshain

Oral examination: .....

The role of non-canonical NF- $\kappa$ B for liver  
homeostasis, chronic liver injury and  
hepatocarcinogenesis

Referees: Prof. Dr. Ralf Bartenschlager  
Prof. Dr. Henning Schulze-Bergkamen

TABLE OF CONTENTS

<b>1. Summary</b> .....	<b>1</b>
<b>2. Zusammenfassung</b> .....	<b>3</b>
<b>3. Introduction</b> .....	<b>6</b>
<b>3.1 The liver</b> .....	<b>6</b>
<b>3.2 Chronic liver diseases</b> .....	<b>8</b>
3.2.1 Chronic liver diseases primarily affecting hepatocytes.....	10
3.2.2 Cholangiopathies.....	10
3.2.3 Ductular reactions .....	11
<b>3.3 Primary liver cancer</b> .....	<b>11</b>
3.3.1 Hepatocellular carcinoma (HCC).....	12
3.3.2 Intrahepatic cholangiocarcinoma (ICC).....	12
<b>3.4 Nuclear factor-<math>\kappa</math>B (NF-<math>\kappa</math>B)</b> .....	<b>13</b>
3.4.1 The NF- $\kappa$ B family and regulating factors.....	13
3.4.2 Mechanism of NF- $\kappa$ B activation.....	14
3.4.3 NF- $\kappa$ B in the murine liver.....	16
3.4.4 NF- $\kappa$ B in the human liver.....	17
3.4.5 NF- $\kappa$ B in hepatocarcinogenesis .....	18
3.4.6 Liver-specific disruption of CYLD .....	19
<b>3.5 Aim of this work</b> .....	<b>20</b>
<b>4. Materials and Methods</b> .....	<b>21</b>
<b>4.1 Mouse Models</b> .....	<b>21</b>
4.1.1 Breeding .....	21
4.1.2 Mouse Genotyping .....	21
4.1.3 Agarose Gel Electrophoresis.....	23
4.1.4 Organ removal and routine serum biochemistry .....	23
4.1.5 Isolation and cultivation of primary murine hepatocytes.....	24
4.1.6 CCl <sub>4</sub> -induced liver fibrosis.....	25
4.1.7 DDC diet.....	25
<b>4.2 Cell culture</b> .....	<b>26</b>
4.2.1 Cultivation of normal human cholangiocytes.....	26
4.2.3 Transfection of cells with siRNA.....	27
4.2.3 Cell stimulation with LT $\alpha$ 1 $\beta$ 2.....	27
<b>4.3 Protein expression analyses</b> .....	<b>27</b>
4.3.1 Protein isolation .....	27
4.3.1.1 Protein isolation from cultured cells.....	28
4.3.1.2 Protein isolation from liver tissues .....	28
4.3.2 Bradford Assay .....	28
4.3.3 SDS-Page.....	29

---

4.3.4 Western Blot .....	30
<b>4.4 Gene expression analysis.....</b>	<b>32</b>
4.4.1 RNA Isolation from murine tissue.....	32
4.4.2 Reverse Transcription.....	33
4.4.3 Real-Time quantitative PCR (qRT-PCR).....	33
<b>4.5 Human liver samples.....</b>	<b>34</b>
<b>4.6 Histopathological Analyses.....</b>	<b>35</b>
4.6.1 Hematoxylin and Eosin Staining.....	35
4.6.2 Sirius Red .....	36
4.6.3 Immunohistochemistry .....	36
4.6.4 In situ hybridization.....	39
<b>4.7 Statistical Analysis.....</b>	<b>40</b>
<b>5. Results.....</b>	<b>41</b>
<b>5.1 The role of RELB for liver homeostasis, chronic injury and hepatocarcinogenesis in mice</b> <b>.....</b>	<b>41</b>
5.1.1 A liver-specific knockout mouse model with increased RELB activation.....	41
5.1.1.1 Generation of a liver-specific CYLD/RELB double knockout mouse.....	41
5.1.1.2 Sustained activation of RELB is crucial for ductular reaction and biliary fibrosis in <i>Cyld<sup>ALPC</sup></i> mice .....	43
5.1.1.3 Reactive biliary epithelial phenotype in <i>Cyld<sup>ALPC</sup></i> mice is dependent on constitutive RELB activation.....	46
5.1.1.4 RELB hyperactivation triggers increased NF- $\kappa$ B signaling in <i>Cyld<sup>ALPC</sup></i> mice .....	51
5.1.2 Hepatocyte-driven fibrosis is RELB independent .....	55
5.1.3 Combined ablation of CYLD and RELB protects from chemically induced biliary damage.....	56
<b>5.2 Non-canonical NF-<math>\kappa</math>B signaling in human chronic liver diseases and liver cancer .....</b>	<b>62</b>
5.2.1 RELB expression is upregulated in human chronic liver diseases .....	62
5.2.2 Nuclear translocation of RELB is increased in human hepatocellular carcinoma .....	64
5.2.3 Expression of nuclear RELB is associated with poor overall survival in HCC patients .....	67
5.2.4 Nuclear RELB expression is elevated in cholangiopathies and intrahepatic cholangiocarcinoma .....	67
5.2.5 Hepatic LT $\beta$ expression as a link to sustained RELB activation.....	69
<b>6. Discussion .....</b>	<b>73</b>
<b>6.1 The role of RELB in a mouse model with ductular reaction and biliary fibrosis.....</b>	<b>73</b>
<b>6.2 The role of RELB in chronic liver injury models.....</b>	<b>78</b>
6.2.1 CCl <sub>4</sub> -induced liver fibrosis.....	78
6.2.2 DDC-induced cholestatic injury.....	79
<b>6.3 The role of RelB for human chronic liver diseases and primary liver cancer .....</b>	<b>80</b>
<b>6.4 Outlook .....</b>	<b>81</b>
<b>7. References.....</b>	<b>83</b>
<b>8. List of Figures.....</b>	<b>101</b>

<b>9. List of Tables .....</b>	<b>102</b>
<b>10. Abbreviations .....</b>	<b>103</b>
<b>11. Contributions.....</b>	<b>107</b>
<b>12. Acknowledgements.....</b>	<b>108</b>

## 1. Summary

Chronic liver diseases such as viral hepatitis and alcoholic liver disease are a major health burden affecting millions of people worldwide. Chronic liver damage can cause fibrosis, which might ultimately progress to cirrhosis as the major risk factor for the development of hepatocellular carcinoma (HCC). HCC is the most common type of primary liver cancers (accounting for ~ 80 %) and originates from hepatocytes, whereas intrahepatic cholangiocarcinoma (ICC, accounting for ~ 15 %) is a malignant liver tumor arising from biliary epithelial cells. Together, they are among the most frequently diagnosed cancers and a leading cause of cancer-related deaths.

NF- $\kappa$ B comprises a family of transcription factors, which regulate the expression of target genes involved in different functions such as inflammation, immunity, cell proliferation, differentiation, and survival. Two major signaling pathways termed as the canonical and non-canonical NF- $\kappa$ B pathway have been described leading to receptor-mediated NF- $\kappa$ B activation. Both pathways are dependent on different signaling components and activate distinct target genes. While activation of canonical NF- $\kappa$ B signaling and its key player RELA have been reported to play a crucial role in chronic liver diseases, the role of non-canonical NF- $\kappa$ B signaling with RELB as its key transcriptional factor remains largely elusive. Therefore, the main objective of this work was to investigate the functional importance of RELB for the liver, chronic liver diseases, and hepatocarcinogenesis.

For this purpose, an established mouse model with a specific disruption of the cylindromatosis gene (*Cyld*) in liver parenchymal cells (LPC) was used. CYLD is a deubiquitinase and acts as a negative regulator of NF- $\kappa$ B signaling. Mice lacking liver-specific full-length CYLD (*Cyld*<sup>ALPC</sup>) exhibit a severe biliary phenotype consisting of ductular reaction and biliary fibrosis, accompanied by highly upregulated RELB expression. To determine whether RELB overexpression contributes to this biliary phenotype, a double knockout mouse containing an additional deletion of RELB (*Cyld/Relb*<sup>ALPC</sup> mice) was generated. Analysis of *Cyld/Relb*<sup>ALPC</sup> mice revealed that nuclear translocation of RELB is essential for the ductular reaction, activation of the oval cell compartment and development of biliary fibrosis in *Cyld*<sup>ALPC</sup> mice, as the spontaneous phenotype of *Cyld*<sup>ALPC</sup> mice is completely reverted in *Cyld/Relb*<sup>ALPC</sup> mice. Moreover, sustained RELB activation induced a specific cytokine response without significant increased immune cell infiltration. The finding that cholangiocytes of *Cyld*<sup>ALPC</sup> mice acquire a reactive phenotype with the ability to express proinflammatory cytokines such as LT $\beta$  points to a perpetuating feedback mechanism of constitutive RELB upregulation ultimately promoting ductular reaction in *Cyld*<sup>ALPC</sup> mice. RELB deficiency also affected the protein expression of NF- $\kappa$ B signaling molecules involved in the canonical and non-canonical signaling pathway. Whereas liver lysates of *Cyld*<sup>ALPC</sup> mice showed elevated NF- $\kappa$ B activation, protein levels of *Cyld/Relb*<sup>ALPC</sup> livers were similar to control mice.

To assess the role of RELB in the injured liver, different chemically induced chronic liver damage models were used. While both RELB and CYLD had no impact on the fibrotic response induced by direct hepatocyte damage, *Cyld*<sup>ALPC</sup> mice showed in a cholangiopathy mouse model the most severe biliary phenotype with cholestasis and biliary fibrosis compared to treated control mice. This pronounced biliary injury was RELB driven, as additional RELB deletion was able to revert this phenotype. Interestingly, *Cyld/Relb*<sup>ALPC</sup> mice were protected against cholestatic damage, maintained body weight, and displayed normal bilirubin levels.

In the second part of this thesis, the importance of RELB for human chronic liver diseases and hepatocarcinogenesis was investigated. In liver parenchymal cells from patients with chronic infection with hepatitis B or C viruses, autoimmune hepatitis, alcoholic liver disease, early stage primary biliary cholangitis (PBC) and primary sclerosing cholangitis (PSC), an increased nuclear translocation of RELB was observable. Especially in cholangiocytes of early disease stage of PBC and PSC, LT $\beta$  acts as a possible upstream trigger leading to sustained RELB activation. In liver tissues from patients with HCC or ICC, nuclear translocation of RELB was significantly increased. Nuclear RELB expression was significantly associated with poor overall survival of HCC patients identifying RELB as a novel prognostic factor to predict the outcome of HCC patients.

Taken together, the results of the present study uncover for the first time a crucial role of non-canonical NF- $\kappa$ B signaling for ductular reaction, progenitor cell activation and biliary driven fibrosis in a mouse model. The finding, that RELB is activated in human diseased liver, HCC, and ICC could harbor broad implications for basic research and clinical application.

## 2. Zusammenfassung

Chronische Lebererkrankungen wie virale Hepatitis und alkoholische Lebererkrankungen sind eine gesundheitliche Belastung für Millionen von Menschen weltweit. Unbehandelt kann eine chronische Leberschädigung zu Fibrose führen, die letztendlich zur Zirrhose als Hauptrisikofaktor für die Entstehung des hepatozellulären Karzinoms (HCC) fortschreiten kann. HCC ist die häufigste Form des primären Leberkrebses (Anteil von ~ 80 %) und entwickelt sich aus Hepatozyten, wohingegen das intrahepatische Cholangiokarzinom (ICC, Anteil von ~ 15 %) ein bösartiger Lebertumor ist, der aus biliären Epithelzellen entsteht. Zusammen gehören sie zu den am häufigsten diagnostizierten Krebsarten und sind eine der häufigsten Ursachen für krebsbedingte Todesfälle.

NF- $\kappa$ B umfasst eine Familie von Transkriptionsfaktoren und reguliert die Expression von Zielgenen, die an verschiedenen Funktionen wie Entzündung, Immunität, Zellproliferation, Differenzierung und Überleben beteiligt sind. Zwei wichtige Signalwege, die als kanonischer und nicht-kanonischer NF- $\kappa$ B Pfad bezeichnet werden, sind bisher beschrieben und führen zu einer rezeptorvermittelten NF- $\kappa$ B Aktivierung. Beide Signalwege sind von verschiedenen Signalkomponenten abhängig und aktivieren unterschiedliche Zielgene. Während die Aktivierung des kanonischen NF- $\kappa$ B Signalwegs und ihrem wichtigsten Faktor RELA eine entscheidende Rolle bei chronischen Lebererkrankungen spielt, bleibt die Rolle des nicht-kanonischen NF- $\kappa$ B Signalwegs über RELB weitgehend unklar. Daher war das primäre Ziel dieser Arbeit, die funktionelle Bedeutung von RELB für die Leber, chronische Lebererkrankungen und der Hepatokarzinogenese zu untersuchen.

Zu diesem Zweck wurde ein etabliertes Mausmodell mit einer spezifischen Störung des Cylindromatose-Gens (CYLD) in Leberparenchymzellen (LPC) verwendet. CYLD ist eine Deubiquitinase und wirkt als negativer Regulator des NF- $\kappa$ B-Signalwegs. Mäuse, denen leberspezifisch Exon 7 und 8 von CYLD fehlt (*Cyld*<sup>ALPC</sup>), weisen einen ausgeprägten biliären Phänotyp auf, bestehend aus duktulärer Reaktion, biliärer Fibrose, begleitet von einer hochregulierten RELB Expression. Um festzustellen, ob die RELB Überexpression zu diesem biliären Phänotyp beiträgt, wurde eine Doppel-Knockout-Maus generiert, die eine zusätzliche Deletion von RELB (*Cyld/Relb*<sup>ALPC</sup> Mäuse) enthält. Die Analyse von *Cyld/Relb*<sup>ALPC</sup> Mäusen ergab, dass die nukleäre Translokation von RELB für die duktuläre Reaktion, die Aktivierung des Progenitor-Zellkompartiments und die Entwicklung der biliären Fibrose in *Cyld*<sup>ALPC</sup> Mäusen verantwortlich ist, da der spontane Phänotyp der *CYLD*<sup>ALPC</sup> Mäuse in *Cyld/Relb*<sup>ALPC</sup> Mäusen vollständig verloren geht. Darüber hinaus führte die anhaltende RELB Aktivierung zu einer spezifischen Zytokinreaktion, jedoch ohne signifikant erhöhte Immunzelleninfiltration. Das Ergebnis, dass Cholangiozyten von *Cyld*<sup>ALPC</sup> Mäusen einen reaktiven Phänotyp erwerben mit der Fähigkeit zur Expression proinflammatorischer Zytokine wie LT $\beta$ . Dies deutet auf einen fortwährenden positiven Feedback-Mechanismus hin, der zu einer konstitutiven RELB Expression führt und letztendlich zum Fortschreiten der duktulären Reaktion bei *Cyld*<sup>ALPC</sup> Mäusen beiträgt. Darüber hinaus beeinflusste die RELB Deletion auch die Expression von NF- $\kappa$ B Signalmolekülen, die sowohl in den kanonischen als auch den nicht-kanonischen Signalweg eingebunden sind. Während die Lebern von *Cyld*<sup>ALPC</sup> Mäusen eine erhöhte NF- $\kappa$ B-Aktivierung zeigten, war die Aktivierung in den *Cyld/Relb*<sup>ALPC</sup> Lebern vergleichbar mit den Kontrollmäusen.

Um die Rolle von RELB für die geschädigte Leber zu beurteilen, wurden verschiedene chemisch induzierte Modelle zur chronischer Leberschädigung verwendet. Während sowohl RELB als auch CYLD keinen Einfluss auf die fibrotische Reaktion durch direkte Hepatozytenschädigung hatten, zeigten *Cyld*<sup>ALPC</sup> Mäuse den am stärksten ausgeprägten biliären Phänotyp in einem Cholangiopathie-Mausmodell, das Cholestase und biliärer Fibrose induzierte. Dieser biliäre Phänotyp wurde erneut durch RELB verursacht, da eine zusätzliche RELB Deletion diesen Phänotyp rückgängig machen konnte. Interessanterweise zeigten *Cyld/Relb*<sup>ALPC</sup> Mäuse nicht nur eine reduzierte duktiläre Reaktion und biliäre Fibrose, sondern waren auch am besten vor den cholestatischen Schäden geschützt, verloren kein Körpergewicht und zeigten keine erhöhten Bilirubinwerte.

Im zweiten Teil dieser Arbeit wurde die Bedeutung von RELB in chronischen Lebererkrankungen und in der humanen Hepatokarzinogenese untersucht. In Leberparenchymzellen von Patienten mit chronischer Infektion mit Hepatitis B oder C-Viren, Autoimmunhepatitis, alkoholischer Lebererkrankung, primärer biliärer Cholangitis (PBC) und primärer sklerosierender Cholangitis (PSC) wurde eine insgesamt erhöhte nukleäre Translokation von RELB nachgewiesen, die eine Aktivierung aufzeigt. Insbesondere in den Cholangiozyten der frühen Krankheitsstadien von PBC und PSC schien LTβ als ein möglicher Trigger zu fungieren, der durch einen positiven Feedback-Mechanismus zur erhöhten RELB Expression beiträgt. Im Lebergewebe von Patienten mit HCC oder ICC translozierte RELB ebenfalls vermehrt in den Kern. Die nukleäre RELB Expression war sogar signifikant mit einem schlechteren Gesamtüberleben von HCC-Patienten assoziiert, was RELB als potentiell neuen prognostischen Faktor zur Vorhersage des Outcomes von HCC-Patienten aufzeigt.

Angesichts der Tatsache, dass eine anhaltende RelB Aktivierung für die duktilären Reaktionen und biliäre Fibrose in einem Mausmodell entscheidend ist und dass nukleäres RELB in verschiedenen chronischen Lebererkrankungen und primärem Leberkrebs überexprimiert wird, könnte die Verminderung des hepatischen RELB Expression bei Lebererkrankungen mit chronisch aktiviertem nicht-kanonischem NF-κB-Signal von Vorteil sein.

Zusammenfassend decken die Ergebnisse der vorliegenden Studie erstmals eine entscheidende Rolle des nicht-kanonischen NF-κB Signalwegs für duktilären Reaktionen, die Aktivierung von Leberprogenitorzellen und die biliäre Fibrose in einem Mausmodell auf. Das Ergebnis, dass RELB in chronischen Lebererkrankungen, HCC und ICC aktiviert ist, könnte von großer Bedeutung für die Grundlagenforschung und die klinische Anwendung sein.

The work presented in the following dissertation was performed from September 2012 until June 2018 in the Division of Medical Oncology at the National Center for Tumor Diseases (NCT) in Heidelberg (Germany) and was supervised by Prof. Dr. Henning Schulze-Bergkamen and Dr. Bruno Christian Köhler.

The majority of results described in this dissertation have been recently published in Gastroenterology in March 2019<sup>1</sup>. Many passages have been quoted verbatim from Elßner et al.<sup>1</sup>. Most of the tables and figures have been adopted.

Declarations according to § 8 (3) b) and c) of the doctoral degree regulations:

b) I hereby declare that I have written the submitted dissertation myself and in this process have used no other sources or materials than those explicitly indicated.

c) I hereby declare that I have not applied to be examined at any other institutions, nor have I used the dissertation in this way or any other form at any other institution as an examination paper, nor submitted it to any other faculty as dissertation.

### 3. Introduction

#### 3.1 The liver

The mammalian liver is a complex organ with a unique regenerative capacity that consists of various cell types of different embryonic origin comprising hepatocytes, cholangiocytes (biliary epithelial cells), stellate cells, sinusoidal endothelial cells, Kupffer cells, and intrahepatic lymphocytes. During embryonic development, endoderm-derived fetal hepatoblasts (bipotential progenitor cells) give rise to two hepatic epithelial cell lineages, hepatocytes, and cholangiocytes. During hepatoblast differentiation, especially NOTCH signaling pathway has been implicated in controlling the lineage specification by regulating the expression levels of different transcription factors such as hepatocyte nuclear factor-1 and 4<sup>2</sup>.

Hepatocytes are the predominant liver cell type and make up two-thirds of the total liver cell population<sup>3</sup>. They are carrying out pivotal roles in glucose homeostasis, protein synthesis, lipid, cholesterol, and amino acid metabolism, production, and secretion of bile, and detoxification<sup>4</sup>. They have a polygonal shape and are arranged in plates/cell layers that separate canalicular bile from sinusoidal blood (Fig. 1). In order to mediate the exchange of macromolecules between these two counter-current flow systems, hepatocytes exhibit a unique polarity with distinct domains on the plasma membrane. The basolateral membrane allows the access to sinusoidal blood, while the apical membrane between two adjacent hepatocytes form capillary-like structures, named as bile canaliculi, serves as a site of bile secretion<sup>5</sup>.

Cholangiocytes are cells that line the intrahepatic and extrahepatic bile ducts, a three-dimensional network of bile ducts named as biliary tree. The main physiological function of cholangiocytes is the formation of ductal bile by modification of primary bile through absorptive and secretory processes. Bile is a complex aqueous secretion with major excretory functions containing endogenous substrates such as cholesterol and bilirubin as well as exogenous toxins, drugs, xenobiotics. Bile acids, which are other biliary constituents, facilitate digestion and absorption of dietary fats in the intestine<sup>6</sup>. Bile is first secreted by hepatocytes into bile canaliculi and transported along the biliary tree (Fig. 1)<sup>7</sup>. From bile canaliculi, which are completely lined by hepatocytes, bile flows into canals of Hering that represent the initial branches of the biliary tree and are formed by both hepatocytes and cholangiocytes. These channels lead to ductules (< 15  $\mu\text{m}$  luminal diameter) that are entirely lined by cholangiocytes and extend to larger interlobular bile ducts (15 - 100  $\mu\text{m}$ ). Joining of biliary branches leads to further increase of the luminal diameter and results in the formation of the right and left hepatic ducts (> 800  $\mu\text{m}$ ), and their extrahepatic fusion to the common hepatic bile duct, from where bile is delivered to the gallbladder and intestine<sup>6,8</sup>.

Besides modifying hepatic bile, it has been reported that biliary epithelial cells and bile have also immunological functions and participate in liver injury and repair. Bile is involved in the transport of immunoglobulins (especially IgA) to the intestine and cholangiocytes are able to secrete chemokines, cytokines, adhesion molecules, and present antigen to natural killer cells<sup>9,10</sup>.

Stellate cells, derived from hematopoietic stem cells, are located in the space between hepatocytes and sinusoidal endothelial cells (space of Disse, Fig. 1) and control sinusoidal vascular tone and blood flow through contraction around sinusoids. Moreover, the majority of retinoids in the body is stored in lipid droplets within the cytoplasm of the stellate cells<sup>11-13</sup>. During chronic liver injury, quiescent stellate

cells get activated and transform into myofibroblast-like cells. This process is accompanied by loss of their lipid droplets, a marked expression of alpha-smooth muscle actin, and excessive matrix deposition leading to fibrosis<sup>14-16</sup>.

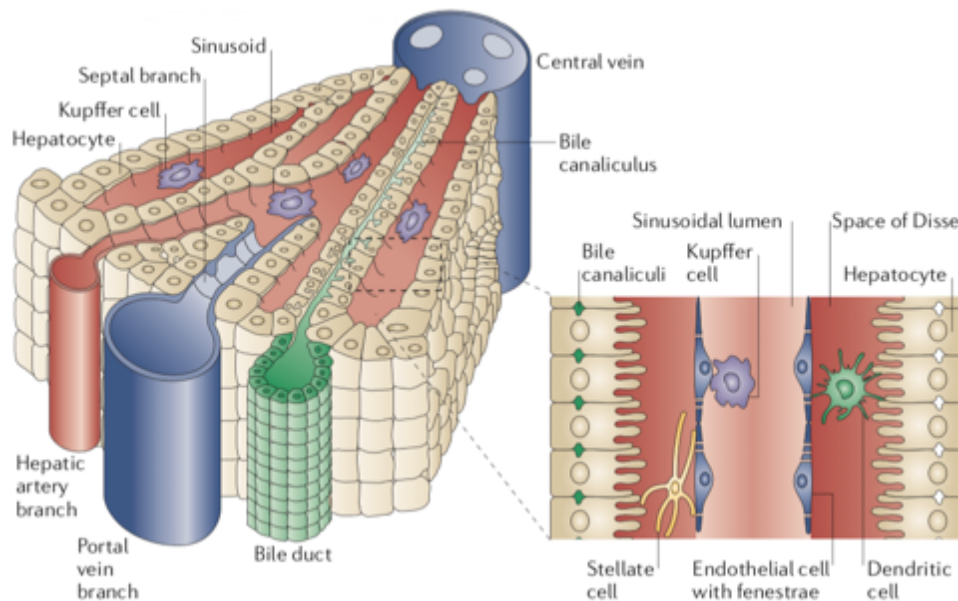


**Figure 1: Illustration showing a three-dimensional structure of a portion of a liver lobule.** Mixed blood from the portal vein and the hepatic artery enters the liver lobule, passes through the sinusoids that are surrounded by plates/cords of hepatocytes, and drain into the central vein. Thereby, the portal veins give rise to a septal branch, whereas the hepatic artery terminates in the sinusoids. Bile, produced from the hepatocytes and secreted into bile canaliculi, is transported in bile ducts to the gallbladder and to the gut. Sinusoids are lined by endothelial cells with unique transmembrane pores called fenestrations and facilitate the exchange and transfer of proteins and plasma components between the sinusoidal blood and hepatocytes. Within the sinusoidal lumen and attached to the endothelium reside phagocytic Kupffer cells, resident macrophages in the liver that carry important filtering functions by removing and processing environmental antigens, dietary and microbial products that arrive from the gastrointestinal tract. The space of Disse is a location between the sinusoids and the hepatocytes and contains hepatic stellate cells and antigen-presenting dendritic cells that can access the space of Disse. The image has been adapted from Adams and Eksteen (2006)<sup>17</sup>.

Liver sinusoidal endothelial cells are a highly specialized endothelial cell population and represent a permeable barrier between blood cells, hepatocytes and stellate cells (Fig. 1). They are characterized by the absence of tight junctions and a distinct basement membrane but possess a unique capacity of forming fenestrations, transmembrane pores ranging in size from 50 to 200 nm in the endothelium that facilitate the exchange and transfer of proteins and particles between the sinusoidal blood and hepatocytes<sup>18,19</sup>. Because of several endocytic receptors, sinusoidal endothelial cells act as the most efficient scavenger cells by removing numerous physiological and foreign waste macromolecules from the blood<sup>20</sup>.

Within the sinusoidal lumen are the resident macrophages of the liver located, designated as Kupffer cells. It has been long believed that they derive from circulating monocytes that originate from bone marrow precursor cells but nowadays it has been reported that Kupffer cells self-renew from resident erythro-myeloid progenitors which develop in the yolk sac during embryonic development and colonize the fetal liver<sup>21-23</sup>. Due to the localization of the Kupffer cells, they play a pivotal role in the clearance of endotoxins and toxic agents (e.g. ethanol) from the circulating blood as well as in the phagocytosis of debris like apoptotic hepatocytes, microorganisms, degenerated cells, and immune

complexes<sup>24</sup>. During liver injury and wound healing, activated Kupffer cells express and secrete inflammatory mediators and acquire therefore pro- or anti-inflammatory roles<sup>25-27</sup>.

Intrahepatic lymphocytes, such as natural killer cells, natural killer T cells, and dendritic cells, are another cell population that is mostly resident in the portal tracts but can be found also scattered within the parenchyma under physiological conditions. Liver-associated lymphocytes are predominated by CD3 positive T lymphocytes and adhere to chemokines and adhesion molecules presented on the surface of sinusoidal endothelial cells. They contribute to the first line of immune defense against pathogens and toxic substances and are involved in the recruitment of circulating lymphocytes during liver injury<sup>28,29</sup>.

The structural unit of the liver is the hepatic lobule (Fig. 1). Nutrient-rich blood originating from the gastrointestinal circulation, spleen, gallbladder, and pancreas enters the liver via the portal vein, which accounts for 75 - 80 % of the blood volume that reaches the liver. 20 - 25% of the blood supply is delivered by the hepatic artery. Together with oxygenated blood from the hepatic artery, blood flows slowly within the sinusoids towards the central vein, to be later drained out of the liver via the hepatic veins<sup>30</sup>. Bile, which is continuously secreted by hepatocytes into bile canaliculi, flows in the opposite direction into larger ducts that form ultimately hepatic bile ducts and gets transported to the gallbladder and finally to the duodenum. The portal triad is an anatomical arrangement and describes the area that is composed of bile ducts, portal vein, and hepatic artery. Each hepatic lobule consists of one central vein in the center and six surrounding portal triads.

### 3.2 Chronic liver diseases

Chronic liver diseases are characterized by persistent liver injury lasting longer than six months and can be caused by multiple etiologies such as viral infections, toxin/drug exposure, metabolic disorders, cholestatic diseases, and autoimmune diseases. Globally, 844 million of the world's population were estimated to have chronic liver diseases with around 2 million deaths per year<sup>31</sup>.

A common pathological consequence of almost every chronic liver disease is liver fibrosis, which is defined by excessive accumulation of extracellular matrix proteins. During acute liver injury, regeneration of parenchymal cells is accompanied by an inflammatory response and restricted production of extracellular matrix. However, when hepatic injury persists, this process can cause liver fibrosis due to a continuously activated wound healing response (Fig. 2)<sup>32</sup>. Thereby, apoptosis of parenchymal cells leads to the activation of quiescent stellate cells, the principal liver cells which promote liver fibrosis and attract and activate Kupffer cells and monocytes through signaling via the chemokine CCL2-CCR2 axis<sup>33,34</sup>. Further secretion of growth factors, fibrogenic and proinflammatory cytokines by Kupffer cells such as tumor necrosis factor- $\alpha$  (TNF- $\alpha$ ), interleukin-6 (IL-6), and transforming growth factor- $\beta$  (TGF- $\beta$ ) lead to the recruitment of T cells and neutrophils and amplification of the inflammatory response. TGF- $\beta$  is also involved in the activation of hepatic stellate cells and their transdifferentiation into myofibroblast-like cells. Activated hepatic stellate cells represent the major source of extracellular matrix-producing cells in chronic injured livers and synthesize large amounts of collagen (type I, III and IV) and  $\alpha$ -SMA<sup>14,35,36</sup>.

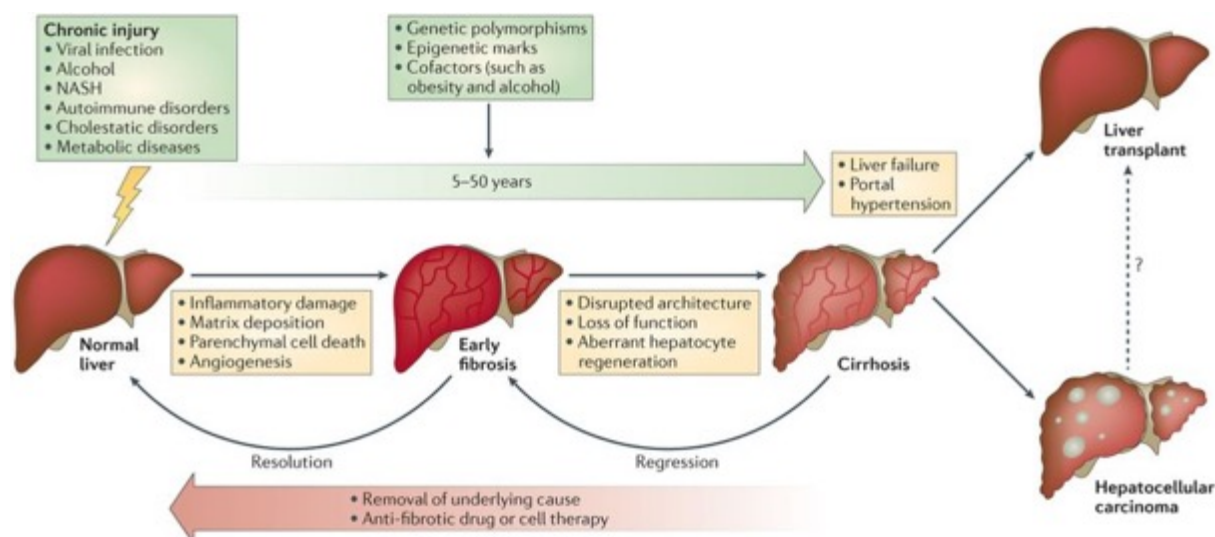


**Figure 2: Natural history of chronic liver disease.** Chronic liver injury caused by viral infections, alcohol, non-alcoholic steatohepatitis, and different liver disorders induce an inflammatory response, cell death of parenchymal cells and fibrosis, resulting from accumulation of extracellular matrix. After eliminating the cause of injury, complete reversal of fibrosis to normal liver architecture is possible. In contrast, advanced liver fibrosis and continued deposition of extracellular matrix leads to irreversible cirrhosis (development of cirrhosis takes years to decades). Then, only regression of fibrosis enables a better clinical outcome. When cirrhosis results in liver failure, transplantation is the only available treatment. Patients with cirrhosis have also a higher risk for primary liver cancer, especially hepatocellular carcinoma, which is a major cause of liver-related deaths. Image has been adapted from Pellicoro et al. (2014)<sup>32</sup>.

If the underlying cause of injury is removed, post-phagocytic macrophages switch to a restorative phenotype and produce anti-inflammatory mediators and growth factors such as hepatocyte growth factor<sup>37-39</sup>. Chemokine-mediated infiltration and activation of monocytes and T cells is drastically reduced. Proinflammatory cytokines decrease, apoptosis of activated hepatic stellate cells occurs and matrix degradation increase due to elevated matrix metalloproteinases levels, favoring the resolution of fibrosis<sup>40,41</sup>.

In contrast, untreated and prolonged injury results in augmented inflammatory cell infiltration and perpetuation of hepatic stellate cell activation which is mediated through several positive feedback loops such as TGF- $\beta$  and platelet derived growth factor<sup>42,43</sup>. A complex interplay between fibrogenic and inflammatory cells stimulating each other in an autocrine and paracrine way causes progressive extracellular matrix deposition, scar accumulation, and distortion of normal liver architecture. Independent of the underlying etiology, following long periods of chronic liver damage, fibrosis can progress to cirrhosis, the end-stage of hepatic fibrosis which is defined by the formation of regenerative nodules surrounded by fibrous septa. Cirrhosis is accompanied by hepatocellular dysfunction, portal hypertension, liver failure and can lead ultimately to hepatocellular carcinoma (HCC)<sup>44,45</sup>.

Depending on the primary damaged target cell, chronic liver diseases can be divided into diseases affecting hepatocytes or cholangiocytes (cholangiopathies).

### 3.2.1 Chronic liver diseases primarily affecting hepatocytes

Among chronic liver diseases, infection with hepatitis B virus (HBV), hepatitis C virus (HCV), alcoholic liver disease (ALD), and nonalcoholic fatty liver disease (NAFLD) have the highest incidence and prevalence and represent a major global health problem. While viral hepatitis accounts predominantly in Asia and Africa as a frequent cause of liver disease, ALD and NAFLD show a higher prevalence in Western countries<sup>31</sup>.

Hepatitis B and C is caused by infection with HBV and HCV. Both viruses infect and replicate in hepatocytes, thereby inducing a cytotoxic host immune response that triggers liver injury. Due to the fact that HBV and HCV are able to persist in the infected host, the majority develops chronic hepatitis which is characterized by continuous hepatic inflammation and liver fibrosis<sup>46</sup>.

ALD comprises a spectrum of diseases that ranges from relatively mild alcoholic fatty liver (steatosis) to alcoholic hepatitis/steatohepatitis, progressive fibrosis, and to the most advanced and severe alcoholic liver cirrhosis<sup>47</sup>. The term steatosis refers to the abnormal accumulation of small lipid droplets (microvesicular) and large lipid droplets (macrovesicular) in hepatocytes. During heavy alcohol consumption, alcohol oxidation leads to increased lipogenesis and simultaneously decreased hepatic lipolysis, followed by accumulation of lipids in hepatocytes. Alcoholic fatty liver can also induce an inflammation response and hepatocellular damage (alcoholic steatohepatitis). Persistency of these conditions increase the risk of progression to more advanced ALD forms<sup>48</sup>.

Histologically similar to ALD is NAFLD, which is defined as well as excess lipid accumulation in hepatocytes but in the absence or low alcohol intake. NAFLD is further categorized in nonalcoholic fatty liver and its more progressive form nonalcoholic steatohepatitis (NASH), and is strongly associated with components of the metabolic syndrome such as obesity and type 2 diabetes<sup>49</sup>. Recently, it has been shown that metabolites derived from an altered gut microbiome might promote the development of NAFLD<sup>50</sup>.

Liver diseases caused by autoimmune damage such as autoimmune hepatitis (AIH) are relatively rare compared with the above-mentioned liver diseases but can also progress rapidly to cirrhosis and liver failure if untreated. AIH is a chronic inflammatory disorder with unknown etiology and is characterized by hepatocyte destruction, interface hepatitis, the presence of autoantibodies and elevated levels of immunoglobulin G<sup>51</sup>.

### 3.2.2 Cholangiopathies

Cholangiopathies refer to a subgroup of chronic liver diseases, in which the biliary tree represents the main target. Damage to the biliary epithelium causes an impaired bile flow from the liver to the duodenum, named as cholestasis, which lead to an accumulation of bile constituents such as bilirubin and bile acids in the liver and systemic circulation<sup>52</sup>. Intrahepatic accumulation of high levels of cytotoxic bile acids results in biliary and hepatocyte injury and liver inflammation. Due to limited effective medical therapies, chronic cholangiopathies often progress to cirrhosis, portal hypertension and ultimately liver failure, thus requiring liver transplantation and accounting for significant morbidity and mortality<sup>53</sup>.

The two most common chronic cholestatic liver diseases are primary biliary cholangitis (PBC) and primary sclerosing cholangitis (PSC). PBC is considered as a slow progressive autoimmune disease

characterized by portal inflammation and immune-mediated destruction of small to medium-sized intrahepatic bile ducts that affects predominantly middle-aged woman<sup>54</sup>. In contrast, PSC is characterized by chronic inflammation of preferentially medium to large intra- and extrahepatic bile ducts, resulting in fibrotic biliary strictures, bile duct obstruction, and can lead to the development of biliary cirrhosis. Moreover, PSC is more common in men and is closely associated with inflammatory bowel disease<sup>55</sup>.

### 3.2.3 Ductular reactions

Although mature hepatocytes can regenerate and proliferate extensively in response to cellular death, hepatocyte cell cycle arrest and senescence attributed to increased cellular turnover have been described in chronic liver diseases including viral hepatitis, ALD, and NASH<sup>56-59</sup>. Regardless of the primary etiology, hepatocyte-specific telomere shortening and senescence correlated with progression of cirrhosis<sup>60</sup>. A role of senescent cholangiocytes contributing to the pathogenesis of the most prevalent cholangiopathies PBC and PSC has been reported as well<sup>61,62</sup>.

When damage of mature liver epithelial cells is combined with impaired and compromised regeneration capacity, activation of the progenitor cell/oval cell compartment and proliferation of ductular structures in the periportal area is initiated<sup>63</sup>. These ductular reactions have been observed in a variety of liver diseases and refer to an increased number of ductules consisting of proliferating existing cholangiocytes, activated progenitor cells, and intermediate hepatocytes, and is associated with inflammation and elevated levels of matrix deposition<sup>64-66</sup>. Cholangiocytes of newly formed bile ducts can acquire a reactive phenotype, thereby expressing adhesion molecules, secreting cytokines, chemotactic mediators, and growth factors<sup>33,67-69</sup>. Since the extent of ductular reaction and oval cell expansion strongly correlate with disease severity in ALD, NASH, and chronic viral hepatitis, it was suggested that ductular reaction promotes a proinflammatory microenvironment and progression of fibrosis<sup>70-72</sup>. Thus, targeting and modulation of ductular reaction might represent a promising strategy to improve liver regeneration and preventing fibrogenesis<sup>73-75</sup>.

### 3.3 Primary liver cancer

Primary liver cancer is one of the most commonly diagnosed cancers worldwide with estimated 850,000 new cases per year and a higher prevalence for men than woman. In 2015, liver cancer was ranked as the fourth leading cause of cancer-related death after lung, colorectal, and stomach cancer<sup>76-78</sup>. Among the different types of primary liver cancers, the most frequently occurring tumors are hepatocellular carcinoma (HCC, accounting for ~ 80 %), which originates from hepatocytes and intrahepatic cholangiocarcinoma (ICC, accounting for ~ 15 %), a malignant tumor arising primarily from epithelial cells lining the bile ducts<sup>79</sup>. Based on demographics and annual percentage changes, a study projecting liver cancer incidence and deaths in the United States to 2030 showed a dramatic increase in cancer-related mortality and ranked liver cancer together with lung and pancreatic cancer as one of the top three leading causes of cancer-related death<sup>80</sup>.

### 3.3.1 Hepatocellular carcinoma (HCC)

HCC largely develops within an established background of chronic liver diseases and cirrhosis (70% - 90% of all detected HCC patients). Major risk factors include chronic HBV and HCV infection, ALD, and NASH<sup>78</sup>. The contribution of underlying etiologies leading to HCC markedly depends on the geographic region. The highest incidence has been reported for East and South-East Asia and sub-Saharan Africa, most likely due to the elevated prevalence of risk factors like chronic HBV and HCV infections<sup>76,81</sup>. Consumption of aflatoxin-contaminated food is an additional risk factor in less developed countries. Whereas liver cancer rates decreased in high-risk countries like China and Japan over the past few decades, an increase could be observed in low-risk areas including Western Europe, North America, and Oceania<sup>82</sup>. Reasons for these elevated rates in developed countries might be partly due to chronic HCV infections, obesity, diabetes mellitus, and alcohol abuse<sup>83,84</sup>. Since HCC is often clinically asymptomatic, it is mostly diagnosed at an advanced stage. After potentially curative resection, recurrence rates are still high compared with other solid cancers<sup>85</sup>. Nevertheless, surgical resection and liver transplantation are the most effective options but many patients with advanced stage are not suitable candidates and organ availability is limited<sup>86,87</sup>. Since conventional systemic chemotherapy lacks efficacy, other therapeutic approaches comprises locoregional therapy such as transarterial chemoembolization (TACE), radiofrequency ablation and targeted therapy<sup>88</sup>. In the last years, improved knowledge of liver carcinogenesis led to the development of first molecularly targeted therapy such as the multi-target tyrosine kinase inhibitor sorafenib, but treatment strategies are still restricted and long-term survival with a median overall survival remains ~ 1 year<sup>88,89</sup>. As the majority of HCC develop in the background of chronic liver diseases, inflammation and cirrhosis, prevention of underlying liver diseases, establishment of better detection strategies and therapeutic breakthroughs are necessary.

### 3.3.2 Intrahepatic cholangiocarcinoma (ICC)

In contrast to HCC, ICC is a relatively rare malignancy and the true etiology remains largely unclear. Although several risk factors such as liver flukes, PSC, viral hepatitis, alcohol abuse, and obesity have been described, many cases of ICC occur sporadic and in the absence of known etiological factors<sup>90,91</sup>. Worldwide, there are tremendous geographic variations in the incidence of ICC, with the highest incidence rates seen in East Asia. These variations are presumably related to differences in the prevalence of certain risk factors, as for example the high incidence of ICC in North-East Thailand is closely associated with liver fluke infections<sup>92</sup>. Although the prevalence of ICC worldwide is considerably low compared with HCC, recent epidemiological studies indicated a progressive increase in the incidence and mortality of ICC over the past decades<sup>93</sup>. Similar to HCC, ICC is usually asymptomatic in early stages with a non-specific clinical presentation which is why ICC is often diagnosed at an advanced stage accompanied by a poor 5-year survival rate and a high recurrence rate<sup>94,95</sup>. Surgical resection represents the only potentially curative therapy for ICC, but unfortunately, only a minority of patients are appropriate surgical candidates. For patients with unresectable ICC, locoregional therapy such as TACE and transarterial radioembolization (TARE) have shown anti-tumor effects with acceptable side effects and systemic chemotherapy including gemcitabine and cisplatin might have beneficial effects on survival<sup>96</sup>. Whereas long-term survival after curative

resection is possible, prognosis for patients with unresectable ICC still remains poor as the majority of patients develop resistance to the treatment after few months leading to a median overall survival of only 6-12 months<sup>97</sup>. Thus, further investigation and better understanding of the cellular origins and molecular mechanisms contributing to pathogenesis, ICC formation, and treatment resistance are essential.

### 3.4 Nuclear factor- $\kappa$ B (NF- $\kappa$ B)

#### 3.4.1 The NF- $\kappa$ B family and regulating factors

NF- $\kappa$ B was discovered in 1986 as a protein capable of localizing to the nucleus where it binds specifically to the DNA sequence 5'-GGGACTTCC-3' within the enhancer of the immunoglobulin  $\kappa$  light chain gene of mature B cells and plasma cells<sup>98</sup>. Following years of research, NF- $\kappa$ B emerged as being expressed in virtually all cell types regulating a multiplicity of target genes involved in innate and adaptive immune responses, cell proliferation, differentiation, survival, and cell death<sup>99</sup>.

The mammalian NF- $\kappa$ B family consists of the inducible transcription factors RELA (also known as p65), RELB, C-REL, p50 and its precursor p105, and p52 and its precursor protein p100. Through combinatorial associations, they can form various homodimeric and heterodimeric complexes that activate the expression of numerous target genes via specifically binding to  $\kappa$ B motifs in their promoter/enhancer region<sup>100</sup>. RELA/p50 heterodimers represent the most abundant REL dimers and can be found in almost all cell types. All subunits share a highly conserved N-terminal REL homology domain (Fig. 3A), which is approximately 300 amino acids long and responsible for dimerization, interaction with inhibitor of NF- $\kappa$ B (I $\kappa$ B) proteins, and DNA-binding<sup>101-104</sup>. Within the REL homology domain lies also a nuclear localization sequence, enabling their nuclear translocation<sup>105</sup>.

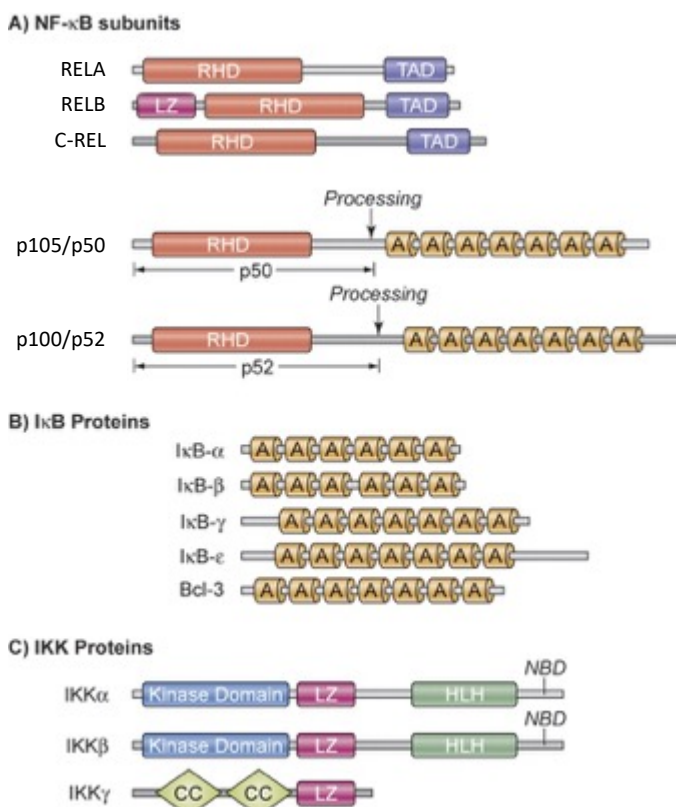


**Figure 3: Structure of NF- $\kappa$ B, I $\kappa$ B, and IKK family members.** (A) The NF- $\kappa$ B family of transcription factors consists of five proteins that share a REL homology domain (RHD), which is responsible for dimerization and DNA-binding. RELA, RELB, and C-REL additionally possess a carboxy-terminal transcription activation domain (TAD), which allows the interactions with regulatory proteins. RELB also contains a leucine zipper (LZ) motif. p105/p50 and p100/p52 contain ankyrin repeats, which mediate the binding to RHD of other NF- $\kappa$ B proteins. Activation leads to processing of the precursor proteins p105 and p100 to p50 and p52. (B) I $\kappa$ B proteins are characterized by 6-7 ankyrin repeats. (C) IKK proteins form a complex containing the catalytic kinases IKK $\alpha$  and IKK $\beta$ , and the regulatory subunit IKK $\gamma$  (NEMO). IKK $\alpha$  and IKK $\beta$  contain a helix-loop-helix region (HLH) and a LZ motif, which are necessary for dimerization. NEMO-binding domain (NBD) enables the interaction of IKK $\alpha$  and IKK $\beta$  with IKK $\gamma$  (NEMO), which possesses a coiled coil (CC) and a LZ domain. Image has been adapted and modified from Jost and Ruland (2007)<sup>106</sup>.

RELA, RELB, and C-REL contain in addition a C-terminal transcription activation domain (Fig. 3A) that is crucial for the activation of gene expression and allows the interaction with transcriptional regulatory proteins<sup>103,107,108</sup>. Among the NF- $\kappa$ B family members, only RELB possesses a N-terminal leucine zipper (Fig. 3A) motif, which is required together with the transcription activation domain for full transactivation<sup>109</sup>. In contrast, p105 and p100 contain in their C-terminal area multiple ankyrin repeats (Fig. 3A), similar to the ankyrin-repeat region found in I $\kappa$ B proteins, rendering the larger precursors as NF- $\kappa$ B inhibitors through cytoplasmic retention of REL proteins<sup>110,111</sup>.

The mature subunits p50 and p52 become active DNA-binding proteins after processing of their precursor molecules p105 and p100, which requires phosphorylation and ubiquitination of the C-terminal domain followed by their partial proteasomal degradation<sup>112,113</sup>. By forming heterodimers with RELA, RELB and C-REL, they finally activate the transcription, while dimers without a transactivation domain also inhibit gene transcription, such as p50 homodimers<sup>114</sup>.

In unstimulated cells, NF- $\kappa$ B subunits are kept in the cytoplasm through interaction with I $\kappa$ B proteins. Members of the I $\kappa$ B family include I $\kappa$ B proteins such as I $\kappa$ B- $\alpha$ , I $\kappa$ B- $\beta$ , I $\kappa$ B- $\gamma$ , I $\kappa$ B- $\epsilon$ , and Bcl-3. Whereas the I $\kappa$ B proteins are predominantly localized in the cytoplasm, Bcl-3 is able to translocate into the nucleus and modulate besides the subcellular localization also the transcriptional activation of p50 and p52 homodimers<sup>115</sup>. All I $\kappa$ B members are characterized by several ankyrin repeats (Fig. 3B), mediating the protein-protein interaction with the REL homology domain of NF- $\kappa$ B transcription factors. Cytoplasmic retention of the NF- $\kappa$ B dimers occurs through masking of their nuclear localization sequence by I $\kappa$ B proteins<sup>116-119</sup>.

Phosphorylation of I $\kappa$ B proteins by I $\kappa$ B kinases (IKK) and subsequent degradation is essential for the release and the nuclear translocation of NF- $\kappa$ B dimers. The IKK family comprises two catalytic subunits IKK $\alpha$  and IKK $\beta$  and one noncatalytic regulatory subunit, IKK $\gamma$  (NEMO for NF- $\kappa$ B essential modulator). IKK $\alpha$  and IKK $\beta$  contain a N-terminal catalytic kinase domain, a leucine zipper motif, and a C-terminal helix-loop-helix region. Helix-loop-helix region and leucine zipper domains are involved in the formation of homo- and heterodimers and in regulating the kinase activity<sup>120</sup>. NEMO possesses no catalytic domain and only a coiled coil and a leucine zipper domain. Interaction between the catalytic kinases and NEMO occurs via NEMO-binding domain<sup>121</sup>.

### 3.4.2 Mechanism of NF- $\kappa$ B activation

In cells under unstimulated conditions, NF- $\kappa$ B subunits exist as inactive hetero- or homodimers in the cytoplasm bound to inhibitory proteins. Since NF- $\kappa$ B is activated by various stimuli that are potentially harmful to the host, activation of NF- $\kappa$ B leads to the transcription of hundreds of target genes mainly involved in the regulation of immune responses, inflammation and cell survival<sup>99</sup>. Stimulation of NF- $\kappa$ B requires different activation steps including phosphorylation, ubiquitination, proteasomal degradation and processing of proteins with inhibitory functions leading to the release of NF- $\kappa$ B dimers and their nuclear translocation where they regulate the transcription of specific target genes. Multiple homodimeric and heterodimeric combinations of the NF- $\kappa$ B subunits enables a unique pattern of transcriptional activation<sup>100</sup>.

NF- $\kappa$ B activation occurs via two distinct signaling pathways: the canonical (classical) and non-canonical (alternative) pathway (Fig. 4). The predominant NF- $\kappa$ B signaling pathway is named as the canonical pathway and is triggered in response to numerous stimuli such as the inflammatory cytokines tumor necrosis factor (TNF), IL-1 and Toll-like receptor (TLR) agonists such as the pathogen-derived molecule patterns lipopolysaccharide (LPS), bacterial and viral RNA/DNA<sup>99</sup>. In the canonical pathway, receptor ligation causes the recruitment of several adaptor proteins including the E3 ubiquitin ligase TNF receptor-associated factor 2 (TRAF2), receptor-interacting protein 1 (RIP1), and cellular inhibitor of apoptosis proteins (C-IAP1/2, Fig.4)<sup>122</sup>.

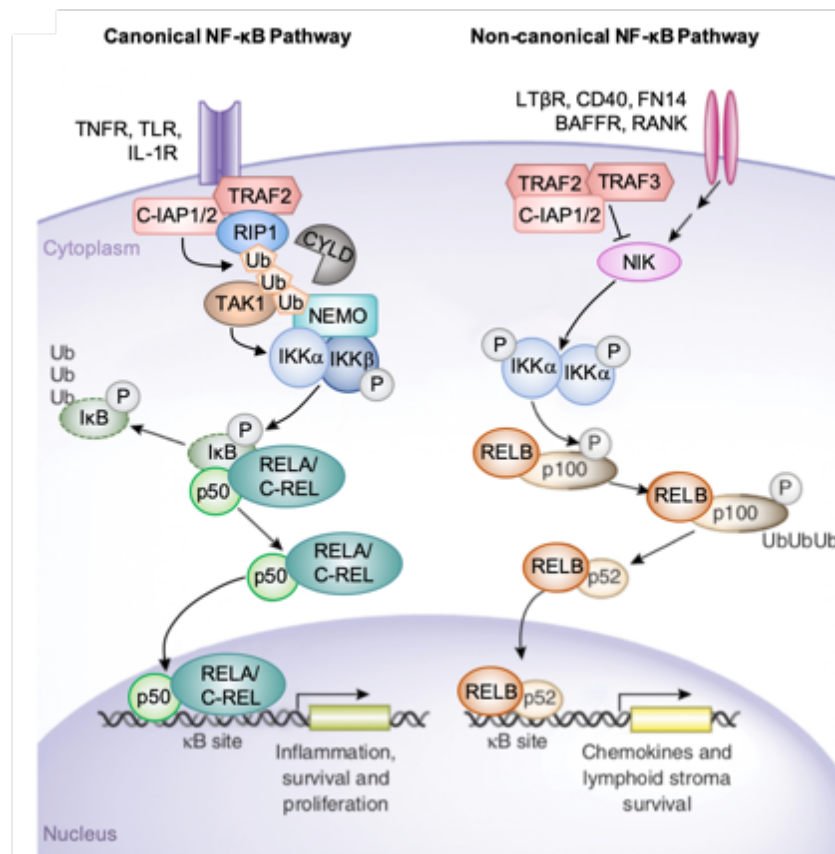


**Figure 4: Canonical and non-canonical NF- $\kappa$ B signaling pathway.** Stimulation of canonical NF- $\kappa$ B (left) leads via K63-linked ubiquitination of different signaling components (TRAF2, RIP1 and TAK1) to activation of the IKK complex. Phosphorylation of I $\kappa$ B, bound to NF- $\kappa$ B dimers such as RELA/p50 or C-REL/p50, results in ubiquitination and following proteasome-induced degradation. NF- $\kappa$ B dimers can then translocate into the nucleus, bind to the DNA (specific  $\kappa$ B sites) and activate the transcription of target genes involved in inflammation, proliferation and survival. The deubiquitinase cylindromatosis (CYLD) negatively regulates NF- $\kappa$ B activation by removing K63-linked ubiquitin chains, inhibiting the recruitment of the IKK complex. Non-canonical NF- $\kappa$ B requires degradation of the ubiquitin ligase complex TRAF2/TRAF3/C-IAP1/2 and activation of NIK, which phosphorylate IKK $\alpha$  homodimers. Phosphorylation of p100 leads to proteolytically processing to p52. Heterodimers RELB/p52 enter the nucleus and activate gene expression from cytokines and that are important for lymphoid organogenesis. Image has been adapted and modified from Gerondakis et al. (2014)<sup>123</sup>.

After formation of this complex, TGF- $\beta$  activated kinase 1 (TAK1) is recruited and activates the IKK complex (IKK $\alpha$ , IKK $\beta$ , and NEMO) by phosphorylation of IKK $\beta$ <sup>124</sup>. Activation of the IKK complex involves K63-linked ubiquitination of different regulator components, including TRAF2, RIP1, TAK1, and NEMO<sup>125</sup>. In this context, deubiquitinases (e.g. CYLD) that are able to remove K63-linked ubiquitin chains play pivotal roles by negatively regulating NF- $\kappa$ B activation<sup>126–128</sup>. Activation of the IKK complex leads to phosphorylation of I $\kappa$ B proteins such as the prototypical I $\kappa$ B member I $\kappa$ B- $\alpha$ ,

its subsequent polyubiquitination at lysine 48 (K48) and proteasomal degradation<sup>129</sup>. Ultimately, release of I $\kappa$ B- $\alpha$  sequestered NF- $\kappa$ B dimers composing predominantly of RELA/p50 results in unmasking their nuclear localization sequence and rapid and transient nuclear translocation, followed by activation of target gene expression involved in cell proliferation, survival, inflammation, epithelial-to-mesenchymal transition, angiogenesis and metastasis<sup>130</sup>.

While canonical NF- $\kappa$ B signaling pathway relies on the degradation of I $\kappa$ B proteins, non-canonical NF- $\kappa$ B pathway depends on processing of p100 to p52 (Fig. 4)<sup>131</sup>. Ligands that stimulate p100 processing have been identified as a subset of TNF receptor family members such as lymphotoxin (LT), LIGHT, receptor activator for nuclear factor  $\kappa$ B ligand (RANKL), B-cell activating factor (BAFF), TNF-like weak inducer of apoptosis (TWEAK), and CD40 ligand (CD40LG)<sup>132–136</sup>. Upon receptor ligation, different TRAF members, particularly TRAF2 and TRAF3, and C-IAP1/2 are recruited to the receptor, where c-IAP1/2 ubiquitinates the TRAF proteins and triggers their degradation (Fig. 4). In unstimulated cells, TRAF/C-IAP1/2 complex keep NF- $\kappa$ B inducing kinase (NIK) levels low by K48 ubiquitination and constant degradation of NIK<sup>137</sup>. After degradation of the TRAFs, NIK accumulates and activates the IKK complex, which consists this time of IKK $\alpha$  homodimers, and phosphorylates the precursor p100 leading to the selective proteolysis of its I $\kappa$ B-like domain<sup>138</sup>. Processing of p100 to the mature subunit p52 results finally in slow and persistent translocation of RELB/p52 dimers into the nucleus and binding to promoters or enhancers of target genes. In contrast to the canonical NF- $\kappa$ B pathway, which is turned on within minutes, activation of the non-canonical pathway takes several hours and involves new protein synthesis important for the development and maintenance of lymphocytes and secondary lymphoid organs<sup>130,139</sup>.

### 3.4.3 NF- $\kappa$ B in the murine liver

Since NF- $\kappa$ B is involved in a wide range of key biological processes, it has become clear that dysregulated and aberrant NF- $\kappa$ B activation is involved in the development of severe diseases such as immunodeficiency, autoimmunity, and cancer, as well as in resistance to chemo- and radiotherapy, which is why NF- $\kappa$ B has been proposed as a potential therapeutic target in the recent years<sup>140–144</sup>. Although pharmacological intervention of NF- $\kappa$ B appears promising, various studies targeting NF- $\kappa$ B regulating proteins have provided inconsistent results regarding the inflammatory activity, cytoprotective and cytotoxic effects of NF- $\kappa$ B. Due to the complexity of the NF- $\kappa$ B pathway and its influence on numerous cellular processes, the differentiation between potential protective and detrimental signaling pathways is a major challenge to minimize off-target effects and unwanted toxicities.

In the liver, especially the interaction with gut-derived bacteria and their products like LPS and LPS-induced TNF needs to be tightly controlled in order to avoid liver damage, as these substances are cytotoxic to hepatocytes. Here, NF- $\kappa$ B induces anti-apoptotic and proinflammatory signals in response to these mediators to ensure hepatocyte survival and immune responses at the same time<sup>145</sup>. The importance of canonical NF- $\kappa$ B member RELA for the liver development was first demonstrated in 1995 in genetic studies by Beg et al., in which RELA knockout mice died on day 15-16 of embryogenesis caused by massive liver degeneration<sup>146</sup>. High sensitivity for endogenous TNF cytotoxicity explained the embryonic lethality, as mice with a double knockout of RELA and either

TNF- $\alpha$  or TNFR type 1 were viable and developed normal livers<sup>147,148</sup>. The phenotype of mice lacking the catalytic subunit of the IKK complex IKK $\beta$  or the regulatory subunit NEMO was consistent with the phenotype of RELA deficient mice. These mice also died from severe fetal liver apoptosis, revealing a critical role of RELA, IKK $\beta$  and NEMO in protecting hepatocytes against TNF- $\alpha$  induced apoptosis during embryogenesis<sup>149,150</sup>.

In the adult liver, the role of the IKK subunits varies from the situation during embryogenesis. Conditional inhibition of RELA, IKK $\beta$  or overexpression of a degradation-resistant form of I $\kappa$ B- $\alpha$  in liver parenchymal cells displayed no spontaneous liver phenotype, indicating no essential liver functions under physiological conditions and in postnatal liver development<sup>151–153</sup>. In contrast, liver-specific deletion of NEMO or TAK1 caused the spontaneous development of HCC. While the liver phenotype of NEMO knockout mice was associated with steatohepatitis, hepatocyte death and compensatory hepatocyte proliferation, livers with TAK1 disruption displayed hepatocyte dysplasia, biliary ductopenia and cholestasis<sup>154,155</sup>. Moreover, hepatic overexpression of IKK $\beta$  led to chronic inflammation and fibrosis, which was partly mediated by the recruitment and activation of macrophages<sup>156</sup>. Compared to RELA, NEMO and IKK $\beta$ , the subunits p50, p52 and RELB appear to be dispensable during liver development and play more important roles in immunity, B cell survival and maturation, nonspecific immune responses to pathogens, and lymphoid organogenesis<sup>157–159</sup>. All the transgenic mouse models with repressed or overactivated expression of different NF- $\kappa$ B signaling components highlight the complexity of the NF- $\kappa$ B pathway and underline the importance for a better understanding of long-term NF- $\kappa$ B modification and its consequences.

#### 3.4.4 NF- $\kappa$ B in the human liver

In human liver diseases, inflammation is an essential component of the wound-healing process in response to hepatic injury. Since NF- $\kappa$ B signaling pathway is a key regulator in immune and inflammatory responses, it is not surprising that NF- $\kappa$ B is activated in a variety of chronic liver disease. In liver biopsies of patients with ASH and NASH, RELA expression was significantly enhanced in hepatocytes, which correlated with disease severity and was highly associated with hepatic apoptosis, suggesting that activation of NF- $\kappa$ B either contributed to apoptosis or occurred in response to hepatocyte death<sup>160</sup>. Immunohistochemical staining and electrophoretic mobility shift assay of HCV-infected liver tissues revealed prominent activation of canonical NF- $\kappa$ B compared to normal liver tissue. In vitro studies showed a sensitizing effect towards TNF- $\alpha$  mediated apoptosis after inhibition of NF- $\kappa$ B activation. From these results, the authors concluded an evasion mechanism by which HCV induced anti-apoptotic strategies to evade host innate immune defense and thus leading to persistent infection<sup>161,162</sup>. Abnormal NF- $\kappa$ B activity was also observed in biliary liver diseases such as PBC, in which RANK, the receptor activator for NF- $\kappa$ B, was found to be strongly expressed by damaged cholangiocytes. Infiltrating T and B lymphocytes in the portal areas represented the cellular source of the ligand RANKL, suggesting that high RANK expression by cholangiocytes led to their recruitment. In addition, hepatic RANKL levels correlated with the disease stage of PBC, indicating a direct effect of RANK/RANKL axis on the pathogenesis of PBC<sup>163</sup>.

Dysregulated NF- $\kappa$ B activation in such a large number of human chronic liver diseases, including ASH, NASH, viral infection, points to an essential role for liver homeostasis, immune cell interaction and wound-healing processes. While previous studies have shown that canonical NF- $\kappa$ B is upregulated

in chronic liver diseases, a contribution of non-canonical NF- $\kappa$ B signaling to chronic liver diseases remains largely unknown.

### 3.4.5 NF- $\kappa$ B in hepatocarcinogenesis

Primary liver cancer, especially HCC, develops in the great majority of cases within an established background of chronic inflammation, fibrosis and cirrhosis, with viral infection, ALD, and NAFLD representing major risk factors. As mentioned in the previous section, NF- $\kappa$ B activation has been observed in the setting of chronic liver diseases. During the development and progression of HCC, NF- $\kappa$ B plays also a decisive role and can function both as tumor promoter and tumor suppressor, as several studies with genetically modified mouse models of HCC have shown. Mice lacking IKK $\beta$  in liver parenchymal cells did not exhibit spontaneous liver dysfunction but exhibited after a single injection of the chemical carcinogen diethylnitrosamine (DEN) significantly increased HCC formation compared with control animals given DEN, which led suggest a tumor suppressor function of NF- $\kappa$ B in this setting<sup>164</sup>. Another study with liver-specific NF- $\kappa$ B inhibition by deletion of NEMO revealed steatohepatitis and spontaneous HCC development<sup>154</sup>. In both studies, it was assumed that hepatocarcinogenesis was caused by increased oxidative stress leading to sustained c-Jun N-terminal kinase (JNK) activity, hepatocyte death, and compensatory proliferation<sup>154,164</sup>. Analysis of liver-specific TAK1 knockout mice revealed ductopenia, cholestasis, hepatocyte apoptosis and dysplasia, and the development of liver tumors at the age of 4 - 8 months, suggesting a liver cancer suppressive role of TAK1<sup>155</sup>. Although the phenotype was partly dependent on defective NF- $\kappa$ B activation in response to TNF- $\alpha$ , additional deletion of NEMO was able to rescue the phenotype of TAK1 knockout mice, surprisingly. In the background of TAK1 ablation, NEMO seemed to act as a tumor promotor, whereas it mediates tumor suppression in liver parenchymal cells with functional TAK1<sup>154,155</sup>.

In contrast to these studies arguing for a general tumor suppressive effect of NF- $\kappa$ B, other studies demonstrated a pro-carcinogenic role of NF- $\kappa$ B in the liver. A tumor promoting effect of NF- $\kappa$ B has been first described using MDR2 knockout mice, in which deletion of the biliary phospholipid exporter MDR2 caused cholestatic hepatitis followed by HCC development<sup>165</sup>. In this inflammation-associated cancer, inhibition of NF- $\kappa$ B by a hepatocyte-specific non-degradable form of I $\kappa$ B $\alpha$  resulted in apoptosis of transformed hepatocytes and suppressed tumor development<sup>166</sup>. In another mouse model, in which overexpression of the cytokine lymphotoxin (LT $\alpha$  and LT $\beta$ ) triggered chronic hepatitis-driven HCC formation, HCC development was dependent on NF- $\kappa$ B activation via IKK $\beta$ , since deletion of IKK $\beta$  prevented HCC formation<sup>167</sup>. In accordance with the murine data, IKK $\alpha$  and IKK $\beta$  were highly expressed in human HCC, combined with increased nuclear RELA expression compared to adjacent tissue. Moreover, downregulation of IKK $\alpha$  and IKK $\beta$  in human HCC cell lines resulted in decreased proliferation and also in inhibited HCC growth in a subcutaneous injection model<sup>168</sup>.

Whereas numerous studies demonstrated the influence of NF- $\kappa$ B in the HCC development, the impact of NF- $\kappa$ B during ICC formation is largely undefined. In an ICC mouse model caused by oxidative stress and in human ICC, the authors observed a dependency on Kupffer cell derived TNF- $\alpha$  which triggered JNK activation and cholangiocellular tumorigenesis. Here, nuclear RELA expression could not be detected in cholangiocytes and was mainly seen in nonparenchymal cells, indicating no relevance of canonical NF- $\kappa$ B signaling in liver parenchymal cells in this ICC mouse model<sup>169</sup>.

Based on the studies described above, it can be concluded that NF- $\kappa$ B signaling plays a critical role in the development of HCC. Although the data seem very contradictory, it should be noted that NF- $\kappa$ B exert different functions depending on the cell populations such as hepatocytes, Kupffer cells and hepatic stellate cells. Therefore, whether NF- $\kappa$ B acts as a tumor promoter or as a tumor suppressor depends on the cell type and experimental setting and also whether the cell compartment is responsible for tumor-promoting proinflammatory mediators. According to current knowledge, it is assumed that NF- $\kappa$ B functions as a tumor promoter rather than a tumor suppressor under relevant physiological conditions in the liver<sup>170</sup>. However, a better understanding of the underlying mechanism leading to pathological NF- $\kappa$ B activity is indispensable to develop specific and effective pharmacologic therapies for the treatment of liver diseases.

### 3.4.6 Liver-specific disruption of CYLD

Ubiquitination, the covalent conjugation of ubiquitin molecules to target proteins, is a crucial mechanism for the activation of NF- $\kappa$ B. This modification is a post-translational and dynamic process and can be counterbalanced by deubiquitinating enzymes. While lysine 48 (K48)-linked ubiquitination targets proteins for proteasomal degradation, K63-linked polyubiquitination facilitate signal transduction, protein-protein interaction, internalization and trafficking<sup>171,172</sup>. CYLD is a tumor suppressor and one of the best characterized deubiquitinases negatively regulating NF- $\kappa$ B activation. By cleaving K63-linked polyubiquitin chains from various NF- $\kappa$ B signaling proteins including NEMO, TRAFs and TAK1, CYLD inhibits the activation of the IKK complex and inhibits ultimately the degradation of I $\kappa$ Bs<sup>126</sup>. CYLD has been originally identified in familial cylindromatosis, a genetic predisposition to multiple tumors originating from the skin appendages, in which CYLD was truncated or lost<sup>173,174</sup>. In recent years, reduced expression of CYLD and persistent NF- $\kappa$ B activation has been observed in several malignancies such as human hepatocellular and colon carcinoma, melanoma and multiple myeloma<sup>175-177</sup>.

In 2012, Urbanik et al. examined the role of CYLD in liver homeostasis and hepatocarcinogenesis *in vivo*. Mice with liver-specific deletion of exon 7 and 8 of the CYLD gene, which were deficient in the expression of full-length CYLD but showed increased expression of the naturally occurring splice variant of CYLD, developed a spontaneous biliary phenotype characterized by ductular reaction and biliary fibrosis.<sup>178</sup> The phenotype was accompanied by periportal T-cell infiltration, increased levels of inflammatory cytokines such as CCL2, TNF- $\alpha$ , TGF- $\beta$ 1, and TGF- $\beta$ 2. Surprisingly, while canonical NF- $\kappa$ B pathway via RELA and p50 was only slightly upregulated, expression levels of non-canonical NF- $\kappa$ B with its key mediators RELB and p52 were remarkably increased. In a DEN/PB-induced hepatocarcinogenesis model, CYLD deficient mice were significantly more sensitive and developed besides HCC also ICC<sup>179</sup>. In another mouse model with a liver-specific truncation and inactivation of CYLD by deletion of exon 9, sustained activation of TAK1 and JNK caused in this case hepatocyte cell death, progressive liver fibrosis, inflammation and even spontaneous development of HCC at 12 months<sup>180</sup>. Both studies demonstrate that CYLD act as an important regulator in parenchymal liver cells and that aberrant NF- $\kappa$ B signaling promotes liver injury, fibrosis and hepatocarcinogenesis.

### 3.5 Aim of this work

The NF- $\kappa$ B signaling pathway is a highly conserved pathway with key regulatory functions in immune and inflammatory responses, cell proliferation, differentiation, and survival<sup>99</sup>. To date, two major signaling pathways have been described leading to NF- $\kappa$ B activation: the canonical pathway via RELA and the non-canonical pathway via RELB. Besides its key roles in inflammation and cell survival in immune cells, NF- $\kappa$ B has been shown to contribute to chronic liver injury, liver fibrosis, and hepatocarcinogenesis<sup>154,155,160,161</sup>. Chronic liver diseases such as viral hepatitis and alcoholic liver disease are a major global health burden affecting millions of people<sup>31</sup>. After long periods of chronic liver damage, fibrosis can progress to cirrhosis, liver failure and ultimately HCC, independent of the underlying etiology<sup>45</sup>. Primary liver cancer is one of the most commonly diagnosed cancers and has been ranked as one of the major causes of cancer-related deaths in 2015<sup>78</sup>. While previous studies only described a crucial role of canonical NF- $\kappa$ B signaling in the liver, a role of non-canonical NF- $\kappa$ B remains largely undefined<sup>146,149,150,157-159</sup>. However, in a study with a liver-specific disruption of the deubiquitinase CYLD in mice, livers displayed a severe biliary phenotype with ductular reaction and biliary fibrosis. Since the biliary phenotype of *Cyld*<sup>ALPC</sup> mice was accompanied by sustained activation of RELB, a contribution of non-canonical NF- $\kappa$ B can be assumed, underlining the necessity of a better understanding of the relevance of RELB in the liver<sup>179</sup>.

Based on these findings, the aim of this thesis was to investigate the functional importance of RELB for the liver, chronic liver diseases and hepatocarcinogenesis. For this purpose, the generation and analysis of a double knockout mouse containing a deletion of full-length CYLD and RELB (*Cyld/Relb*<sup>ALPC</sup> mice) was intended. To further elucidate the function of RELB for the liver under stress conditions, different chemically induced chronic liver damage models mimicking a) hepatocyte driven fibrosis and b) cholestasis with biliary fibrosis should be performed. The second part of this thesis aimed at evaluating the expression of RELB in human healthy liver tissue and in samples from patients with chronic liver diseases (viral hepatitis, AIH, ALD, NASH), cholangiopathies (PBC, PSC) and primary liver cancer (HCC, ICC).

## 4. Materials and Methods

### 4.1 Mouse Models

All mice studies were performed in accordance with relevant guidelines and regulations approved by the local governmental animal use and care committee and animal experiments were performed according to Institutional, National, and European guidelines.

#### 4.1.1 Breeding

Mice expressing Cre recombinase under the control of the albumin promoter (AlbCre) and mice carrying loxP sites flanking exon 7 of CYLD (CYLD<sup>FF</sup>) were kindly provided by the group of Prof. Dr. Waisman (Institute for Molecular Medicine, University of Mainz, Germany). Mice carrying loxP-flanked alleles of *Relb* (*Relb*<sup>FF</sup>) were obtained from Prof. Dr. Falk Weih (Leibniz Institute of Aging, Jena, Germany). All mice were bred on a C57BL/6 genetic background. To generate the liver parenchymal cell (LPC) specific knockout mice CYLD<sup>ALPC</sup> and *Relb*<sup>ALPC</sup>, AlbCre transgenic mice were crossed with the respective flox-strains, with complete recombination by 6 weeks of age<sup>181,182</sup>. Crossing of CYLD<sup>FF</sup> mice with AlbCre mice lead to an alternative splicing from exon 6 to exon 9 and knockout of full-length CYLD<sup>178,179</sup>. Double knockout in LPCs (*Cyld/Relb*<sup>ALPC</sup>) were established by intercrossing the respective lines. In all experiments, knockout mice were compared with their AlbCre control littermates (referred to as control), since it has been reported that in the absence of loxP-flanked alleles, expression of Cre recombinase led to metaplasia and profound atrophy of the epithelium in the stomach<sup>183</sup>. Mice were housed in a 12 h light/dark, temperature controlled and specific pathogen-free (SPF) animal facility of the University Heidelberg, Germany with *ad libitum* feeding.

#### 4.1.2 Mouse Genotyping

Ethylenediaminetetraacetic acid (EDTA)	# 8040.3, Roth, Karlsruhe, Germany
Magnesium chloride (MgCl <sub>2</sub> )	# M8266, Sigma-Aldrich, Munich, Germany
Proteinase K	# EO0491, Thermo Fisher, Schwerte, Germany
RedTaq Ready PCR Reaction Mix	# R2523, Sigma-Aldrich, Munich, Germany
Sodium dodecyl sulfate (SDS)	# CN30.3, Roth, Karlsruhe, Germany
Tris Hydrochloride (Tris-HCl)	# 9090.1, Roth, Karlsruhe, Germany

Proteinase K buffer: 100 mM Tris-HCl (pH 7.6), 20 mM EDTA (pH 8.0), 0.5 % (w/v) SDS

To determine the genotype of the mice, 2 mm ear punches from 3-week-old mice were used for the isolation of the DNA. First, each tissue was digested with 50 µl of proteinase K solution, followed by incubation overnight at 56 °C. The proteinase K solution was prepared before each genotyping by mixing freshly thawed proteinase K and buffer in a 1:10 ratio. After the digestion, 1 ml MilliQ H<sub>2</sub>O was added to each sample and samples were stored at 4 °C until further use. For the Cre and CYLD polymerase chain reaction (PCR), an additional 1:10 dilution with MilliQ H<sub>2</sub>O of each sample was needed. The RedTaq Ready PCR Reaction Mix, which comprises already a thermostable DNA

polymerase Taq and dNTPs, was supplemented with primers, MgCl<sub>2</sub> and H<sub>2</sub>O to prepare a master mix for each target gene (Table 1).

**Table 1. Components for the preparation of the indicated PCR master mixes.**

<b>Cre</b>	<b>1x [μl]</b>	<b>Cyld</b>	<b>1x [μl]</b>	<b>Relb</b>	<b>1x [μl]</b>
Cre: 310 bp, Actin: 510 bp		wt: 325 bp, flox: 426 bp		wt: 225 bp, flox: 275 bp	
RedTaq	7.5	RedTaq	7.5	RedTaq	15
MgCl <sub>2</sub>	0.6	MgCl <sub>2</sub>	0.6	MgCl <sub>2</sub>	1.2
Primer Cre for	0.25	Primer Cre for	0.375	Primer Cre for	0.75
Primer Cre rev	0.25	Primer Cre rev	0.375	Primer Cre rev	0.75
Primer Act for	0.5	H <sub>2</sub> O	5.4	H <sub>2</sub> O	10.8
Primer Act rev	0.5				
H <sub>2</sub> O	4.65				
14.25 μl per tube + 2 μl DNA (1:10 diluted)		14.2 μl per tube + 1 μl DNA (1:10 diluted)		28.4 μl per tube + 1 μl DNA	

The master mix for the Cre PCR contained an additional Actin primer pair to differentiate between Cre negative samples and failures in the PCR procedure. Primer sequences are listed in Table 2 and the corresponding PCR programs are shown in Table 3.

**Table 2. PCR primer sequences for mouse genotyping.**

<b>Target Gene</b>	<b>Primer Sequence</b>
<i>Cyld</i>	for 5'-CCTATGTGGTACTGACCAGA-3'
	rev 5'-CATGGAAGGAGGCTGCGGAGGAGAT-3'
<i>Relb</i>	for 5'-TCCAAAAAACCACCAACAAC-3'
	rev 5'-GTTTTCCCTGCTTGTTCTGC-3'
<i>Cre recombinase</i>	for 5'-GCA CTG ATT TCG ACC AGG TT-3'
	rev 5'-CCC GGC AAA ACA GGT AGT TA-3'
<i>Actin</i>	for 5'-TGT TAC CAA CTG GGA CGA CA-3'
	rev 5'-GAC ATG CAA GGA GTG CAA GA-3'

Primers were synthesized by Eurofins (Jena, Germany).

**Table 3. PCR programs.**

<b>Cre/Cyld PCR program</b>		<b>Relb PCR program</b>	
1 cycle	95 °C for 5 min	1 cycle	94 °C for 5 min
	95 °C for 30 sec		94 °C for 30 sec
40 cycles	59 °C for 30 sec	40 cycles	56 °C for 40 sec
	72 °C for 45 sec		72 °C for 40 sec
1 cycle	72 °C for 5 min → 4 °C	1 cycle	72 °C for 5 min → 4 °C

### 4.1.3 Agarose Gel Electrophoresis

Acetic acid	# 3738.1, Roth, Karlsruhe, Germany
Agarose	# 2267.4, Roth, Karlsruhe, Germany
Ethidium Bromide 1%	# A1152, AppliChem, Darmstadt, Germany
EDTA	# 8040.3, Roth, Karlsruhe, Germany
GeneRuler 50 bp DNA ladder	# SM0373, Thermo Fisher, Schwerte, Germany
Tris-HCl	# 9090.1, Roth, Karlsruhe, Germany

50x TAE buffer: 2 M Tris-HCl, 1 M acetic acid, 50 mM EDTA (pH 8.0)

The agarose gel electrophoresis enables the separation of DNA fragments in a size-dependent manner. To analyze the amplified DNA products from the PCR, agarose powder (2 %, w/v) was dissolved in 1x TAE buffer and heated up in a microwave until it became completely transparent. After the agarose solution cooled down to about 50 °C, the DNA-intercalating substance ethidium bromide was added to a final concentration of approximately 0.05 µl/ml. Then, the agarose solution was poured into a gel tray with a well comb already in place. After the gel became completely solidified, the gel was placed into a gel box filled with 1x TAE buffer. The comb was removed, DNA ladder and samples were loaded into the wells and an electric tension of 120 V was applied. After the run, the DNA fragments were visualized by illuminating the gel with UV-light ( $\lambda = 254$  nm). Ethidium bromide intercalates unspecifically into double-stranded DNA molecules and excitation to UV-light leads to an emission of detectable fluorescence ( $\lambda = 605$  nm).

### 4.1.4 Organ removal and routine serum biochemistry

37 % Formaldehyde solution	# F1635, Sigma-Aldrich, Munich, Germany
Ketamine 10%	belapharm, Vechta, Germany
OCT mounting medium	# SA62550, Science Services, Munich, Germany
Phosphate buffered saline (PBS)	# 14190-094, Thermo Fisher, Schwerte, Germany
Sodium chloride (NaCl)	# 9265.1, Roth, Karlsruhe, Germany
Xylavet (20 mg Xylazin)	CD Pharma, Burgdorf, Germany

In order to analyze liver morphology and clinically relevant serum parameters, mice were anesthetized by intraperitoneal injections of ketamine 10 % (120 mg/kg) and xylazine (16 mg/kg) diluted in isotonic 0.9 % NaCl. Blood was obtained by cardiac puncture from deeply anesthetized mice followed by rapid dislocation of the cervical spine. Liver was removed, rinsed in PBS and cut in different sections. Thereby, the left lateral lobe was used for histological and immunohistochemical analyses and the right medial lobe was used for protein and RNA analyses. For protein and RNA analyses, liver tissue was transferred into a reaction tube and snap frozen in liquid nitrogen. For histological analyses, liver tissue was transferred into a 4 % neutral buffered formaldehyde solution and stored at room temperature until further processing. For additional immunohistochemical analyses, liver tissue was covered with OCT mounting medium and was gradually frozen in the gas phase of liquid nitrogen. After removal of the liver, whole blood samples were centrifuged at 1500 x g for 10 min, serum was

collected from the supernatant and stored at -20 °C until analysis. Serum (400 µl, if necessary diluted with 1x PBS) was then analyzed for aspartate transaminase (AST), alanine transaminase (ALT), alkaline phosphatase (AP), and bilirubin by the Diagnostic Center of the Heidelberg University Hospital according to standard procedures.

#### 4.1.5 Isolation and cultivation of primary murine hepatocytes

Acetic acid	# 3738.1, Roth, Karlsruhe, Germany
Calcium chloride (CaCl <sub>2</sub> )	# CN93.1, Roth, Karlsruhe, Germany
Collagen	# C9791, Sigma-Aldrich, München
Collagenase NB 4	# 17454.01 Serva, Heidelberg
DMEM Medium	# 61965-026, Thermo Fisher, Schwerte, Germany
Fetal calf serum (FCS)	# 16000044, Thermo Fisher, Schwerte, Germany
HEPES	# 9105.4, Roth, Karlsruhe, Germany
Insulin	# 01843315, Sanofi-Aventis, Frankfurt, Germany
Ketamine 10%	bela-pharm, Vechta, Germany
Penicillin/Streptomycin (10000 U/ml)	# P4333, Sigma-Aldrich, Munich, Germany
Potassium chloride (KCl)	# 104936, Merck, Darmstadt, Germany
NaCl	# 9265.1, Roth, Karlsruhe, Germany
Xylavet (20 mg Xylazine)	CD Pharma, Burgdorf, Germany

Buffer A: 140 mM NaCl, 7 mM KCl, 10 mM HEPES (pH 7.4)

Buffer B: 70 mM NaCl, 7 mM KCl, 5 mM CaCl<sub>2</sub>, 100 mM HEPES (pH 7.6), 0.5 mg/ml Collagenase

Buffer C: 140 mM NaCl, 7mM KCl, 1mM CaCl<sub>2</sub>, 10 mM HEPES (pH 7.4)

Attachment medium: DMEM with 10 % FCS, 100 U/ml Pen/Strep, 20 mM HEPES, 0.05 % (20 IE/L)

Insulin

Culture medium: DMEM with 0.5 % FCS, 100 U/ml Pen/Strep, 20 mM HEPES, 0.05 % (20 IE/L)

Insulin

The principle of this method is based on a two-step collagenase perfusion technique to isolate hepatocytes<sup>184</sup>. First, a calcium-free medium containing a calcium chelator removes calcium ions from epithelial cells resulting in the destruction of intercellular junctions and the loss of cell-cell contacts<sup>185</sup>. In the second step, the enzyme collagenase causes the disruption of the supporting extracellular matrix. After the isolation, parenchymal hepatocytes can be separated from other non-parenchymal cells which include sinusoidal endothelial cells, cholangiocytes, hepatic stellate cells, Kupffer cells, and intrahepatic lymphocytes. Hepatocytes were used then for a short-term culture of 48 h to verify the liver parenchymal cell-specific knockout of CYLD and RELB.

All solutions were first heated up to 37 °C. 8-week-old mice were anesthetized with ketamine 10 % (120 mg/kg) and xylazine (16 mg/kg) injections diluted in isotonic 0.9 % NaCl and livers were exposed surgically. The peripheral venous catheter was inserted into the *vena portae*, the *vena cava inferior* was cut and the liver was perfused with 100 ml of buffer A. Then, the perfusion medium was changed for buffer B (50 ml), a collagenase solution that digests the connective tissue in the liver. After perfusion, the entire liver was removed and transferred into a petri dish containing buffer C. By using

two pairs of forceps, the liver lobes were dissociated and the hepatocyte solution was filtered through a gauze mesh filter into a 50 ml sterile tube. After centrifugation (5 min, 30 x g), the supernatant was discarded and the pellet was washed twice with 50 ml DMEM. This procedure allows the separation of parenchymal hepatocytes from dead hepatocytes and other liver populations, which remain in the supernatant. Hepatocytes were suspended in 30 ml attachment medium and cell number and viability was determined using Trypan Blue staining. Per mouse, 20 - 30 x 10<sup>6</sup> cells with a viability of 70 - 80 % could be isolated. 2.5 x 10<sup>6</sup> cells were then seeded onto collagen coated 6-well plates, since primary murine hepatocytes require collagen for attachment.

For the collagen coating, 5 mg collagen was dissolved in 20 ml 10 % acetic acid overnight at room temperature overnight (stirring) and sterile filtered. This collagen solution was diluted 50-fold with MilliQ H<sub>2</sub>O and transferred into 6-well plates covering the surface. 30 min later, excess fluid from the coated surface was removed, dried overnight and stored at room temperature until further usage.

The isolated hepatocytes were incubated at 37 °C and 5 % CO<sub>2</sub> for at least 3 hours. Afterwards, the attachment medium was replaced with culture medium. Cells were collected 24 hours later, followed by western blot analysis.

#### 4.1.6 CCl<sub>4</sub>-induced liver fibrosis

Carbon tetrachloride (CCl <sub>4</sub> )	# 289116, Sigma-Aldrich, Munich, Germany
Sunflower Seed Oil Sigma Aldrich S5007	# S5007, Sigma-Aldrich, Munich, Germany

Liver fibrosis occurs as a response to almost every type of chronic liver injury<sup>186</sup>. Prolonged administration of CCl<sub>4</sub> is a widely used toxin-based experimental model for the induction of non-cholestatic liver fibrosis<sup>187</sup>. CCl<sub>4</sub> was diluted 1:7 in sunflower oil and 8-week-old male mice (n = 5 per group) were injected intraperitoneally at a dose of 1 ml/kg bodyweight. Mice were injected twice a week for 6 weeks and were daily monitored. Control mice (n = 5 per group) received the same amount of sunflower oil during the experimental time. Mice were sacrificed 3 days after the last CCl<sub>4</sub> injection.

#### 4.1.7 DDC diet

3,5-diethoxycarbonyl-1,4-dihydrocollidine	# 137030, Sigma-Aldrich, Munich, Germany
Standard mouse diet	# 1324, Altromin, Lage, Germany

Chronic exposure to the biliary toxin 3,5-diethoxycarbonyl-1,4-dihydrocollidine (DDC) is a model to study xenobiotic-induced chronic cholangiopathies<sup>69</sup>. Therefore, 8-week-old male mice (n = 5 per group) were fed *ad libitum* with a diet supplemented with 0.1% DDC for up to 6 weeks. Control mice (n = 5 per group) received a standard mouse diet.

## 4.2 Cell culture

### 4.2.1 Cultivation of normal human cholangiocytes

DMEM F12 with glutamax (Gibco)	# 10565018, Thermo Fisher, Schwerte, Germany
Fetal calf serum (FCS)	# 16000044, Thermo Fisher, Schwerte, Germany
Penicillin/Streptomycin (10 000 U/ml)	# P4333, Sigma-Aldrich, Munich, Germany
Trypsin-EDTA Solution	# T3924, Sigma-Aldrich, Munich, Germany
Phosphate Buffered Saline (PBS) (Gibco)	# 14190-094, Thermo Fisher, Schwerte, Germany
MEM non-essential amino acids solution	# 11140050, Thermo Fisher, Schwerte, Germany
MEM vitamine solution (Gibco)	# 11120037, Thermo Fisher, Schwerte, Germany
Soyben Trypsin Inhibitor	# 17075029, Thermo Fisher, Schwerte, Germany
Insulin Transferrin Selenium (Gibco)	# 51500056, Thermo Fisher, Schwerte, Germany
Bovine Pituitary Extract	# 13028014, Thermo Fisher, Schwerte, Germany
Dexamethasone	# D4902, Sigma-Aldrich, Munich, Germany
T3 (3, 3' 5-triiodo-L-thyronine sodium salt)	# T6397, Sigma-Aldrich, Munich, Germany
Epidermal growth factor (EGF)	# E9644, Sigma-Aldrich, Munich, Germany
Lipid mixture, chemically defined	# L0288, Sigma-Aldrich, Munich, Germany
Forskolin	# F3917, Sigma-Aldrich, Munich, Germany

Normal human cholangiocytes were isolated and characterized by the group of Jesus Maria Banales (Department of Liver and Gastrointestinal Diseases, Biodonostia Health Research Institute-Donostia University Hospital, University of the Basque Country, San Sebastian, Spain) and afterwards kindly provided for experiments<sup>188</sup>. Adherent cells were grown in cell culture flasks and were maintained at 37°C, 5% CO<sub>2</sub> in a humid atmosphere. Cells were cultured in Dulbecco's Modified Eagle's Medium (DMEM) F12 with glutamax, supplemented with 10% FCS, 1% Penicillin/Streptomycin, 1% MEM non-essential aminoacids, lipid mixture, 1% MEM vitamine solution, 25 mg soyben trypsin inhibitor, 1% insulin transferrin selenium, 6.7 mg bovine pituitary extract, 0.2 mg dexamethasone, 1.7 mg T3, 0.5 mg EGF, and 2 mg Forskolin. Cells were provided in a frozen vial on dry ice. To thaw the cell suspension, the vial was placed in a 37°C water bath and the cell suspension was transferred to 10 ml of cell culture medium. In order to remove DMSO (dimethyl sulfoxide), the cell suspension was centrifuged for 5 min at 100 x g, supernatant was discarded and cells were resuspended in preheated cell culture medium. Then, the cells were seeded into a cell culture flask (25 cm<sup>2</sup>) and incubated at 37°C. After 24 h the medium was changed to fresh medium. To split the cells, culture medium was discarded, cells were washed with PBS and detached by trypsinization for 5 minutes at 37°C. Trypsin-mediated digestion of cells was stopped by adding fresh cell culture medium. Cell suspension was then transferred into a 15 ml falcon and centrifuged for 5 min at 100 x g. After discarding the trypsin-containing supernatant, the cell pellet was resuspended in culture medium and the cell suspension was seeded 1:2 into a new cell culture flask. The total medium volume in the flask was adjusted with fresh and preheated medium. The cells were routinely controlled for any contaminations.

### 4.2.3 Transfection of cells with siRNA

Lipofectamine RNAiMAX	# 13778150, Thermo Fisher, Schwerte, Germany
OptiMEM (Gibco)	# 31985070, Thermo Fisher, Schwerte, Germany
Phosphate Buffered Saline (PBS) (Gibco)	# 14190-094, Thermo Fisher, Schwerte, Germany

For knockdown experiments, 180,000 cells were seeded into a 12 well plate. After 24 h, cells were transfected with 80nM small interfering RNA (siRNA) targeting *Relb* by using Lipofectamine RNAiMAX according to the manufacturer's protocol.

The following siRelb sequence was applied (purchased by MWG Biotech, Ebersberg, Germany):

5'- GAACCAUCAGGAAGUAGACTT-3' (sense) and 5'-GUCUACUCCUGAUGGUUCTT-3' (anti-sense).

### 4.2.3 Cell stimulation with LT $\alpha$ 1 $\beta$ 2

Recombinant human LT $\alpha$ 1 $\beta$ 2	# 678-LY, R&D Systems, Minneapolis, United States
---	---

LT $\beta$  is a ligand stimulating non-canonical NF- $\kappa$ B signaling. For specific LT $\beta$  receptor ligation, cells were incubated with 250 ng/ml recombinant human LT $\alpha$ 1 $\beta$ 2. After 48 hours of incubation, cells were harvested, diluted 1:2 with trypan blue, and counted using a Neubauer counting chamber to determine the relative cell count. Trypan blue was used to distinguish between dead, fragmented cells and vital cells.

## 4.3 Protein expression analyses

To determine protein expression and activation of signaling pathways, total protein was isolated from cultured primary murine hepatocytes or murine liver tissue. Proteins were separated by SDS polyacrylamide gel electrophoresis (SDS-PAGE) and were analyzed by Western blot using specific primary and secondary antibodies.

### 4.3.1 Protein isolation

1,4 Dithiothreitol (DTT)	# 6908.2, Roth, Karlsruhe, Germany
Nonylphenylpolyethylenglycol (NP-40)	# 28324, Thermo Fisher, Schwerte, Germany
Phenylmethylsulphonyl fluoride (PMSF)	# 6367.2, Roth, Karlsruhe, Germany
PBS	# 14190-094, Thermo Fisher, Schwerte, Germany
Protease inhibitor cocktail (PI)	# 04693116001, Roche, Mannheim, Germany
NaCl	# 9265.1, Roth, Karlsruhe, Germany
Sodium dodecyl sulfate (SDS)	# CN30.3, Roth, Karlsruhe, Germany
Sodium fluoride (NaF)	# 2618.1, Roth, Karlsruhe, Germany
Sodium orthovanadate	# 450243, Sigma-Aldrich, Munich, Germany
Tris-HCl	# 9090.1, Roth, Karlsruhe, Germany

2x Radioimmunoprecipitation Assay buffer (RIPA buffer): 240 mM NaCl, 100 mM Tris/HCl (pH 8.0), 2% (v/v) NP-40, 0.2% (w/v) SDS

1x RIPA lysis buffer: 428  $\mu$ l MilliQ H<sub>2</sub>O, 500  $\mu$ l 2x RIPA buffer, 40  $\mu$ l NaF, 20  $\mu$ l PI, 10  $\mu$ l PMSF, 1  $\mu$ l DTT, 1  $\mu$ l Vanadate

### 4.3.1.1 Protein isolation from cultured cells

Cells were washed twice with precooled 1x PBS. Depending on the cell confluence, freshly prepared 1x RIPA lysis buffer was added (70-150  $\mu$ l per well), cells were mechanically detached with a cell scraper and transferred into a reaction tube. After incubation on ice for 15 min, the suspension was centrifuged at 13000 x g, 4 °C for 20 min to get rid of the cellular debris. The protein-containing supernatant was transferred into a new reaction tube and samples were stored at -80 °C.

### 4.3.1.2 Protein isolation from liver tissues

Tissue specimens of 20 mg were pestled with a mortar in liquid nitrogen and the frozen tissue was transferred into a pre-cooled reaction tube. The reaction tube was placed on ice and 500-800  $\mu$ l freshly prepared 1x RIPA lysis buffer was added. Samples were incubated on ice for 15 min (vortexing in between) and centrifuged at 13000 x g, 4 °C for 20 min. The supernatant was transferred into a new reaction tube and samples were stored at -80 °C.

### 4.3.2 Bradford Assay

Bovine Serum Albumin (BSA)-Standard # 23209, Thermo Fisher, Schwerte, Germany

Bradford Dye Reagent # 5000205, Bio-Rad, Munich, Germany

To determine the total protein concentration, the colorimetric Bradford assay was performed. Based on the properties of the dye Coomassie Brilliant Blue G-250, the color and absorbance maximum of Coomassie Blue shifts from red (470 nm) to blue (595 nm) upon binding to proteins.

First, samples were diluted with MilliQ H<sub>2</sub>O (cell lysates 1:5, tissue lysates 1:20) and 5  $\mu$ l of each sample were transferred into a 96-well plate. After adding 250  $\mu$ l of the Bradford Reagent, samples were incubated for 5 min in the dark at RT and absorbance was quantified by spectrometric measurement at 595 nm. For the standard curve, 5  $\mu$ l of a BSA protein standard (0, 0.25, 0.5, 0.75, 1, 1.25, 1.5  $\mu$ g/ $\mu$ l) were used and allowed later the protein quantification via linear regression. All measurements were done in duplicates.

### 4.3.3 SDS-Page

30% Acrylamide	# A124.1, Roth, Karlsruhe, Germany
Ammonium persulfate (APS)	# 9592.5, Roth, Karlsruhe, Germany
$\beta$ -Mercaptoethanol	# 444203, Merck, Darmstadt, Germany
Bromphenol Blue	# B0126, Sigma-Aldrich, Munich, Germany
Glycerol	# 6962.1, Roth, Karlsruhe, Germany
Glycine	# A1067, AppliChem, Darmstadt, Germany
2-Propanol	# I9516, Sigma-Aldrich, Munich, Germany
ProSieve Quad Color Protein Markers	# 830537, Biozym, Oldendorf, Germany
SDS	# CN30.3, Roth, Karlsruhe, Germany
Tetramethylethylenediamine (TEMED)	# 2367.1, Roth, Karlsruhe, Germany
Tris	# A1086, AppliChem, Darmstadt, Germany

5x Sample buffer: 50 % (v/v) Glycerol, 10 % (w/v) SDS, 50 mM Tris, 25 % (v/v)  $\beta$ -Mercaptoethanol, 0.25 mg/ml Bromphenol Blue

10x Running buffer: 1 % (w/v) SDS, 25 mM Tris, 190 mM Glycine

SDS-PAGE was used to separate proteins by size. Noncovalently binding of the detergent SDS to proteins leads to protein denaturation and an overall negative charge by masking the intrinsic charge of the protein. Because of the proportional binding of SDS to the protein mass (one SDS molecule per two amino acids), complexes with a similar charge-to-mass ratio are formed. This results in a protein migration within a polyacrylamide gel depending primarily on its size and enabling molecular weight estimation. The polyacrylamide gel can be divided into a stacking gel and a separating gel, in which the acrylamide concentration in the separating gel depends on the size of the target protein. In this case, 12 % acrylamide gels were prepared (Table 4).

**Table 4. Components for the preparation of two 12 % polyacrylamide gels.**

	Separating Gel (12 %)	Stacking Gel
H <sub>2</sub> O [ml]	3.3	2.7
30 % acrylamide [ml]	4.0	0.67
1.5 M Tris [ml]	2.5	-
1 M Tris [ml]	-	0.5
10 % SDS [ul]	100	40
10 % APS [ul]	100	40
TEMED [ul]	4	4

The separating gel solution was poured between the glass plates, which were fixed in casting frames (Bio-Rad), and 2-propanol was immediately added on top. After polymerization, 2-propanol was discarded, the stacking gel was poured until overflow and a comb was inserted for slot formation. 20 - 50  $\mu$ g total protein of each lysate was mixed with 5x sample buffer in a 1:5 ratio and boiled for 5 min at 95 °C. The polymerized gel was then transferred into an electrophoresis chamber (Bio-Rad), filled with 1x running buffer and the comb was removed. After loading the protein marker and the samples

into the wells, an electric tension of 90 V was applied and increased to 120 V when the dye front reached the separating gel.

#### 4.3.4 Western Blot

BSA	# T844.4, Roth, Karlsruhe, Germany
Enhanced Chemiluminescence Substrate	# NEL103001EA, PerkinElmer, Rodgau, Germany
Glycine	# A1067, AppliChem, Darmstadt, Germany
Methanol	# 32213, Sigma-Aldrich, Munich, Germany
PBS	# 14190-094, Thermo Fisher, Schwerte, Germany
Powdered milk	# T145.2, Roth, Karlsruhe, Germany
Sodium azide	# 08591, Sigma-Aldrich, Munich, Germany
Tris	# A1086, AppliChem, Darmstadt, Germany
Tween 20	# P2287, Sigma-Aldrich, Munich, Germany

10x Transfer buffer: 25 mM Tris, 190 mM Glycine

1x Transfer buffer: 100 ml 10x transfer buffer, 700 ml MilliQ H<sub>2</sub>O, 200 ml methanol

For the immunodetection of specific proteins, SDS polyacrylamide gels were blotted on a Immobilon-P PVDF membrane (Merck) using a Mini Trans-Blot Module wet transfer device (Bio-Rad). According to the manufacturer's instructions, a blot sandwich consisting of a separating gel, a methanol activated PVDF membrane, six sheets of Whatman paper, and two sponges was inserted into the wet transfer device filled up with 1x transfer buffer. Blotting was performed for 2 h at 4 °C with a constant tension of 90 V using a PowerPac HC power supply (Bio-Rad). Afterwards, the membrane was blocked with 5 % milk or 5 % BSA (both w/v) in PBS-T (0.1 % Tween 20 in PBS) on an orbital shaker for 1 h at RT to prevent non-specific binding. The membrane was then rinsed three times for 5

min in PBS and was incubated with the appropriate primary antibody overnight at 4 °C on a rotating shaker. The primary antibody was diluted in milk or BSA containing PBS-T, supplemented with 1 % sodium azide as indicated (Table 5). The day after, unbound antibody was removed by washing the membrane 3x 5 min in PBS, followed by the incubation with a secondary antibody for 1 h on a rotating shaker at RT. Again, the membrane was washed three times for 5 min with PBS and the horseradish peroxidase-coupled secondary antibody was visualized by enhanced chemiluminescence reaction. Therefore, the ECL reaction agents were mixed in a 1:1 ratio and poured onto the membrane. The resulting chemiluminescence was detected with the Fusion SL system (Vilber Lourmat, Eberhardzell, Germany) and analyzed with the Fusion Imaging Software.

Table 5. Antibodies used for Western blot analyses.

Primary Antibodies	Species	Dilution	Source	Identifier
ACTIN	Rabbit	1:500 in PBS-T	Santa Cruz	# sc-1616
$\beta$ -CATENIN	Rabbit	1:1000 in 5% BSA	Cell Signaling	# 9587
BCL-2	Rabbit	1:1000 in 5% BSA	Cell Signaling	# 2876
BCL-3	Rabbit	1:100 in 2.5% BSA	Santa Cruz	# sc-185
BCL-X <sub>L</sub>	Rabbit	1:1000 in 5% BSA	Cell Signaling	# 2764
CASPASE 3	Rabbit	1:1000 in 5% milk	Cell Signaling	# 9664
CL. CASPASE 3	Rabbit	1:1000 in 5% milk	Cell Signaling	# 9662
C-IAP1/2	Goat	1:200 in 5% milk	Santa Cruz	# sc-12410
KRT7	Rabbit	1:1000 in PBS-T	abcam	# ab181598
C-MYC	Rabbit	1:100 in 5% BSA	Cell Signaling	# sc-788
C-REL	Rabbit	1:750 in 5% BSA	Cell Signaling	# 4774
CYCLIN D1	Mouse	1:1000 in 5% BSA	Cell Signaling	# 2926
CYLD	Mouse	1:100 in 5% milk	Santa Cruz	# sc-74434
ERK1/2	Rabbit	1:1000 in 5% milk	Cell Signaling	# 9102
P-ERK1/2 (Thr202/Tyr204)	Mouse	1:1000 in 5% milk	Cell Signaling	# 9106
HES1	Mouse	1:100 in 5% milk	Santa Cruz	# sc-25392
I $\kappa$ B $\alpha$	Rabbit	1:1000 in 2.5% milk	Santa Cruz	# sc-371
P-I $\kappa$ B $\alpha$	Mouse	1:500 in 5% milk	Santa Cruz	# sc-8404
IKK $\alpha$	Mouse	1:200 in 5% milk	Santa Cruz	# sc-52932
IKK $\beta$	Rabbit	1:2500 in 5% milk	abcam	# ab32135
P-IKK $\alpha/\beta$ (Ser176/Ser177)	Rabbit	1:500 in 2.5% BSA	Cell Signaling	# 2078
JAGGED1	Mouse	1:100 in 5% milk	Santa Cruz	# sc-390177
JNK (JNK1, JNK2, and JNK3)	Rabbit	1:1000 in 5% BSA	Cell Signaling	# 9252
P-JNK (Thr183/Tyr185)	Rabbit	1:1000 in 5% BSA	Cell Signaling	# 9251
MCL-1	Rabbit	1:2000 in 5% milk	Rockland	#600-401-394
NEMO	Rabbit	1:50 in 2.5% BSA	Santa Cruz	# sc-8256
NIK	Mouse	1:200 in PBS-T	Santa Cruz	# sc-8417
NOTCH1	Goat	1:250 in 5% milk	Santa Cruz	# sc-6014
CL. NOTCH1	Rabbit	1:600 in 5% milk	Cell Signaling	# 4147
NOTCH2	Goat	1:250 in 5% milk	Santa Cruz	# sc-7423
NOTCH3	Rabbit	1:100 in 5% milk	Santa Cruz	# sc-5593
p38	Rabbit	1:1000 in 5% BSA	Cell Signaling	# 9212
P-p38 (Thr180/Tyr182)	Rabbit	1:1000 in 5% BSA	Cell Signaling	# 9211
p50/p105	Rabbit	1:200 in 5% milk	Santa Cruz	# sc-114
p52/p100	Rabbit	1:1000 in 5% BSA	Cell Signaling	# 4882
RELA	Rabbit	1:200 in 2.5% BSA	Santa Cruz	# sc-109
P-RELA (Ser536)	Rabbit	1:1000 in 5% milk	Cell Signaling	# 3033
RELB	Rabbit	1:500 in 2.5% BSA	Cell Signaling	# 4954
RIP1	Rabbit	1:500 in 5% milk	Cell Signaling	# 4926
TAK1	Rabbit	1:1000 in 5% BSA	Cell Signaling	# 4505

P-TAK1	Rabbit	1:500 in 5% BSA	Cell Signaling	# 4536
TRAF2	Rabbit	1:500 in 5% milk	Cell Signaling	# 4712
TRAF3	Rabbit	1:1000 in 2.5% BSA	Cell Signaling	# 4729
TUBULIN	Mouse	1:5000 in PBS-T	Sigma-Aldrich	#T8203
<b>Secondary Antibodies</b>	<b>Species</b>	<b>Dilution</b>	<b>Source</b>	<b>Identifier</b>
Anti-goat	donkey	1:10000 in 0.5% milk	Santa Cruz	# sc-2056
Anti-mouse	Goat	1:10000 in 0.5% milk	Santa Cruz	# sc-2031
Anti-mouse IgG1 (TUBULIN)	Goat	1:10000 in 0.5% milk	Southern Biotech	# 1070-05
Anti-rabbit	Goat	1:10000 in 0.5% milk	Santa Cruz	# sc-2030

#### 4.4 Gene expression analysis

In order to investigate the gene expression in murine liver tissues, real-time quantitative polymerase chain reaction (qRT-PCR) was performed to quantify the mRNA abundance of a specific target gene. Therefore, RNA was isolated and first transcribed into complementary DNA (cDNA) by a RNA-dependent DNA polymerase. The cDNA was then used as a template for the qRT-PCR reaction, which enables the analysis of the relative gene expression by normalizing target gene expression to the housekeeping genes GAPDH and Rps6.

##### 4.4.1 RNA Isolation from murine tissue

TRI reagent	# T9424, Sigma-Aldrich, Munich, Germany
Chloroform	# C2432, Sigma-Aldrich, Munich, Germany
2-Propanol	# I9516, Sigma-Aldrich, Munich, Germany
Ethanol absolute	# 32205, Sigma-Aldrich, Munich, Germany

For RNA isolation, tissue specimens of 20 mg were pestled in liquid nitrogen. The frozen tissue was transferred into a reaction tube, placed at RT and 1 ml TRI reagent was immediately added. The solution was incubated for 5 min at RT, vortexed in between, and 200  $\mu$ l chloroform were added. The mixture was vortexed for 10 sec until it became milky and was incubated for 10 min at RT. The following centrifugation step for 13 min at 16000 x g, 4 °C resulted in a phase separation, whereby the upper aqueous phase (about 400  $\mu$ l) was carefully transferred into a new reaction tube. RNA was precipitated by adding 500  $\mu$ l 2-propanol. After inverting the tube for several times, the mixture was incubated for 10 min at RT and centrifuged for 1 h at 14000 x g, 4 °C. Pellet was washed twice with 500  $\mu$ l 75 % ethanol, centrifuged for 3 min at 7500 x g, 4 °C, and air-dried for several hours until it became transparent. Finally, the RNA was dissolved in 40-60  $\mu$ l of RNase-free water overnight at 4 °C and the concentration was determined by using an Epoch Microplate Spectrophotometer (BioTek, Winooski, VT, USA). The quality was confirmed by measuring an OD260/OD280 > 2.0. For long time storage, RNA was kept at -80 °C until further usage.

#### 4.4.2 Reverse Transcription

Omniscript Reverse Transcription Kit # 205111, Qiagen, Hilden, Germany  
 Oligo dT 16 Primer # N8080128, Thermo Fisher, Schwerte, Germany

For the transcription of RNA into cDNA, the Omniscript Reverse Transcription Kit was used according to the manufacturer's instructions. For each reaction, 1 µg of total RNA was filled up with RNase-free water to a total volume of 14.5 µl. The secondary structure of the RNA was denatured by incubation for 5 min at 65 °C. The samples were subsequently placed on ice and 5.5 µl of the reverse transcription master mix (Table 6), containing the enzyme, oligo dT primer and deoxynucleotide triphosphates (dNTPs), were added.

**Table 6. Components for the Reverse Transcriptase Master Mix.**

Reverse Transcriptase Master Mix	1x [µl]
10x Reverse Transcriptase Buffer	2
dNTPs (5 mM)	2
Reverse Transcriptase	1
Oligo dT Primer (10 µM)	0.5
5.5 µl per tube + 14.5 µl diluted RNA (1 µg RNA)	

The reverse transcription was carried out at 37 °C for 1 h. Afterwards, the samples were diluted 1:2 with RNase-free water and stored at 4 °C for up to one week, or at -20 °C for long-time storage.

#### 4.4.3 Real-Time quantitative PCR (qRT-PCR)

QuantiTect SYBR-Green PCR Kit # 204143, Qiagen, Hilden, Germany

In order to quantify mRNA expression, qRT-PCR was performed by using the QuantiTect SYBR-Green PCR Kit according to the manufacturer's instructions. Like a conventional PCR, qRT-PCR amplifies DNA segments, in which specific primers define the DNA target region by binding to the 3' ends and thereby serving as starting point for the DNA polymerase. To detect and measure the products generated during each PCR cycle, the DNA-intercalating dye SYBR Green is used, which emits a fluorescence signal after DNA-binding. The number of cycles is then plotted against the fluorescence. The first cycle that shows a detectable increase in fluorescence greater than the background signal/threshold due to the formation of PCR products is called crossing point (Cp). This Cp value is used to determine the template amount in each sample since it depends on the initial amount of target DNA and thereby on the level of gene expression. For the relative quantification, the expression of each target gene was normalized to the expression of the housekeeping genes GAPDH and Rps6, which showed stable expression under various conditions.

For each reaction, 9 µl master mix consisting of 5 µl SYBR Green, 3 µl RNase-free water and 1 µl primer (listed in Table 7), were transferred into a white 96-well TW-MT plate (Biozym) and

supplemented with 1.5  $\mu$ l cDNA. All measurements were done in technical duplicates and a negative control for each primer pair was generated by replacing the cDNA with H<sub>2</sub>O. After sealing the plate with Adhesive Clear qPCR Seals (Biozym), the plate was centrifuged at 100 x g for 30 sec and the qRT-PCR run was performed with the LightCycler 480 Instrument II (Roche, Basle, Switzerland). The program started with a denaturation step for 15 min at 95 °C, followed by 35 PCR cycles, each consisting of 15 sec at 95 °C (denaturation step), 30 sec at 55 °C (annealing step), and 30 sec at 72 °C (elongation step). After each cycle, fluorescence was measured and data analysis was done by using the Light Cycler 480 SW 1.5 software.

**Table 7. qRT-PCR primers.**

qPCR Primer	Identifier
<i>Baff</i>	QT00117215
<i>Bsep</i>	QT00161896
<i>Ccl2</i>	QT00167832
<i>Cd40lg</i>	QT00101437
<i>Krt7</i>	QT00173649
<i>Col1a1</i>	QT00162204
<i>Gapdh</i>	QT01658692
<i>Light</i>	QT00164080
<i>Lta</i>	QT01046206
<i>Lt<math>\beta</math></i>	QT00107443
<i>Mdr2</i>	QT00164010
<i>Mrp2</i>	QT00120379
<i>Mrp3</i>	QT00251006
<i>Mrp4</i>	QT01199226
<i>Ntcp</i>	QT01045177
<i>Rankl</i>	QT02589496
<i>Tgf<math>\beta</math>1</i>	QT00145250
<i>Tgf<math>\beta</math>2</i>	QT00106806
<i>Tnf-<math>\alpha</math></i>	QT00104006
<i>Tweak</i>	QT00170681

Primers were synthesized by Qiagen (Hilden, Germany).

#### 4.5 Human liver samples

Tissue samples of normal liver (n = 10), early stage PSC (n = 4), late stage PSC (n = 9), early stage PBC (n = 5), late stage PBC (n = 7), HCV-induced hepatitis (n = 7), HBV-induced hepatitis (n = 7), AIH (n = 5), and NASH (n = 2) were provided by the tissue bank of the National Center for Tumor Diseases (NCT, Heidelberg, Germany) in accordance with the regulations of the tissue bank and the approval of the ethics committee of the University of Heidelberg. Late stage PBC and PSC specimens were obtained from explanted organs showing progressed cirrhosis representing end stage liver disease, while all the other samples included only liver biopsies.

Tissue samples of NASH (n = 4) and ALD (n = 21) were kindly provided by Prof. Dr. Sebastian Mueller (Salem Medical Center and Center for Alcohol Research, University of Heidelberg). To obtain tissue, guided liver biopsy were performed according to recommendations of the Barcelona Conference<sup>189</sup>. By using the Menghini technique under ultrasound, liver specimens were obtained percutaneously, fixed in formalin, and finally embedded in paraffin. Histological staging was assessed by the liver pathologists Prof. Dr. Thomas Longerich and PD Dr. Benjamin Goeppert from the Department of Pathology at Heidelberg University Hospital using the appropriate entity-specific staging systems (e.g. Ludwig and Scheuer, Desmet, and NAS)<sup>190–193</sup>.

For the analysis of different HCC specimens, a tissue microarray (TMA) containing HCC samples of 92 patients was utilized, with corresponding tumorous liver and normal liver tissue samples as previously described<sup>194</sup>. All patients were treated at the University Hospital in Heidelberg, Germany, between 2000 and 2013. Thereby, tissue was obtained from 65 HCC patients undergoing liver resection and 27 patients undergoing liver transplantation. The histological grade of tumor differentiation was assigned in line with the Edmondson Grading System<sup>195</sup>. The HCC TMA was kindly provided by PD Dr. Kai Breuhahn from the Department of Pathology at Heidelberg University Hospital.

In accordance with the Declaration of Helsinki, all experiments were done after the governmental and institutional guidelines and were authorized by the ethic committee of the University Hospital of Heidelberg (206/2005). Written informed consent was obtained from all patients and specimens were provided in a pseudonymized form.

## 4.6 Histopathological Analyses

### 4.6.1 Hematoxylin and Eosin Staining

Eosin	# HT110380, Sigma-Aldrich, Munich, Germany
37 % Formaldehyde Solution	# F1635, Sigma-Aldrich, Munich, Germany
Hematoxylin	# GHS380, Sigma-Aldrich, Munich, Germany
PBS	# 14190-094, Thermo Fisher, Schwerte, Germany
Roti Histokitt II mounting medium	# T160.1, Roth, Karlsruhe, Germany
Xylene	# 247642, Sigma-Aldrich, Munich, Germany

Hematoxylin and eosin (H&E) staining is a commonly used staining technique in histopathology that allows the discrimination of different cellular components. Hematoxylin in combination with aluminum salts acts as a basic dye and reacts with negatively charged, basophilic cell structures, such as nucleic acids. Stained nuclei appear in a deep blue-purple color. Eosin is an acidic dye and binds to positively charged, acidophilic components in the tissue, such as amino groups in proteins in the cytoplasm. This stain results in a pink color.

If cryosections were stained, slides were fixed in 4 % paraformaldehyde (PFA) for 15 min, washed three times for 10 min in PBS and rinsed in running ddH<sub>2</sub>O for 1 min. If paraffin-embedded tissue sections were stained, slides were first deparaffinized using xylene (2x 10 min) and a series of graded alcohols (99 %, 96 %, 70 %, 5 min each) and were washed in ddH<sub>2</sub>O for 5 min. The following staining protocol was applicable for both, cryosections and paraffin-embedded tissue sections. Slides were

incubated in hematoxylin for 5 min at RT and subsequently blued for 5 min in tap water. After rinsing in ddH<sub>2</sub>O for 1 min, slides were stained with eosin for 1 min at RT and immediately dehydrated by rinsing the slides in a series of graded alcohols. An additional incubation step in 99 % ethanol for 1 min followed and sections were finally incubated in xylene for 5 min and mounted with Roti Histokitt II mounting medium. Histopathologic evaluation was then performed by two experienced pathologists.

#### 4.6.2 Sirius Red

Direct Red 80 (Sirius Red)	# 365548, Sigma-Aldrich, Munich, Germany
Picric acid solution	# P6744, Sigma-Aldrich, Munich, Germany
Acetic acid	# 3738.1, Roth, Karlsruhe, Germany
Weigert's hematoxylin	# 1.15973.0002, VWR, Darmstadt, Germany
Roti Histokitt II mounting medium	# T160.1, Roth, Karlsruhe, Germany

Picosirius Red Solution: 0.1 g Sirius red, 100 ml saturated aqueous solution of picric acid

For the histological visualization of collagen fibers in paraffin-embedded tissue sections, a Sirius Red staining was performed. Sirius Red is a hydrophilic dye with sulphonic acid groups, which reacts with basic groups in the collagen molecule<sup>196</sup>. Thereby, the stained collagen appears red and cytoplasm yellow in light microscopy. Liver tissue slides were deparaffinized by incubating the slides twice in xylene for 10 min, followed by a serial incubation in graded alcohols (99 %, 96 %, 70 %) for 5 min each. After staining of the nuclei with Weigert's hematoxylin for 20 min, slides were washed twice in tap water (10 min) and distilled water (5 min), and were incubated in picosirius red solution for 1 h. Following two quick changes of 0.5 % acetic acid, slides were dehydrated in three changes of 99 % ethanol. Finally, slides were incubated for 5 min in xylene and covered with anhydrous Roti Histokitt II mounting medium.

To quantify the fibrotic area in liver tissue samples, slides were digitized with an Aperio whole slide scanner (Leica Biosystems, Wetzlar, Germany). Eight representative rectangular regions of interests (ROIs) were manually selected from each image so that at least 30 % of the total tissue section was captured. Matlab R2016b (Mathworks, Natick, USA) was used for image analysis. Images were converted from RGB to the CIE 1976 L\*a\*b\* color space so that the a\* intensity contained only Sirius red positive image areas. These areas were segmented by a locally adaptive threshold using a sensitivity parameter of 0.4. The fraction of positive pixels was subsequently quantified and averaged over all eight ROIs for each whole slide image.

#### 4.6.3 Immunohistochemistry

Aquatex mounting medium	# 1.08562.0050, Merck, Darmstadt, Germany
Citric acid	# 251275, Sigma-Aldrich, Munich, Germany
Ethanol absolute	# 32205, Sigma-Aldrich, Munich, Germany
37 % Formaldehyde Solution	# F1635, Sigma-Aldrich, Munich, Germany
NaCl	# 9265.1, Roth, Karlsruhe, Germany

NovoLink Polymer Detection System	# RE7290-CE, Leica Biosystems, Wetzlar, Germany
PBS	#14190-094, Thermo Fisher, Schwerte, Germany
Tris-HCl	# 9090.1, Roth, Karlsruhe, Germany
Trisodium citrate	# S1804, Sigma-Aldrich, Munich, Germany
Triton X 100 (TTX)	# 3051.2, Roth, Karlsruhe, Germany
Xylene	# 247642, Sigma-Aldrich, Munich, Germany

Citrate buffer (1l, pH 6.0): 18 ml solution A (24.4 g Trisodium citrate in 1l MilliQ H<sub>2</sub>O), 82 ml solution B (10.5 g Citric acid in 500 ml MilliQ H<sub>2</sub>O)

10x TBS (pH 7.5): 150 mM NaCl, 7.7 mM Tris-HCl

TBS-TTX: 1 % TBS, 0.1 % TTX

Immunohistochemical staining allows the visualization of differentially expressed proteins and analysis of their distribution and localization within single cells and whole tissue specimens. According to the manufacturer's instructions, staining was performed by using the NovoLink Polymer Detection System, which contains a peroxidase-blocking reagent, a protein-blocking reagent, a polymer solution, a diaminobenzidine (DAB) solution and hematoxylin.

Paraffin-embedded human normal liver, PBC, PSC, NASH, ALD, HCC (TMA) tissue slides were first dewaxed and rehydrated by 2x 10 min xylene incubation and a series of graded alcohols (99 %, 96 %, 70 %, 5 min each), followed by a rinsing in ddH<sub>2</sub>O for 5 min. For the staining of murine cryosections, tissue slides were fixed in 4 % PFA for 15 min at RT under light exclusion, washed five times in PBS for 10 min each and rinsed in ddH<sub>2</sub>O for 5 min. The following staining steps were applicable for both, cryosections and paraffin-embedded tissue sections. All washing steps were performed on a rotating shaker.

To perform the heat-induced antigen retrieval, tissue slides were transferred into cuvettes filled with citrate buffer (pH 6.0) and boiled five times for 3 min. After cooling down to RT, slides were washed for 5 min in ddH<sub>2</sub>O and incubated for 15 min with the peroxidase-blocking reagent to inhibit endogenous peroxidase levels and reducing background staining. Subsequently, the sections were rinsed for 1 min in running ddH<sub>2</sub>O followed by two washing steps in TBS-TTX for 5 min each, and incubation for 10 min in the protein-blocking reagent to reduce unspecific binding sites. Slides were washed again twice in TBS-TTX for 5 min before the diluted primary antibody (Table 8) was poured onto the tissue specimens. Depending on the primary antibody, tissue slides were incubated in a wet chamber at RT or at 4 °C overnight. Thereafter, specimens were washed three times for 5 min in TBS-TTX and were further incubated with the polymer solution for 30 min, which contains HRP-coupled anti-rabbit secondary antibody. During three washing steps for 5 min in TBS-TTX, the DAB working solution for detection was prepared by diluting the DAB chromogen with the DAB-substrate buffer in a 1:20 ratio. The DAB working solution was poured onto the specimens and was incubated under light exclusion for 3-5 min, thereby HRP converts the hydrogen peroxide which lead to an oxidation-induced color change of the DAB-chromogen. This reaction was terminated by washing the slides three times for 5 min with ddH<sub>2</sub>O. At last, nuclei were counterstained for 3-5 min with hematoxylin followed by bluing in tap water for 5 min and rinsing in ddH<sub>2</sub>O for 5 min. Finally tissues slides were coated with aqueous medium and covered with cover slips. Images were taken using a Keyence BZ-

9000 microscope and the accompanying software BZ II viewer and BZ II analyzer (Keyence, Osaka, Japan).

To quantify A6, KI67, CD3, CD68, and CD11B, scanned slides were analyzed using QuPath, an open-source software for quantitative pathology<sup>197</sup>. For CD68 and CD11B, representative rectangular ROIs of the whole liver section were taken and quantified using the positive cell detection feature with empirical parameters. Since A6, KI67, and CD3 positive cells were mainly observed in the periportal surrounding, ten representative periportal regions for each animal were manually selected and the fraction of positive pixels was quantified and averaged for each whole slide image.

For the semi-quantitative immunohistochemical assessment of RELB expression, an immunohistochemical score (IHC score, ranging from 0 to 12) was obtained by multiplying staining quantity by intensity<sup>194,198</sup>. Staining quantity was categorized as 0 = no expression, 1 = positivity in less than 1 % of cells, 2 = positivity in 1 - 9 % of cells, 3 = positivity in 10 - 50 % of cells, and 4 = positivity in more than 50 %. Staining intensity was categorized as 0 = negative, 1 = low, 2 = medium, and 3 = high. To analyze the relationship between RELB expression, clinicopathological features and survival of HCC patients, patients were classified into the negative/low-expression group (<sup>nuc</sup>RELB<sup>-</sup>, n = 41) and patients with an equal or higher expression level were classified into the positive/high-expression group (<sup>nuc</sup>RELB<sup>+</sup>, n = 45).

**Table 8. Antibodies used for immunohistochemical staining.**

Primary Antibodies	Dilution	Incubation	Source	Identifier
Reactivity: human				
RELB	1:150 in PBT	1 h, RT	Sigma-Aldrich	# HPA040506
CYLD	1:50 in PBT	30 min, RT	abcam	# ab137524
RELA	1:50 in PBT	20 h, 4 °C	Santa Cruz	# sc-109
IκBα	1:50 in PBT	1 h, RT	Santa Cruz	# sc-371
Reactivity: mouse				
KRT7	1:8000 in PBT	30 min, RT	abcam	# ab181598
RELA	1:500 in PBT	30 min, RT	Thermo Fisher	# RB-1638
RELB	1:400 in PBT	30 min, RT	Santa Cruz	# sc-226
KI67	1:500 in PBT	30 min, RT	abcam	# ab16667
CD3	1:100 in PBT	30 min, RT	abcam	# ab16669
CD11B	1:1600 in PBT	30 min, RT	LSBio	# LS-C141892
CD68	1:3000 in PBT	20 h, 4 °C	abcam	# ab125212
VCAM1	1:600 in PBT	1 h, RT	GeneTex	# GTX63001

#### 4.6.4 *In situ* hybridization

Anti-Digoxigenin-AP	# 11093274910, Basle, Roche
BSA	# T844.4, Roth, Karlsruhe, Germany
DIG RNA Labeling KIT (SP6/T7)	# 11175025910, Basle, Roche
<i>E. coli</i> tRNA	# TRNAMRE-RO, Basle, Roche
Ficoll	# CN90.3, Roth, Karlsruhe, Germany
Levamisole	# 196142, Sigma-Aldrich, Munich, Germany
MgCl <sub>2</sub>	# M8266, Sigma-Aldrich, Munich, Germany
NaCl	# 9265.1, Roth, Karlsruhe, Germany
NBT/BCIP	# 11697471001, Basle, Roche
Polyvinylpyrrolidone	# PVP10, Sigma-Aldrich, Munich, Germany
Tris-HCl	# 9090.1, Roth, Karlsruhe, Germany
Trisodium citrate	# S1804, Sigma-Aldrich, Munich, Germany

20x saline sodium citrate (SSC, 1l): 3 M NaCl, 300 mM Trisodium citrate, pH 7.0

100x Denhardt's solution (0.5l): 10 g Ficoll, 10 g polyvinylpyrrolidone, 10 g BSA

Buffer 1: 100 mM Tris-HCl pH 7.5, 150 mM NaCl

Buffer 2: 100 mM Tris-HCl pH 9.5, 150 mM NaCl, 50 mM MgCl<sub>2</sub>, containing 1mM Levamisole, Nitroblue tetrazolium chloride/5-bromo-4-chloro-3-indolyl phosphate (NBT/BCIP)

*In situ* hybridization for Lymphotoxin  $\beta$  (LT $\beta$ ) was performed as published by Haybaeck et al. 2009<sup>167</sup>. Sense and antisense probes derived from a pGEM plasmid containing the Sau3AI fragment of mLT $\beta$  (GenBank: U06950). For Digoxigenin (DIG)-labeling of the cRNA probe, a DIG labeling Kit was used according to the instructions of the manufacturer. Paraffin-embedded sections were deparaffinized, post fixed in 4% PFA, and acetylated in 0.1 M triethanolamine and 0.25% acetic anhydride. Prehybridization was performed in 5x SSC, 50% formamide, 5x Denhardt's solution, and 250  $\mu$ g/ml *E. coli* tRNA for 3 h at RT. Probes were denatured at 85 °C for 5 min and then placed on ice. Hybridization was performed with the prehybridization solution containing the 50 ng/50  $\mu$ l DIG-labelled RNA probe. Prehybridization solution was removed and the hybridization solution was added. After covering the sections with a cover slip, sections were sealed in a box, heated to 85 °C for 30 min and incubated overnight at 58 °C. Afterwards, samples were washed for 1 h at 65 °C in pre-warmed 0.2 and 0.1x SSC and incubated with anti-DIG alkaline phosphatase (1:2000) at RT for 2-3 h. After washing in buffer 1 for 20 min twice, detection was performed in buffer 2. Reaction was stopped in 10 mM Tris pH 8.0 and 1 mM EDTA. Finally, samples were mounted in DAKO mounting medium and analyzed using a Keyence BZ-9000 microscope and the accompanying software.

#### 4.7 Statistical Analysis

Statistical analyses were performed using GraphPad Prism 7 (GraphPad Software Inc., La Jolla, USA) and IBM SPSS Statistics version 22 (IBM Corp., Armonk, USA). To evaluate statistical significance, human data (IHC score) was subjected to non-parametric analysis of variance (ANOVA) Kruskal-Wallis with the post hoc Dunn's multiple comparison test to compare three or more groups or subjected to two-sided non-parametric Mann-Whitney *U* test for comparison of two groups. The correlation between IHC score and patient's gender, age, Edmonson grading, tumor size, vascular infiltration, viral hepatitis, bilirubin, serum AFP and Child-Pugh, alcohol consumption and treatment was analyzed using the Spearman's rank correlation coefficient. Parameters not available for the analysis were depicted as 'NA'. Overall survival (OS) was calculated from the date of surgery (event = death by any cause). Survival time of patients who did not experience an event was 'censored'. OS was evaluated by the Kaplan-Meier method and differences assessed by log-rank (Mantel-Cox) test.

Results obtained from mice experiments were analyzed by one-way ANOVA with the post hoc Tukey multiple comparison test or by two-way ANOVA followed by Bonferroni's multiple comparison test. Statistical significance was defined as follows: \* $p < 0.05$ , \*\* $p < 0.01$ , \*\*\* $p < 0.001$ , and \*\*\*\* $p < 0.0001$ .

## 5. Results

### 5.1 The role of RELB for liver homeostasis, chronic injury and hepatocarcinogenesis in mice

#### 5.1.1 A liver-specific knockout mouse model with increased RELB activation

In order to gain more insight into the function of RELB for liver homeostasis as well as for chronic liver injury, an established mouse model with highly upregulated RELB expression was utilized (Fig. 5). Mice lacking liver-specific full-length CYLD (*Cyld*<sup>ALPC</sup>), but expressing naturally occurring CYLD splice variant, exhibited a spontaneous phenotype characterized by ductular reaction and biliary fibrosis (Fig. 5)<sup>179</sup>.

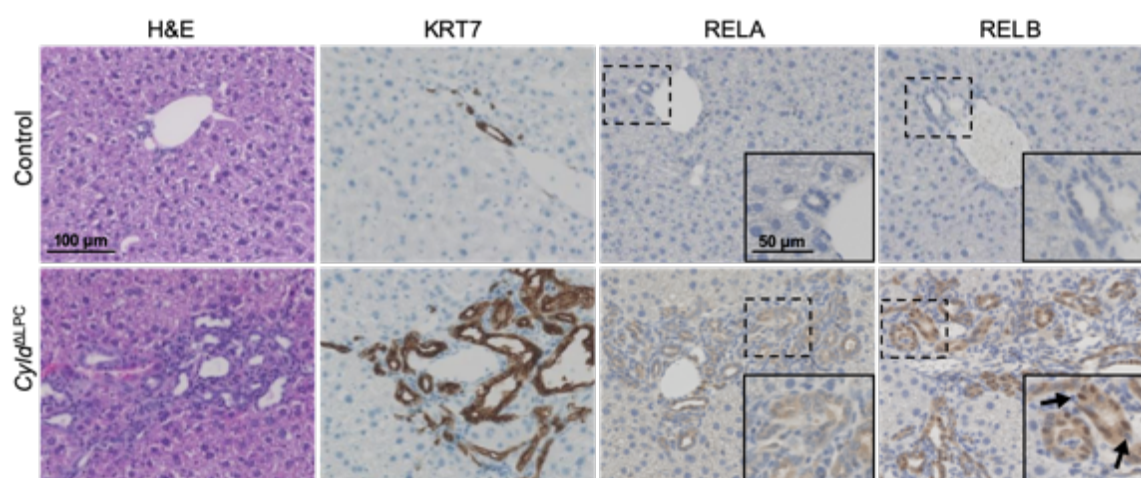


**Figure 5. Increased RELB expression in *Cyld*<sup>ALPC</sup> mice.** Haematoxylin and eosin (H&E) and IHC staining for KRT7 (biliary epithelial cell marker), RELA, and RELB on liver paraffin sections of 9-month-old control and *Cyld*<sup>ALPC</sup> mice, showing RELB overexpression mainly in cholangiocytes of *Cyld*<sup>ALPC</sup> livers. Arrows indicate nuclear RELB expression. Scale bars as indicated. Adapted from Eißner et al. (2019)<sup>1</sup>.

Since NF- $\kappa$ B proteins are known targets of CYLD, the phenotype was associated with increased NF- $\kappa$ B signaling<sup>179</sup>. Surprisingly, not the canonical NF- $\kappa$ B pathway via RELA showed the most profound alteration, instead the expression of the key mediator of the non-canonical pathway RELB was remarkably increased in *Cyld*<sup>ALPC</sup> livers (Fig. 5). IHC staining for RELA revealed only slight upregulation in the cytosol of hepatocytes and biliary epithelial cells, whereas RELB was highly upregulated predominantly in the biliary compartment (KRT7 positive cells) and was also located in the nucleus of cholangiocytes, indicating its activation (Fig. 5). Hepatocytes of *Cyld*<sup>ALPC</sup> mice displayed no increased RELB expression in the IHC staining.

##### 5.1.1.1 Generation of a liver-specific CYLD/RELB double knockout mouse

To determine if RELB overexpression contributes to the biliary phenotype of *Cyld*<sup>ALPC</sup> mice, a double knockout mouse with a liver-specific deficiency in full-length CYLD and RELB (*Cyld/Relb*<sup>ALPC</sup>) was generated.

First, a liver-specific RELB knockout mouse (*Relb*<sup>ALPC</sup>) was established via crossbreeding of mice harboring two loxP-sites flanking the *Relb* gene (*Relb*<sup>FF</sup>) with a strain expressing the *Cre recombinase*

under control of the albumin promoter (*AlbCre*). Because murine expression of Cre recombinase has been shown to induce gastric epithelial atrophy and metaplasia in the absence of floxed alleles, *AlbCre* transgenic mice were chosen as control animals for all experiments<sup>183</sup>. To verify the genotype of *Relb*<sup>ALPC</sup> mice, 2 mm ear punches from 3-week-old mice were taken and DNA was isolated. After performing a PCR with gene specific primers and subsequent agarose gel electrophoresis, the amplified DNA products were analyzed (Fig. 6A).

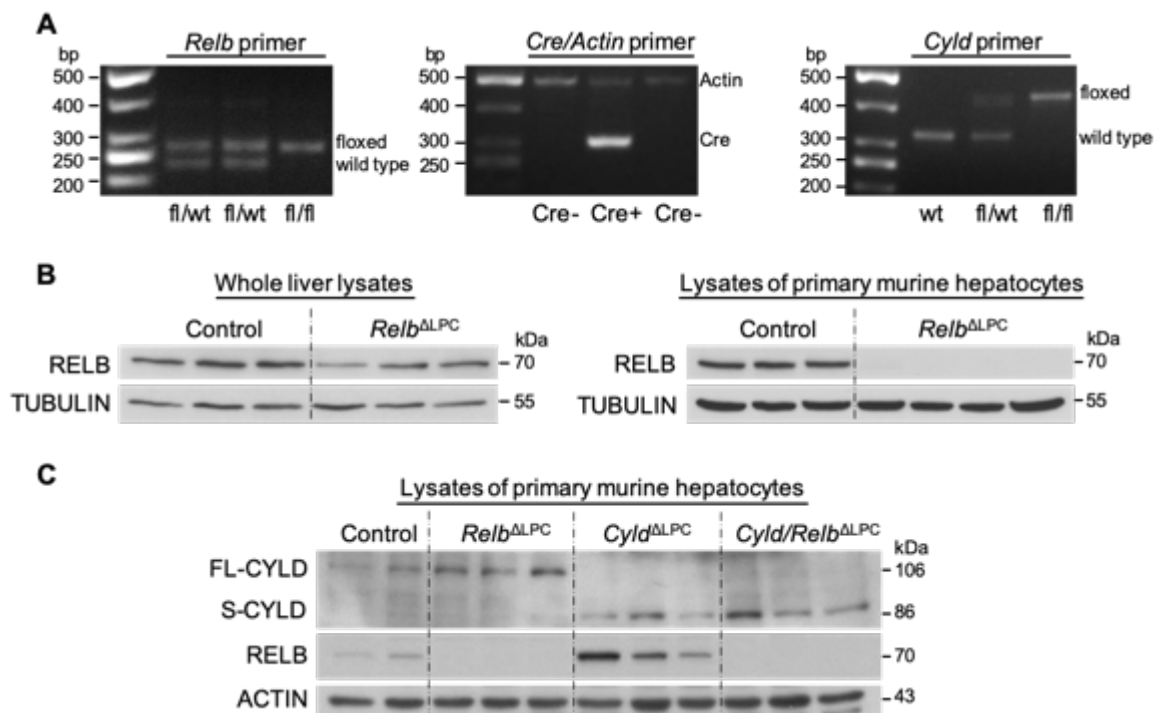


**Figure 6. Generation of liver-specific RELB and CYLD/RELB knockout mice.** (A) Gene expression of wild type (wt) or floxed (fl) *Relb* and *Cyld* was analyzed. DNA was isolated from ear punch biopsies of mice. A positive PCR for fl/fl and *Cre* (*Cre*+) confirmed the *Relb*<sup>ALPC</sup> and *Cyld/Relb*<sup>ALPC</sup> genotype. Actin primers in the *Cre* PCR were used as an internal positive control. (B) Western blot analysis of liver lysates and primary murine hepatocytes for RELB expression in 8-week-old *Relb*<sup>ALPC</sup> and control littermates. TUBULIN was used as loading control. (C) Western blot analysis of CYLD and RELB expression in primary murine hepatocytes of *Relb*<sup>ALPC</sup>, *Cyld*<sup>ALPC</sup>, *Cyld/Relb*<sup>ALPC</sup> mice and control littermates. Actin served as loading control. Adapted from Elßner et al. (2019)<sup>1</sup>.

Integrated loxP-sites/floxed alleles resulted in a larger PCR product compared with the wild type allele and enabled thereby the differentiation between flox and wild type status. For the *Cre* PCR, *Actin* was additionally detected as an internal positive control to avoid failures in the PCR procedure because biopsies from *Cre* negative mice would show no signal. The offspring of *Relb*<sup>FF</sup> and albumin *Cre*<sup>+</sup> mice were further bred until littermates displayed homozygosity regarding their flox status.

Efficiency of the deletion was then evaluated on protein level (Fig. 6B). Surprisingly, Western blot analysis of RELB in whole liver lysates showed no difference in the expression levels between *Relb*<sup>ALPC</sup> mice and control mice. Since whole liver lysates consists of parenchymal liver cells and non-parenchymal cells like sinusoidal endothelial cells, hepatic stellate cells, Kupffer cells, and intrahepatic lymphocytes, which are still expressing RELB, the visible RELB expression could be attributed to these cells. For this reason, primary murine hepatocytes were isolated, cultured for 24 h to allow the separation from the other non-parenchymal cells, and harvested. Lysates of primary murine hepatocytes revealed a complete and organ specific deletion of RELB in *Relb*<sup>ALPC</sup> mice compared with control mice (Fig. 6B).

Further crossbreeding of *Relb*<sup>ALPC</sup> mice with *Cyld*<sup>ALPC</sup> mice generated finally the liver-specific double knockout mouse *Cyld/Relb*<sup>ALPC</sup> (Fig. 6A and C). In accordance with previous findings, *Cyld*<sup>ALPC</sup> mice and *Cyld/Relb*<sup>ALPC</sup> mice did not express full-length CYLD but showed an increased expression of a naturally occurring shorter splice variant of the CYLD protein (Fig. 6C)<sup>178,179</sup>. RELB deletion was confirmed in *Relb*<sup>ALPC</sup> and *Cyld/Relb*<sup>ALPC</sup> mice (Fig. 6C). In contrast to the IHC staining for RELB (Fig. 5), Western Blot analysis also revealed highly upregulated RELB expression in primary murine hepatocytes of *Cyld*<sup>ALPC</sup> mice compared with control mice.

#### 5.1.1.2 Sustained activation of RELB is crucial for ductular reaction and biliary fibrosis in *Cyld*<sup>ALPC</sup> mice

In order to analyze liver morphology and clinically relevant serum parameters in the newly generated knockout mouse model, blood was obtained by cardiac puncture and livers were removed. As shown in Fig. 7A, livers obtained from 3- and 9-month-old *Relb*<sup>ALPC</sup>, *Cyld*<sup>ALPC</sup>, and *Cyld/Relb*<sup>ALPC</sup> mice appeared macroscopically similar to control mice. At the age of 3 months, liver/body weight ratios of *Relb*<sup>ALPC</sup> (0.049,  $p = 0.0002$ ) and *Cyld/Relb*<sup>ALPC</sup> mice (0.049,  $p = 0.0002$ ) were significant reduced compared with control mice (0.058, Fig. 7B). Liver/body weight ratio of *Cyld/Relb*<sup>ALPC</sup> mice was also significant reduced to the ratios of *Cyld*<sup>ALPC</sup> mice (0.056,  $p = 0.0035$ ). At the age of 9 months, liver/body weight ratios of the transgenic mice were not significantly changed compared with control mice (Fig. 7C).

To monitor potential liver damage, blood was examined for biochemical liver function parameters such as aspartate transaminase (AST), alanine transaminase (ALT), and alkaline phosphatase (AP) (Fig. 7B and C). In all 3- and 9-month-old knockout mice, serum AST and AP levels were not different from control mice. In contrast, ALT serum levels were significantly elevated in 3-month-old *Cyld*<sup>ALPC</sup> mice compared with control mice (35.29 vs. 19.50,  $p = 0.0183$ ) and 9-month-old *Cyld*<sup>ALPC</sup> mice (47.75 vs. 17.19,  $p = 0.0094$ ), confirming the already reported liver damage in these mice<sup>179</sup>. Serum analysis of 3- and 9-month old *Cyld/Relb*<sup>ALPC</sup> mice resulted in reduced ALT levels compared with *Cyld*<sup>ALPC</sup> mice, suggesting a diminished liver injury.

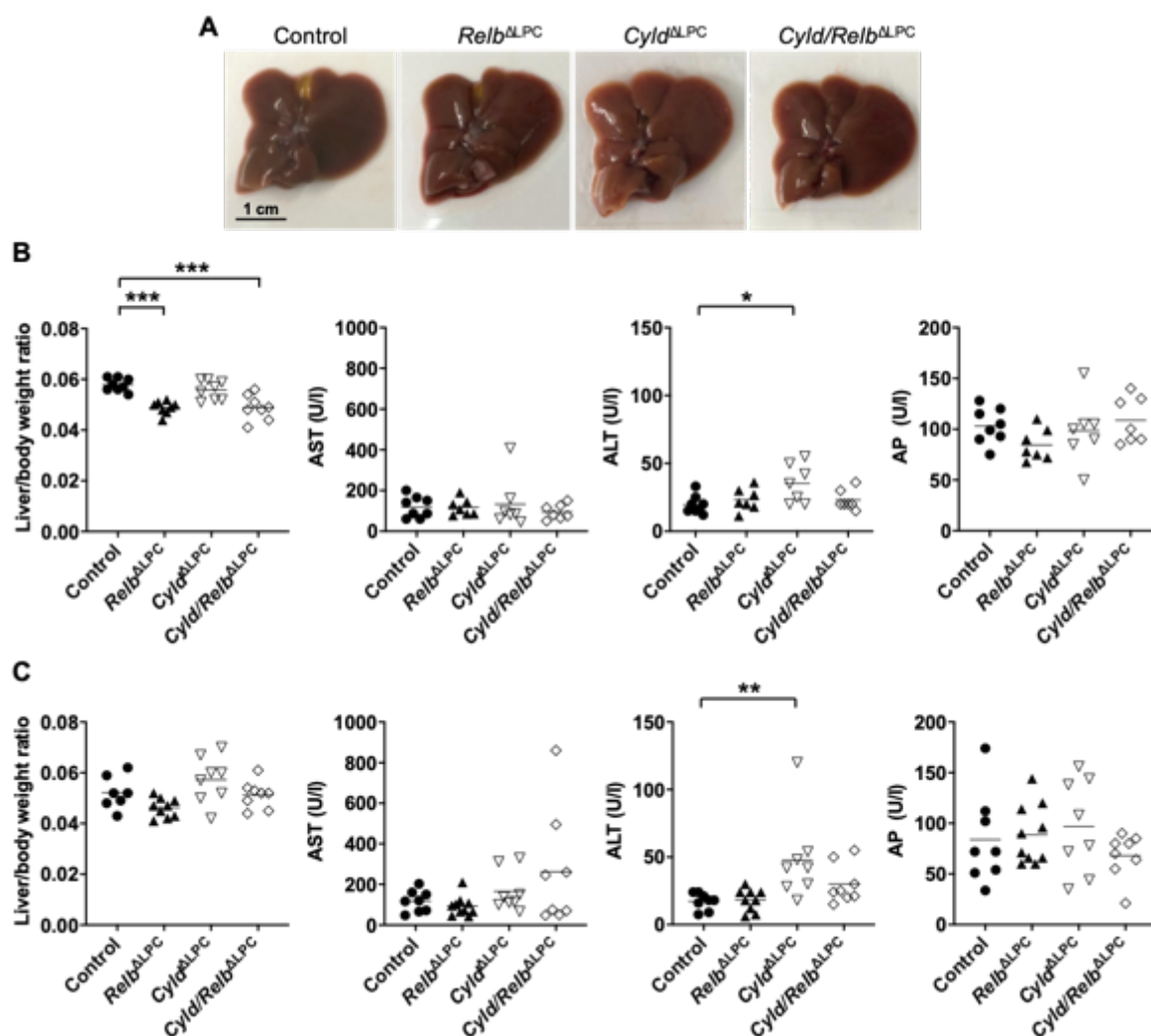


**Figure 7. Basal characterization of *Cyld/Relb*<sup>ALPC</sup> mice.** (A) Representative macroscopic pictures of livers obtained from 9-month-old control, *Relb*<sup>ALPC</sup>, *Cyld*<sup>ALPC</sup>, and *Cyld/Relb*<sup>ALPC</sup> mice. (B and C) Liver/body weight ratio and serum analysis of the liver enzymes aspartate transaminase (AST), alanine transaminase (ALT), and alkaline phosphatase (AP) for the indicated genotypes of 3-month-old (B) and 9-month-old mice (C). Each symbol represents one individual mouse. Results are shown as means, n = 7-10 mice per group, \*p<0.05, \*\*p<0.01, \*\*\*p<0.001 by one-way ANOVA and Tukey's multiple comparisons test. Adapted from Elßner et al. (2019)<sup>1</sup>.

Murine livers were then histologically analyzed (Fig. 8A). Whereas liver-specific RELB single knockout mice showed no phenotype and were comparable to control littermates, generation of *Cyld/Relb*<sup>ALPC</sup> mice revealed that the histological phenotype of *Cyld*<sup>ALPC</sup> livers strictly depends on the prolonged activation of RELB (Fig. 8). Additional deletion of RELB in *Cyld*<sup>ALPC</sup> mice led to a complete abrogated liver phenotype in *Cyld/Relb*<sup>ALPC</sup> mice. Quantification of Sirius Red staining (Fig. 8B) as well as assessment of mRNA expression of collagen displayed significantly reduced biliary fibrosis in *Cyld/Relb*<sup>ALPC</sup> livers compared with *Cyld*<sup>ALPC</sup> livers (Sirius Red staining p = 0.0084, *Coll1a1* mRNA: p = 0.0006). Furthermore, dramatic increase of periportal ductules in *Cyld*<sup>ALPC</sup> mice, as proven by KRT7 IHC staining (Fig. 8A), mRNA analysis (Fig. 8B, p < 0.0001), and Western Blot (Fig. 8C) was significantly reduced in double knockout mice (*Krt7* mRNA: p < 0.0001) and was comparable to control mice.

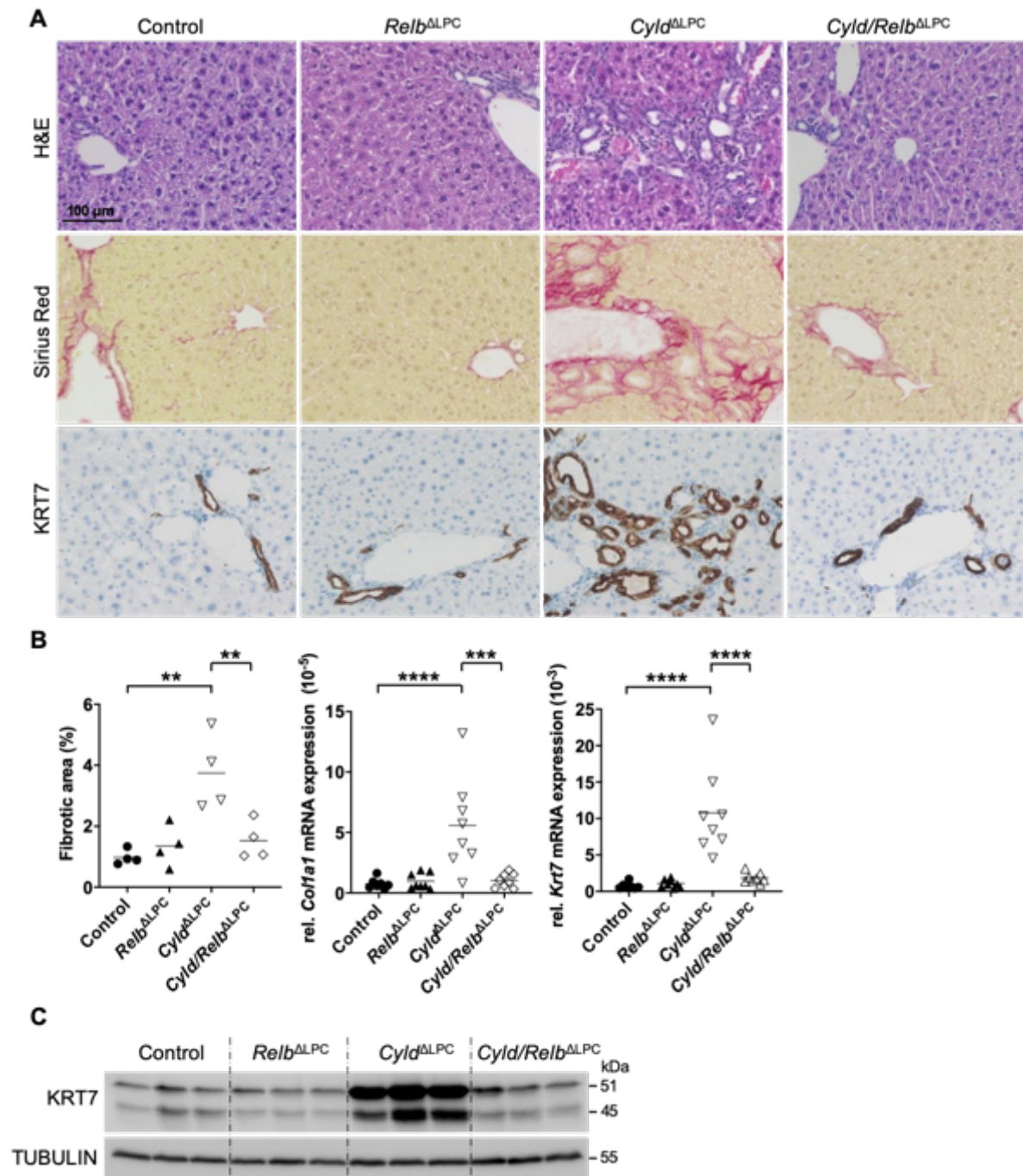


**Figure 8. Sustained activation of RELB is required for the biliary phenotype in *Cyld*<sup>ΔLPC</sup> mice.** (A) Liver histology (H&E) and fibrosis (Sirius Red) were examined on liver paraffin sections of 9-month-old control, *Relb*<sup>ΔLPC</sup>, *Cyld*<sup>ΔLPC</sup>, and *Cyld/Relb*<sup>ΔLPC</sup> mice. Cryosections of similar mouse livers were stained for KRT7 (biliary epithelial cell marker). Scale bars as indicated. (B) Quantification of Sirius Red staining (n = 4 mice per group). Eight images for each mouse were averaged and analyzed). Quantitative real-time PCR analysis of *Col1a1* and *Krt7* mRNA expression in murine livers (n = 8). Results are presented as expression relative to *Gapdh* and *Rps6*. Each symbol represents one individual mouse. Data are shown as means, \*\*p<0.01, \*\*\*p<0.001 and \*\*\*\*p<0.0001 by one-way ANOVA and Tukey's multiple comparisons test. (C) Western Blot analysis for KRT7 expression in whole liver extracts of 9-month-old *Relb*<sup>ΔLPC</sup>, *Cyld*<sup>ΔLPC</sup>, and *Cyld/Relb*<sup>ΔLPC</sup> mice and control littermates. TUBULIN was used as loading control. Adapted from Elßner et al. (2019)<sup>1</sup>.

Since *Cyld*<sup>ΔLPC</sup> mice showed increased proliferation in the surrounding of periportal biliary ductules, the proliferative capacity was evaluated by KI67 staining (Fig. 9A)<sup>179</sup>. Quantification of KI67 positive

cells revealed a decreased number of KI67 positive cells in the periportal regions of *Cyld/Relb*<sup>ALPC</sup> mice compared with *Cyld*<sup>ALPC</sup> mice (Fig. 9B,  $p = 0.0312$ ).

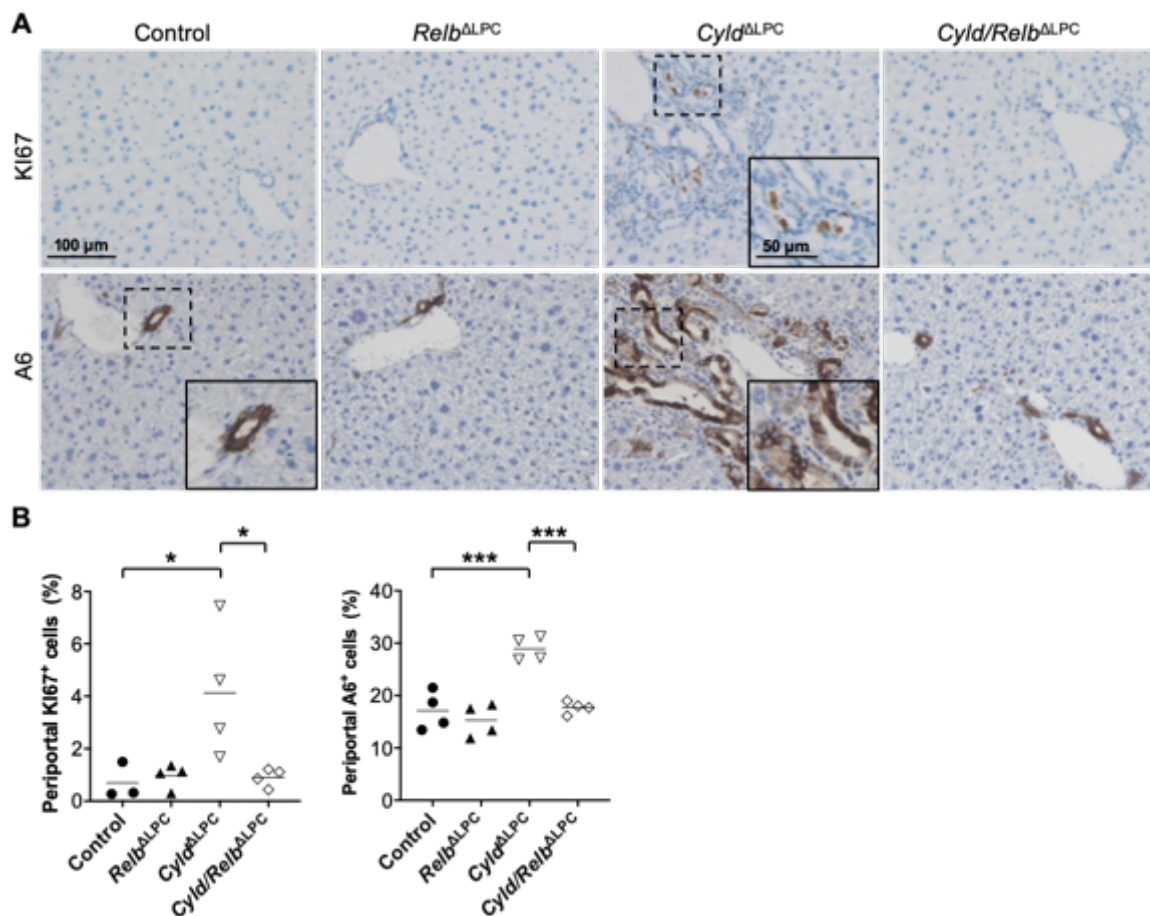


**Figure 9. Increased proliferation and oval cell activation in *Cyld*<sup>ALPC</sup> mice can be abolished by additional RELB deletion.** (A) Liver cryosections of 9-month-old control, *Relb*<sup>ALPC</sup>, *Cyld*<sup>ALPC</sup>, and *Cyld/Relb*<sup>ALPC</sup> mice were stained for KI67 (proliferation marker) and A6 (oval cell marker). Scale bars as indicated. (B) Quantification of KI67 and A6 positive cells in the periportal surrounding ( $n = 4$  mice per group). Ten representative periportal regions for each animal were selected, quantified and averaged for each whole slide image. Each symbol represents one individual mouse. Data are represented as means, \* $p < 0.05$  and \*\*\* $p < 0.001$  by one-way ANOVA and Tukey's multiple comparisons test. Adapted from Elßner et al. (2019)<sup>1</sup>.

In addition, the significant increased activation of the progenitor cell/oval cell compartment in *Cyld*<sup>ALPC</sup> mice, demonstrated by A6 positive cells (Fig. 9A and B), was completely abolished in *Cyld/Relb*<sup>ALPC</sup> mice (Fig. 9A and B,  $p = 0.0004$ ).

Taken together, these findings identify RELB as the driving force for biliary injury, ductular reaction, oval cell activation, and subsequent fibrosis in *Cyld*<sup>ALPC</sup> mice.

### 5.1.1.3 Reactive biliary epithelial phenotype in *Cyld*<sup>ALPC</sup> mice is dependent on constitutive RELB activation

The phenotype of *Cyld*<sup>ALPC</sup> livers is accompanied by few portal T cell infiltrates and strongly increased mRNA expression of proinflammatory cytokines<sup>179</sup>. To investigate, whether sustained RELB activation is also responsible for this phenomenon in *Cyld*<sup>ALPC</sup> mice, livers of 9-month-old knockout

mice were immunohistochemically stained for CD3 (T cells), CD11B (neutrophils), and CD68 (macrophages), as shown in Fig. 10A.

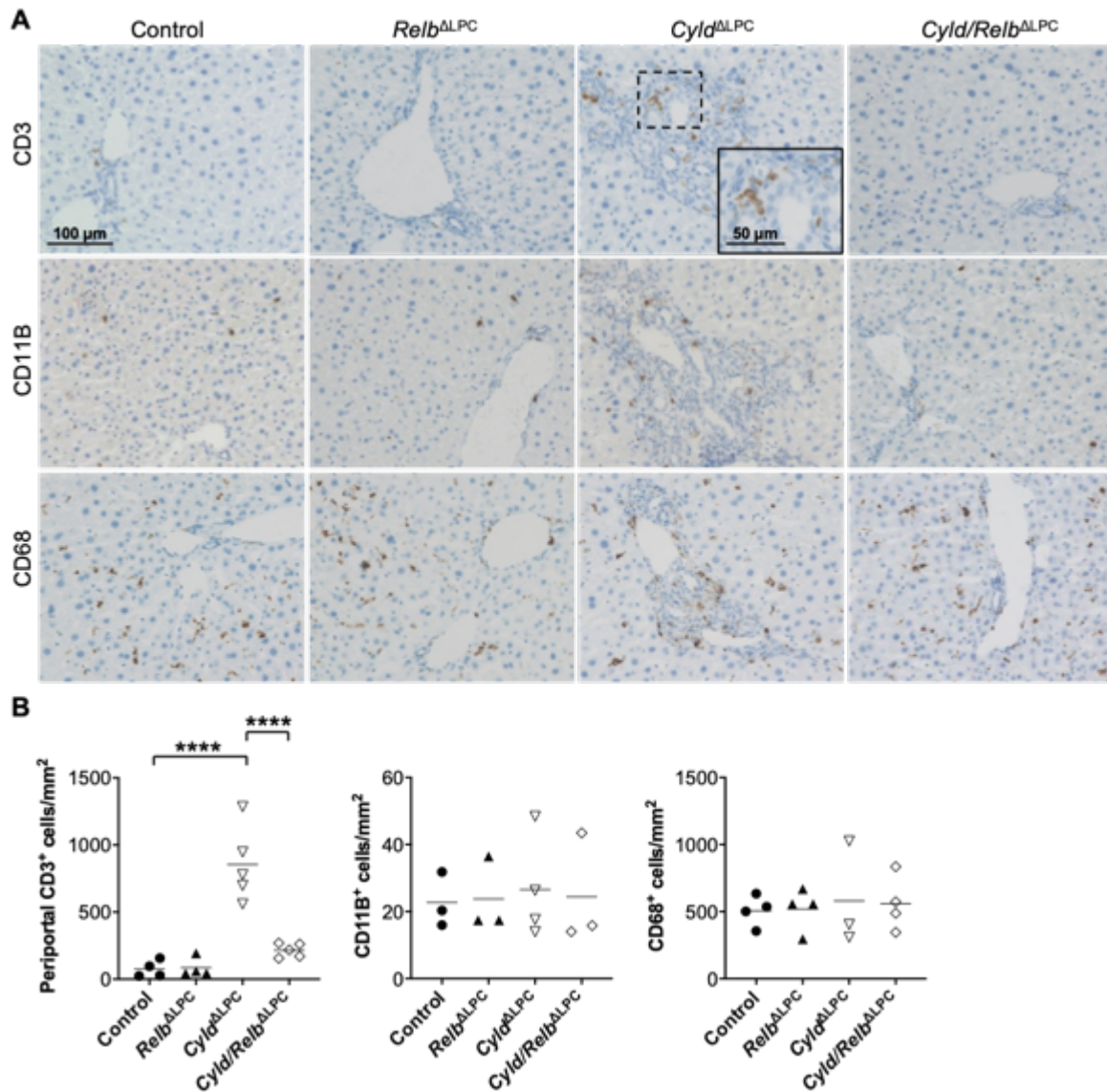


**Figure 10. Deletion of RELB reduces infiltration of CD3 positive cells in *Cylb* $\Delta$ LPC mice.** (A) Representative IHC staining of liver cryosections for CD3 (T-cells), CD11B (neutrophils), and CD68 (macrophages). (B) Quantification of CD3, CD11B, and CD68. For the evaluation of CD3 positive cells in the periportal surrounding (n = 4 mice per group), ten representative periportal regions for each animal were selected, quantified and averaged for each whole slide image. For CD11B and CD68 (n = 4 mice per group), representative rectangular ROIs of the whole liver section were taken and quantified. Each symbol represents one individual mouse. Data are represented as means, \*\*\*\*p<0.0001 by one-way ANOVA and Tukey's multiple comparisons test. Adapted from Elßner et al. (2019)<sup>1</sup>.

Since infiltrating CD3<sup>+</sup> cells were solely located in the periportal areas, evaluation was performed specifically for this area. As seen in Fig. 10B, quantification revealed that RELB deletion was able to reduce the infiltration of CD3<sup>+</sup> cells in *Cylb/Relb* $\Delta$ LPC mice compared with *Cylb* $\Delta$ LPC mice (p < 0.0001). For macrophages (CD68<sup>+</sup> cells) and neutrophils (CD11B<sup>+</sup> cells), no significant increase was observed in *Cylb* $\Delta$ LPC mice (Fig. 10B).

Results of the qRT-PCR analysis showed that mRNA levels of the inflammatory mediators *Ccl2*, *Tnfa*, and *Tgfb2* were repressed in *Cyld/Relb*<sup>ALPC</sup> mice at the age of 3 months (Fig. 11A,  $p < 0.0001$ ) and 9 months compared with *Cyld*<sup>ALPC</sup> mice (Fig. 11B, *TNF- $\alpha$* :  $p = 0.0009$ , *TGF- $\beta$ 2*:  $p < 0.0001$ ). Slightly elevated expression levels of *TGF- $\beta$ 1* in 9-month-old *Cyld*<sup>ALPC</sup> mice were also reduced in *Cyld/Relb*<sup>ALPC</sup> mice (Fig. 11A and B).

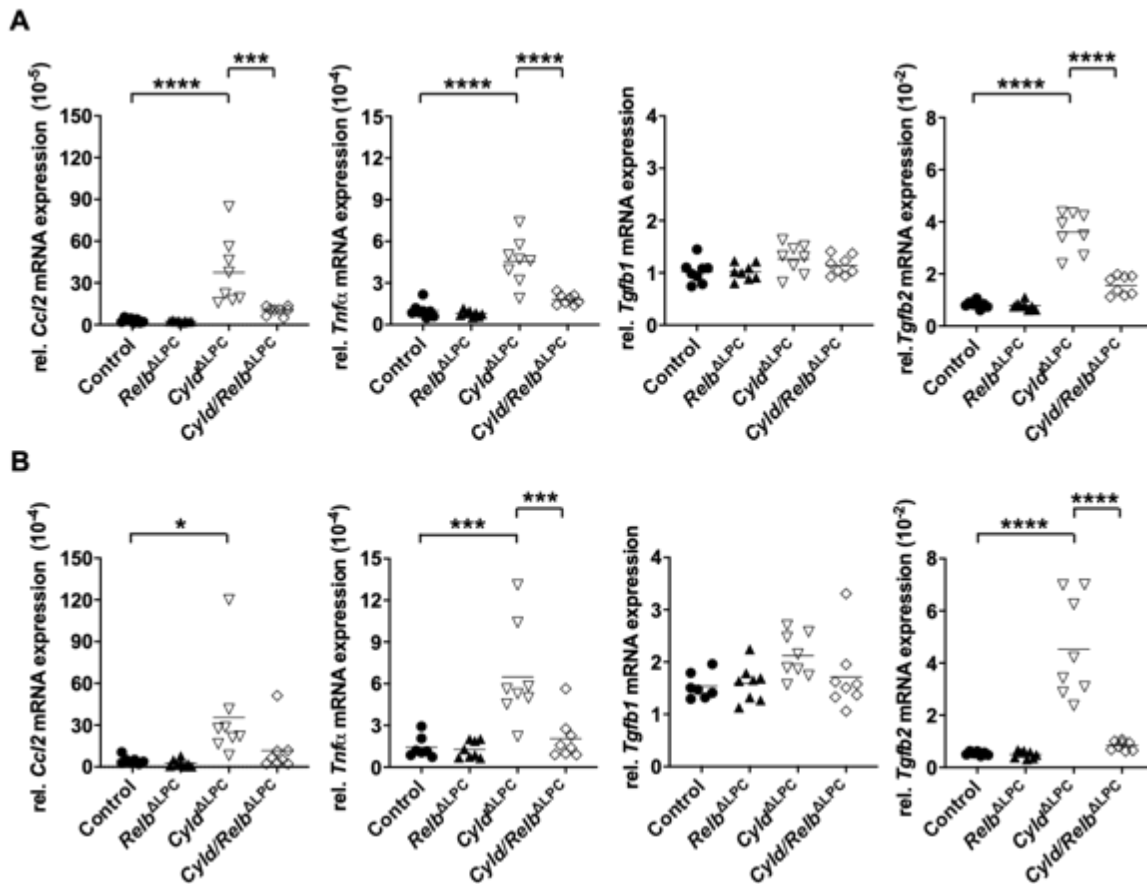


**Figure 11. Deletion of RELB dampens the elevated cytokine milieu in *Cyld*<sup>ALPC</sup> mice.** q-RT PCR analysis for pro-inflammatory markers and cytokines of livers from 3-month-old (A) and 9-month-old mice (B). Expression levels are normalized to housekeeping genes *Gapdh* and *Rps6*. Each symbol represents one individual mouse. Results are shown as means, \* $p < 0.05$  \*\* $p < 0.01$ , \*\*\* $p < 0.001$  and \*\*\*\* $p < 0.0001$  by one-way ANOVA and Tukey's multiple comparisons test. Adapted from Elßner et al. (2019)<sup>1</sup>.

Next, potential changes in the expression of cytokines that directly target the non-canonical NF- $\kappa$ B pathway and might promote prolonged activation of RELB in *Cyld*<sup>ALPC</sup> mice were addressed (Fig. 12). Whereas *Lta*, *Tweak*, *Cd40lg*, and *Light* mRNA levels remained unchanged in 3-month-old *Cyld*<sup>ALPC</sup> mice, a 3-fold upregulation of *Rankl* ( $p = 0.0013$ ) and *Baff* ligands ( $p = 0.0001$ ) were detected compared with control mice (Fig. 12A). *Lt $\beta$*  levels were even more elevated, with a 6-fold difference ( $p < 0.0001$ ), respectively. At later time points, the differences were more prominent: *Lt $\beta$*  showed a 9-fold upregulation ( $p < 0.0001$ ), *Rankl* levels were 6-fold upregulated ( $p = 0.0015$ ), and *Baff* 4-fold (Fig. 12B,  $p = 0.0001$ ). In addition, qRT-PCR of 9-month-old *Cyld*<sup>ALPC</sup> mice revealed also slight elevated expression levels of *Cd40lg* (3-fold,  $p = 0.0418$ ) and *Light* (2-fold,  $p = 0.0127$ ). Again, in *Cyld/Relb*<sup>ALPC</sup> mice, transcription levels of all upregulated cytokines were profoundly repressed (Fig. 12A and B, *Lt $\beta$* :  $p < 0.0001$ , *Rankl*:  $p = 0.0009$ , *Baff*:  $p = 0.0004$ , *Light*:  $p = 0.0232$ ).

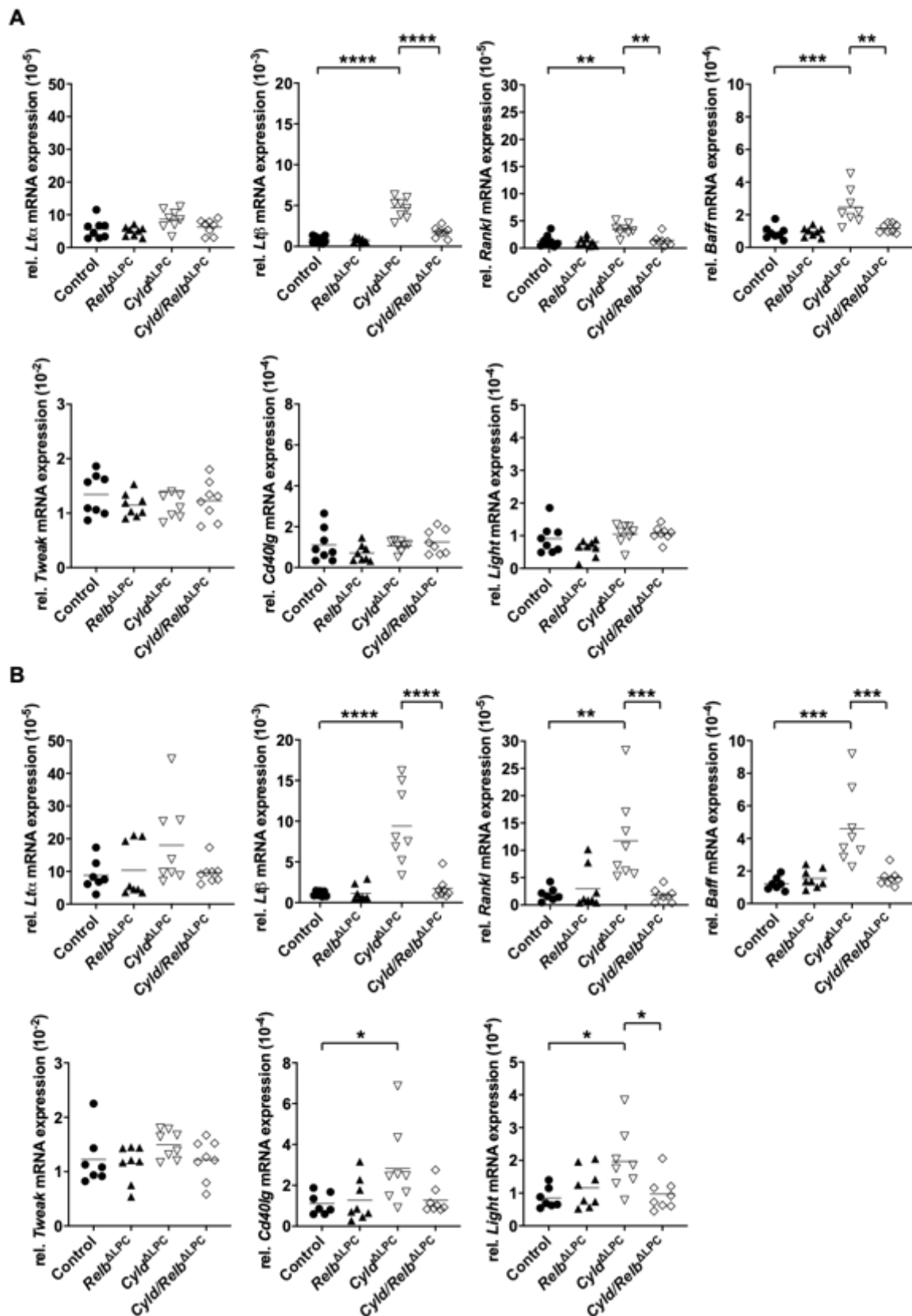


**Figure 12. Increased expression of cytokines targeting the non-canonical NF- $\kappa$ B pathway in *Cytld*<sup>ΔLPC</sup> mice is RELB dependent.** q-RT PCR analysis of livers from 3-month-old (A) and 9-month-old mice (B) for cytokines stimulating the non-canonical NF- $\kappa$ B. Expression levels are normalized to housekeeping genes *Gapdh* and *Rps6*. Each symbol represents one individual mouse. Results are shown as means, \* $p < 0.05$ , \*\* $p < 0.01$ , \*\*\* $p < 0.001$  and \*\*\*\* $p < 0.0001$  by one-way ANOVA and Tukey's multiple comparisons test. Adapted from Eißner et al. (2019)<sup>1</sup>.

The significant discrepancy between the strong activation of cytokine production and the mild cellular inflammation in *Cyld*<sup>ALPC</sup> mice questions the cellular origin, which is responsible for this significantly elevated cytokine transcription. Ductular reaction, as seen in many forms of liver injury and also in *Cyld*<sup>ALPC</sup> livers, refers to an increased number of bile ductules accompanied by fibrosis and inflammatory infiltrates<sup>66</sup>. These newly formed bile ducts are composed of reactive cholangiocytes, which acquire the ability to express proinflammatory cytokines, chemotactic mediators, growth factors, and adhesion molecules such as VCAM1<sup>199</sup>. To investigate whether cholangiocytes display a reactive biliary phenotype, an IHC staining for vascular cell adhesion molecule (VCAM1) was performed (Fig. 13). The IHC staining demonstrated a highly upregulated expression in biliary epithelial cells of *Cyld*<sup>ALPC</sup> mice, indicating the transformation of the bile duct cells into a reactive phenotype.

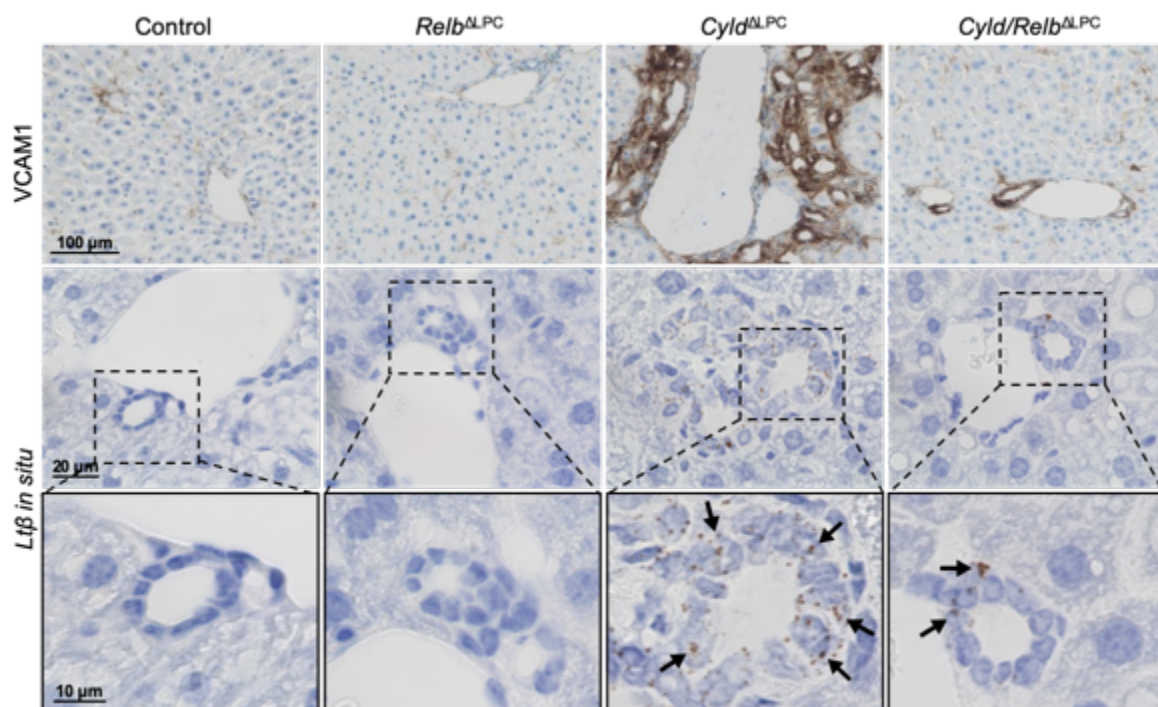


**Figure 13. Reactive biliary epithelial phenotype in *Cyld*<sup>ALPC</sup> mice depends on sustained RELB activation.** Representative IHC staining of liver cryosections of 9-month-old mice for vascular cell adhesion molecule (VCAM1) indicating transformation of cholangiocytes into a reactive phenotype. Representative image for *in situ* hybridization of *Ltβ* in *Cyld*<sup>ALPC</sup> livers demonstrating biliary epithelial origin of the cytokine. Arrows indicate positive *Ltβ* foci. Scale bars as indicated. Adapted from Elßner et al. (2019)<sup>1</sup>.

Although *Cyld/Relb*<sup>ALPC</sup> mice exhibited no ductular reaction and less KRT7 positive cells (Fig. 8), the biliary epithelial cells maintained a reactive phenotype to a lower extent, as demonstrated by VCAM1 positive bile duct cells (Fig. 13). In order to trace the cellular origin responsible for the elevated cytokine secretion, *Ltβ* *in situ* hybridization was performed, since *Ltβ* expression levels showed the strongest upregulation. As presented in Fig. 13, activated cholangiocytes represented indeed the source of *Ltβ* in *Cyld*<sup>ALPC</sup> mice. In *Cyld/Relb*<sup>ALPC</sup> mice, *Ltβ* was also expressed by reactive cholangiocytes, but in a significant lower amount.

Altogether, these data indicate that reactive cholangiocytes in *Cyld*<sup>ALPC</sup> mice contribute to the increased cytokine levels, pointing to a perpetuating feedback mechanism of constitutive RELB activation.

#### 5.1.1.4 RELB hyperactivation triggers increased NF- $\kappa$ B signaling in *Cyld*<sup>ALPC</sup> mice

As CYLD negatively regulates NF- $\kappa$ B signaling by deubiquitination, *Cyld*<sup>ALPC</sup> mice showed an increased and activated NF- $\kappa$ B signaling<sup>179</sup>. Since RELB deficiency histologically abolished the effects of *Cyld*<sup>ALPC</sup> mice, protein levels of NF- $\kappa$ B subunits (Fig. 14) and regulating factors (Fig. 15) were analyzed to investigate if RELB deletion was also affecting the expression of the NF- $\kappa$ B expression levels. Whole liver lysates were used to determine the effect of RELB for both, hepatocytes and cholangiocytes, as they were both affected by albumin Cre recombinase. Low expression levels of full-length CYLD in *Cyld*<sup>ALPC</sup> and *Cyld/Relb*<sup>ALPC</sup> livers as well as of RELB in RELB deleted livers (Fig. 14) were attributed to non-parenchymal cells like sinusoidal endothelial cells, hepatic stellate cells, Kupffer cells, and intrahepatic lymphocytes. As already shown for primary murine hepatocytes, full-length CYLD deletion was accompanied by enhanced expression of a naturally occurring shorter CYLD splice variant and upregulated RELB expression.

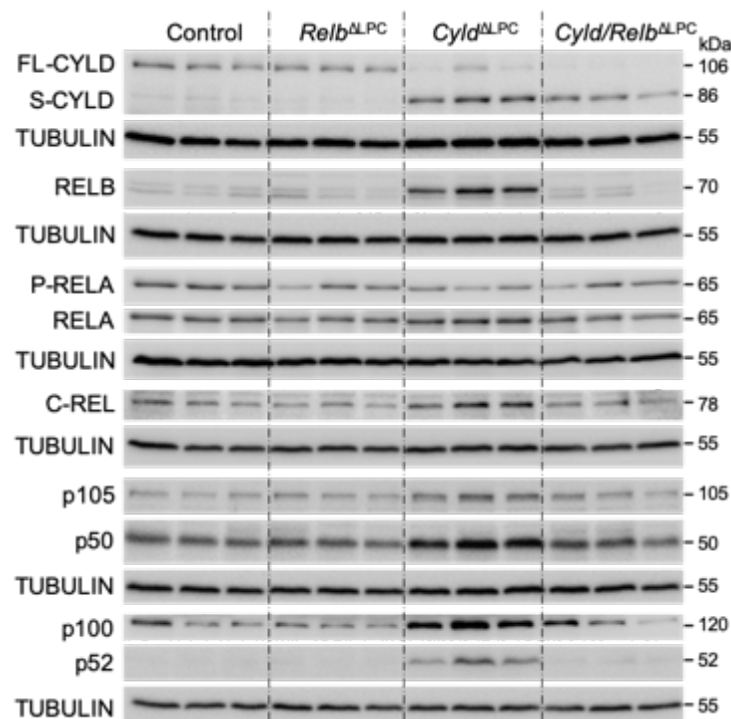


**Figure 14. Increased NF- $\kappa$ B activation in *Cyld*<sup>ALPC</sup> mice is rescued by RELB deletion.** Western blot analysis of liver extracts from 9-month-old control, *Relb*<sup>ALPC</sup>, *Cyld*<sup>ALPC</sup> and *Cyld/Relb*<sup>ALPC</sup> mice for CYLD, members of the canonical NF- $\kappa$ B pathway (RELA, C-REL, p105, p50) and non-canonical NF- $\kappa$ B pathway (RELB, p100, p52). Elevated protein levels in *Cyld*<sup>ALPC</sup> mice are reduced in *Cyld/Relb*<sup>ALPC</sup> mice to normal level. TUBULIN served as loading control. Adapted from Elßner et al. (2019)<sup>1</sup>.

Expression of RELA, which was slightly elevated in *Cyld*<sup>ALPC</sup> mice but not activated, as demonstrated by the unaltered phosphorylated RELA expression, was unchanged in *Cyld/Relb*<sup>ALPC</sup> livers compared with control mice. Induced expression of C-REL, p50, p52, and its precursor proteins p105, p100 was completely abolished in *Cyld/Relb*<sup>ALPC</sup> mice.

Hepatic expression levels of proteins involved in the regulation of NF- $\kappa$ B signaling were afterwards assessed. Whereas TRAF3, NIK, C-IAPs, P-IKK $\alpha/\beta$ , P-I $\kappa$ B $\alpha$ , and BCL-3 remained unchanged (Fig. 15), NEMO, TRAF2, RIP1, all direct enzymatic targets of CYLD, were upregulated in *Cyld*<sup>ALPC</sup> mice but showed normal expression levels in *Cyld/Relb*<sup>ALPC</sup> mice.

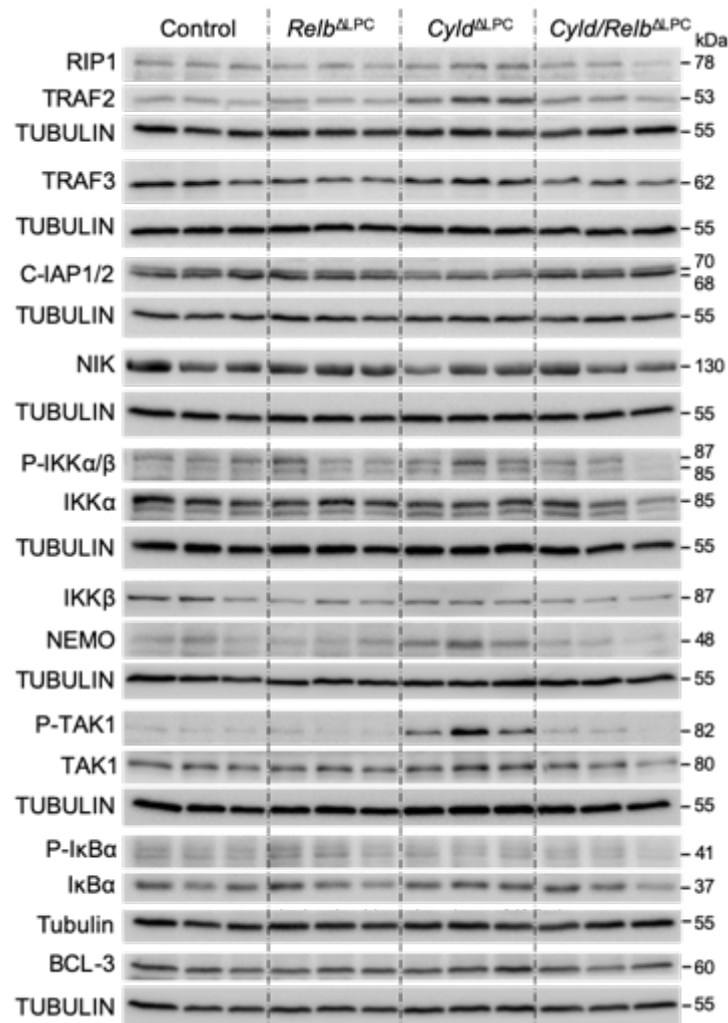


**Figure 15. Increased expression of NF- $\kappa$ B regulating factors in *Cyld*<sup>ΔLPC</sup> mice is rescued by RELB deletion.** Western blot analysis of liver extracts from 9-month-old control, *Relb*<sup>ΔLPC</sup>, *Cyld*<sup>ΔLPC</sup> and *Cyld/Relb*<sup>ΔLPC</sup> mice for proteins involved in the NF- $\kappa$ B signaling pathway. Elevated protein levels of TRAF2, NEMO and P-TAK1 in *Cyld*<sup>ΔLPC</sup> mice are decreased in *Cyld/Relb*<sup>ΔLPC</sup> mice to control level. TUBULIN served as loading control. Adapted from Elßner et al. (2019)<sup>1</sup>.

Strong phosphorylation of TAK1 was completely reverted in *Cyld/Relb*<sup>ΔLPC</sup> mice and similar to control levels.

Collectively, Western blot analysis of the NF- $\kappa$ B signaling pathway revealed that prolonged activation of RELB triggered the increased expression of NEMO, TRAF2, RIP1, phosphorylated TAK1, C-REL, p105/p50 (involved in canonical NF- $\kappa$ B pathway), and p52/p100 (involved in non-canonical NF- $\kappa$ B pathway) in *Cyld*<sup>ΔLPC</sup> mice. These findings suggest a yet unknown interaction between canonical and non-canonical NF- $\kappa$ B pathway and identify RELB as a key player driving the overall increased NF- $\kappa$ B signaling in *Cyld*<sup>ΔLPC</sup> livers.

To investigate whether additional signaling pathways contribute to the development of the biliary phenotype in *Cyld*<sup>ALPC</sup> mice, signaling pathways addressing apoptosis, proliferation, and biliary differentiation were analyzed.

In a similar model of CYLD disruption and spontaneous TAK1 activation, c-Jun N-terminal kinase (JNK) was reported to be activated, which is a known trigger of cell death in several cell types<sup>180</sup>. However, only a weak activation of JNK was observed in *Cyld*<sup>ALPC</sup> mice (Fig. 16), as demonstrated by slightly enhanced protein levels of phosphorylated JNK compared with control mice. Levels of total JNK1, JNK2 or JNK3 protein (shown by detection of JNK, Fig. 16) were unchanged.

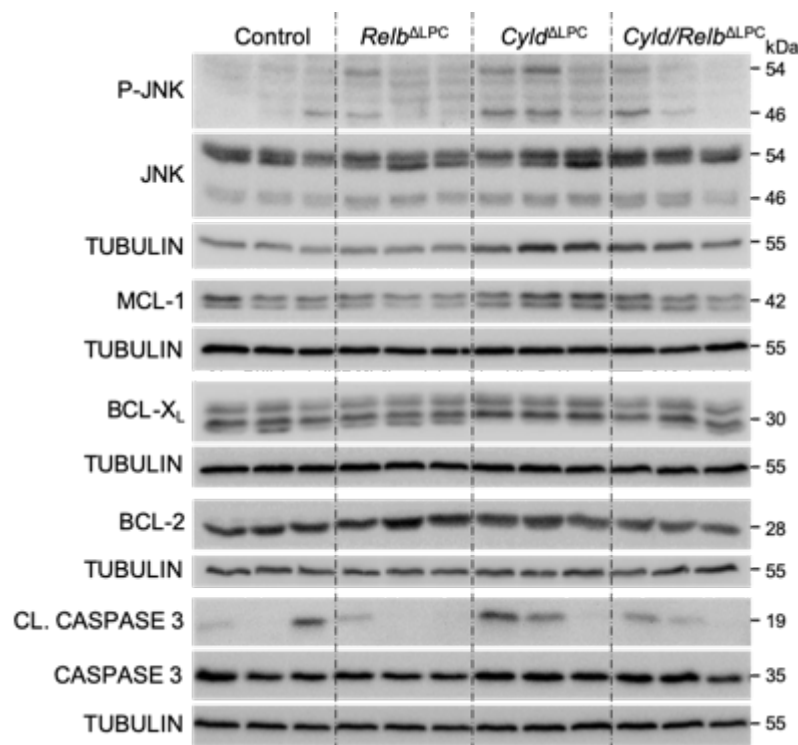


**Figure 16. Analysis of cell death and anti-apoptotic BCL-2 proteins.** Western blot analysis of liver extracts from 9-month-old control, *Relb*<sup>ALPC</sup>, *Cyld*<sup>ALPC</sup> and *Cyld/Relb*<sup>ALPC</sup> mice for JNK (detection of JNK1, JNK2, and JNK3) and the anti-apoptotic BCL-2 proteins MCL-1, BCL-X<sub>L</sub>, and BCL-2 and the apoptotic effector CASPASE 3 demonstrating no differences in the protein expression. TUBULIN served as loading control.

Western blot analysis of anti-apoptotic BCL-2 proteins such as MCL-1, BCL-X<sub>L</sub> and BCL-2 also revealed no significant changes in *Cyld*<sup>ALPC</sup> mice compared with control mice. As the main executors of apoptosis, caspases and their cleavage and activation are responsible for the amplification of the apoptotic signal and executing the cellular destruction<sup>200</sup>. In *Cyld*<sup>ALPC</sup> mice, the most important effector caspase, namely CASPASE 3, seemed to be not affected by the deletion of full-length CYLD (Fig. 16), suggesting that apoptosis of liver parenchymal cells is not accountable for the biliary phenotype in this mouse model.

Next, the question was addressed whether other mitogen-activated protein kinases and increased proliferation might contribute to the biliary phenotype of *Cyld*<sup>ALPC</sup> mice. While ERK1/2 and p38 were shown to be dysregulated after CYLD suppression in recent studies, in *Cyld*<sup>ALPC</sup> livers these pathways were unchanged (Fig. 17)<sup>201,202</sup>. Furthermore, CYLD expression correlates negatively with the expression of C-MYC, CYCLIN D1 and β-CATENIN, which is why potential changes in these

proteins were also examined<sup>203,204</sup>. As presented in Fig. 17, no alterations could be found in the different knockout mice compared with control mice.

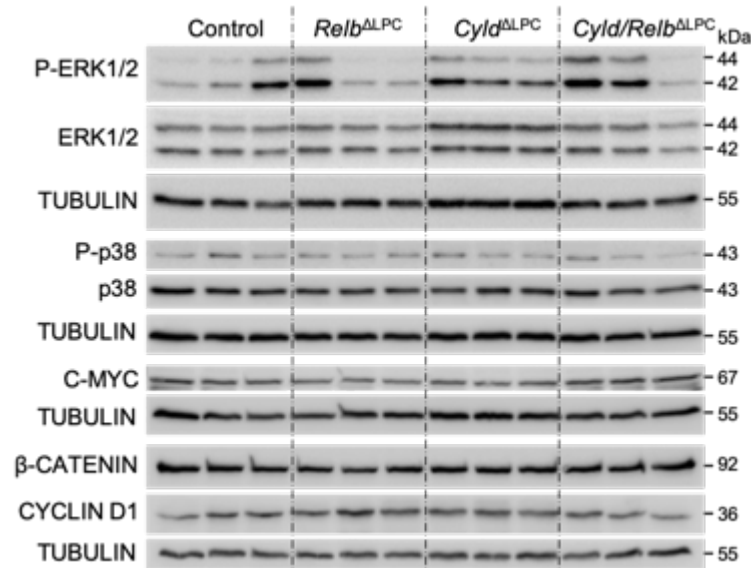


**Figure 17. Analysis of proliferation and mitogen-activated protein kinases.** Western blot analysis of liver extracts from 9-month-old control, *Relb*<sup>ΔLPC</sup>, *Cyl*<sup>ΔLPC</sup> and *Cyl*<sup>ΔLPC</sup>/*Relb*<sup>ΔLPC</sup> mice for ERK1/2, p38, C-MYC, β-CATENIN, and CYCLIN D1. No alterations in the protein expression could be observed. TUBULIN served as loading control.

In the recent years, NOTCH signaling pathway has been implicated in the lineage specification of cholangiocytes and hepatocytes and in the process of bile duct proliferation<sup>205,206</sup>. In order to determine whether the ductular reaction in *Cyl*<sup>ΔLPC</sup> mice was caused by impaired NOTCH signaling, NOTCH signaling was assessed on protein levels of murine liver extracts (Fig. 18).

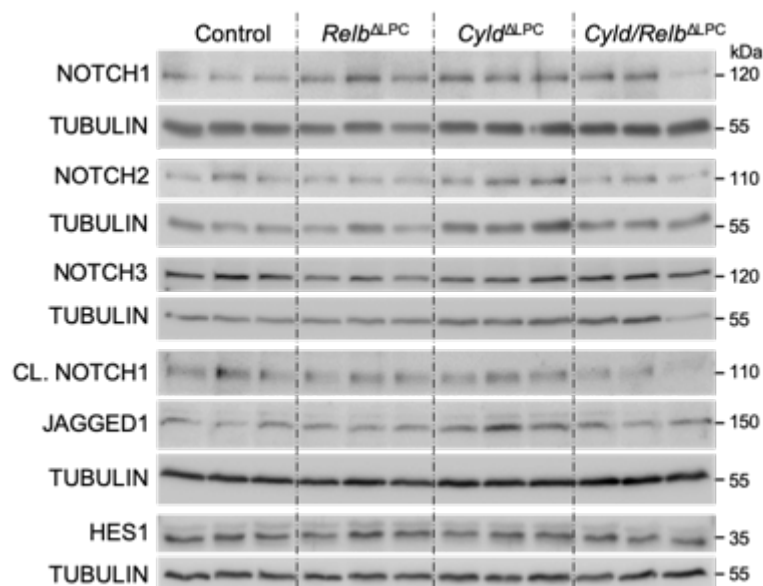


**Figure 18. Analysis of NOTCH signaling pathway.** Western blot analysis of liver extracts from the indicated genotypes for proteins involved in the NOTCH signaling pathway, showing no alteration in the protein expression. TUBULIN served as loading control.

Similar to the findings above, full-length CYLD deficiency did not result in markedly increased protein expression of neither NOTCH receptors (NOTCH1, 2, 3) nor activated NOTCH (CLEAVED

NOTCH1), NOTCH ligand (JAGGED1) and NOTCH target (HES1), indicating that NOTCH signaling is not essential for the development of ductular reaction and biliary fibrosis in *Cyld*<sup>ALPC</sup> mice.

### 5.1.2 Hepatocyte-driven fibrosis is RELB independent

Liver-specific lack of full-length CYLD led to a biliary phenotype associated with fibrosis. The observation that additional deletion of RELB rescued the spontaneous phenotype of *Cyld*<sup>ALPC</sup> mice raised the question whether RELB alone has any functional impact for persistent liver injury and fibrosis development. Liver fibrosis can be driven by injury to both types of hepatic cells, hepatocytes and cholangiocytes<sup>207</sup>. In order to determine if RELB is causatively involved in the development of fibrosis in a model for hepatocyte driven fibrosis, mice were injected twice a week for 6 weeks with CCl<sub>4</sub> (control mice received the same amount of sunflower oil). After long-term CCl<sub>4</sub>-intoxication, livers were examined for fibrosis and the fibrotic response was determined (Fig. 19A and B).

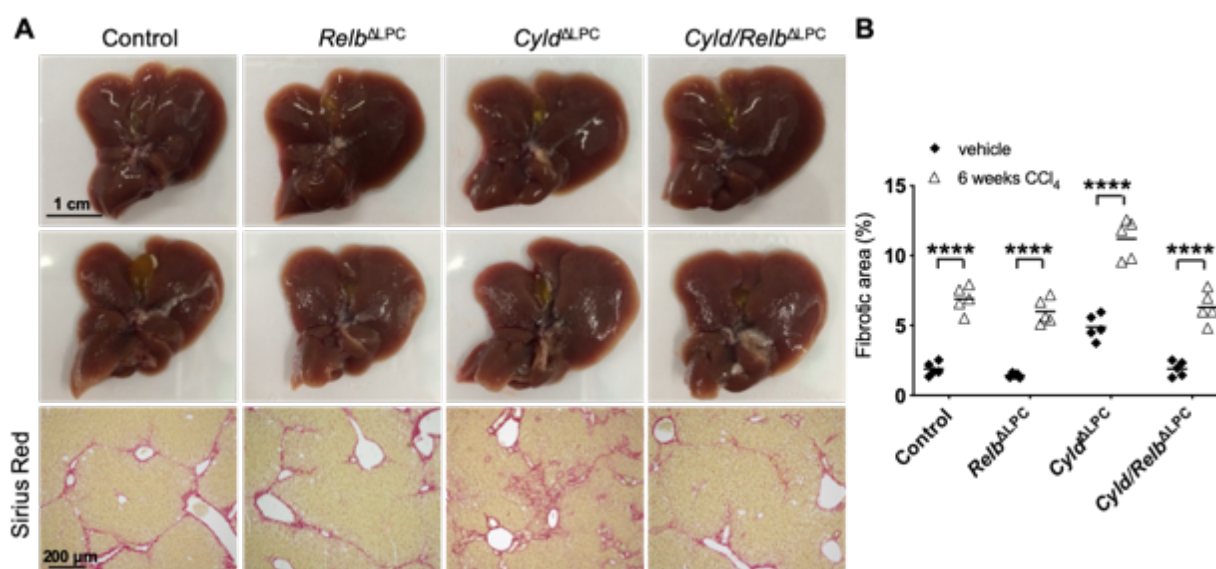


**Figure 19. CCl<sub>4</sub>-induced liver fibrosis.** (A) Representative macroscopic pictures of livers before (upper row) and after CCl<sub>4</sub>-injections (lower row). CCl<sub>4</sub>-treated livers were examined for fibrosis using Sirius Red. (B) Quantification of Sirius Red staining (n = 5 mice per group). Eight images for each mouse were averaged and analyzed. Each symbol represents one individual mouse. Data are represented as means, \*\*\*\*p<0.0001 two-way ANOVA and Bonferroni's multiple comparison test. Adapted from Elßner et al. (2019)<sup>1</sup>.

Using this model, quantification of Sirius Red staining showed no differences in the fibrosis induction between the different knockout mouse models (Fig. 19B). The mean difference ( $\Delta$ ) in fibrotic area between vehicle and CCl<sub>4</sub>-treated mice was not significantly altered between the mouse strains (in control mice:  $\Delta = 5.0$ , in *Relb*<sup>ALPC</sup> mice:  $\Delta = 4.6$ , in *Cyld*<sup>ALPC</sup> mice:  $\Delta = 6.3$ , and in *Cyld/Relb*<sup>ALPC</sup> mice:  $\Delta = 4.4$ , in all groups: p < 0.0001). From these findings, it could be hypothesized that RELB was rather involved in biliary driven fibrosis mediated through cholangiocytes and had no impact on liver fibrosis induced by hepatocyte damage.

### 5.1.3 Combined ablation of CYLD and RELB protects from chemically induced biliary damage

To examine if RELB regulates chronic biliary injury in a xenobiotic-induced cholestatic mouse model, a DDC-supplemented diet was used, which leads to cholestasis and biliary fibrosis. After 4 weeks of chronic exposure, DDC-fed control mice became jaundiced (Fig. 20A) and lost 30% body weight (Fig. 20B). Serum analyses of DDC-fed control mice revealed a significant increase in AST and ALT levels, indicative for hepatocyte damage, followed by significant elevations of cholestasis parameter such as AP and bilirubin levels compared with untreated control mice (Fig. 20D and Table 9). Elevated bilirubin levels, clearly seen in serum of control mice after DDC feeding, proved cholestatic injury (Fig. 20C).

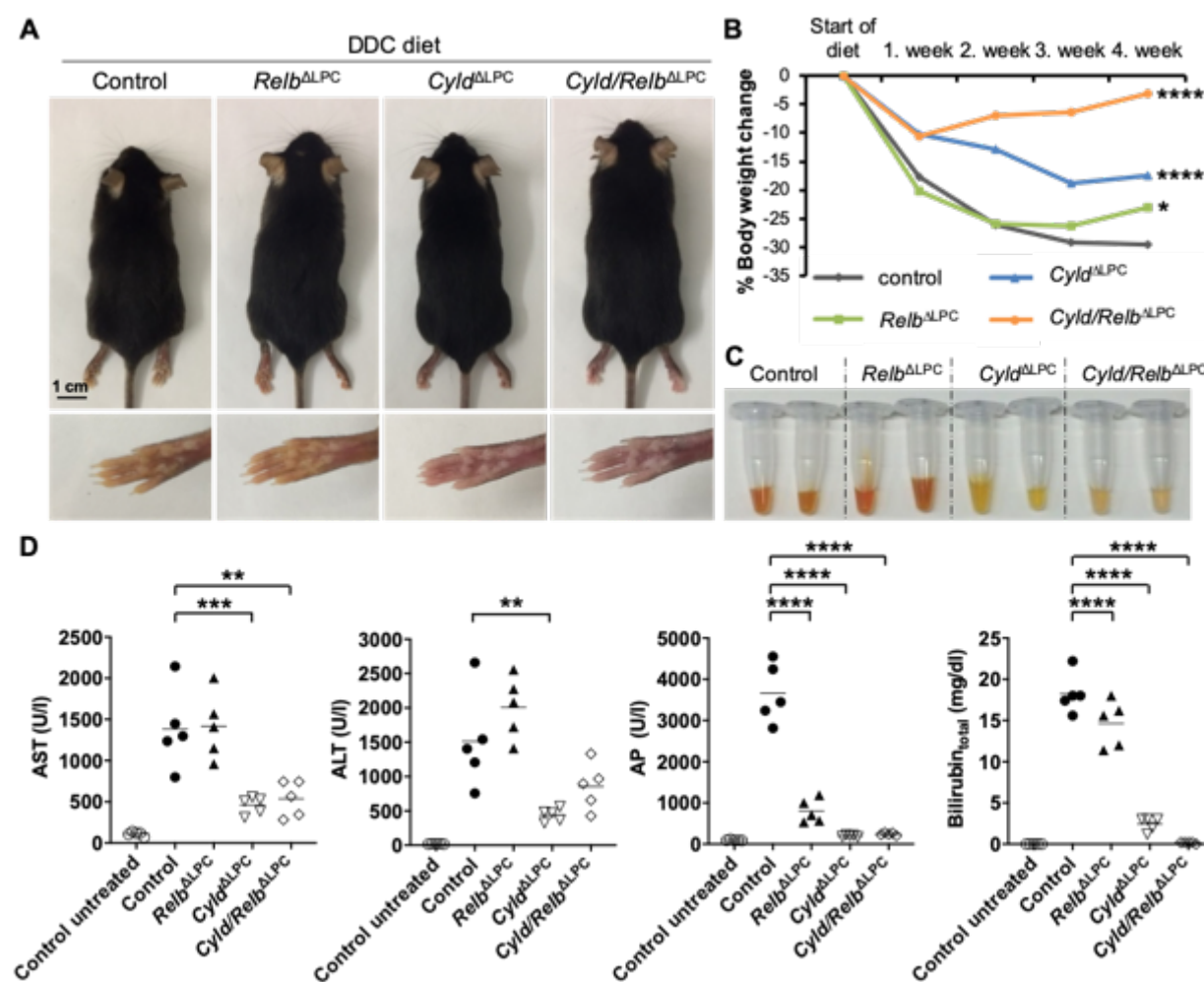


**Figure 20. Combined ablation of full-length CYLD and RELB protects from chemically induced biliary damage.** (A) Mice after 4 weeks of DDC feeding. The skin is jaundiced in control mice but not in *Cyld/Relb*<sup>ΔLPC</sup> mice. (B) Body weight change (%) during the period of DDC feeding with the lowest weight loss seen in *Cyld/Relb*<sup>ΔLPC</sup> mice. (C) Representative macroscopic picture of sera obtained from mice fed with DDC. (D) Serum analysis of AST, ALT, and total bilirubin after DDC feeding. Each symbol represents one individual mouse. Results are shown as means, n = 5 mice per group, \*\*p<0.01, \*\*\*p<0.001 and \*\*\*\*p<0.0001 by one-way ANOVA and Tukey's multiple comparisons test. Adapted from Elßner et al. (2019)<sup>1</sup>.

**Table 9. Serum analyses of untreated control mice and DDC-fed mice.** Results are shown as means  $\pm$  SD. ND = not detectable.

Variables	Control untreated	Control	<i>Relb</i> <sup>ALPC</sup>	<i>Cyld</i> <sup>ALPC</sup>	<i>Cyld/Relb</i> <sup>ALPC</sup>
AST (U/l)	111 $\pm$ 26.1	1384 $\pm$ 487.7	1418 $\pm$ 401.8	458.8 $\pm$ 105.8***	536.4 $\pm$ 217.5**
ALT (U/l)	18 $\pm$ 2.7	1513 $\pm$ 705.5	2009 $\pm$ 451.6	440.2 $\pm$ 96.0**	854.2 $\pm$ 340.4
AP (U/l)	96 $\pm$ 13.9	3660 $\pm$ 720.1	800.4 $\pm$ 284.4****	198.6 $\pm$ 21.3****	243.8 $\pm$ 29.4****
Total Bilirubin	ND	18.2 $\pm$ 2.4	14.6 $\pm$ 2.8****	2.4 $\pm$ 0.8****	0.2 $\pm$ 0.1****

Interestingly, although AP and bilirubin levels were significantly lower in DDC treated *Relb*<sup>ALPC</sup> mice compared with DDC-fed control mice (each  $p < 0.0001$ ), DDC-induced a similar phenotype in *Relb*<sup>ALPC</sup> mice as observed in control mice, indicating RELB independent effects in this chemically induced cholangiopathy model. In contrast, DDC feeding of *Cyld*<sup>ALPC</sup> mice, who exhibit untreated already a chronic biliary disease, led to body weight loss of only 17% (Fig. 20B) and significantly lower serum transaminases and bilirubin levels compared with DDC-fed control mice (Fig. 20D, Table 9).

The finding that ductular reaction and biliary fibrosis of untreated *Cyld*<sup>ALPC</sup> mice was RELB dependent and completely abolished in *Cyld/Relb*<sup>ALPC</sup> mice led to the hypothesis that DDC feeding of *Cyld/Relb*<sup>ALPC</sup> mice would lead to results comparable to control mice. Surprisingly, DDC-treated *Cyld/Relb*<sup>ALPC</sup> mice were healthy and maintained their body weight with only 3% body weight loss (Fig. 20A and B). Serum AST and ALT levels and AP levels of *Cyld/Relb*<sup>ALPC</sup> mice were comparable to *Cyld*<sup>ALPC</sup> mice after DDC exposure and significantly lower compared with DDC-fed control mice while bilirubin levels were not increased (Fig. 20D, Table 9). These data suggest protective mechanism against this biliary toxin in *Cyld*<sup>ALPC</sup> and *Cyld/Relb*<sup>ALPC</sup> mice.

Next, livers were examined macroscopically (Fig. 21) and histologically (Fig. 22). DDC-treated livers turned to dark-brown (Fig. 21A, lower panel) and liver/body weight ratio increased significantly in all mice (Fig. 21B,  $p < 0.0001$  in all groups). However, only in DDC-treated *Cyld*<sup>ALPC</sup> and *Cyld/Relb*<sup>ALPC</sup> mice were liver weights significantly increased, demonstrating a robust proliferative/regenerative response.

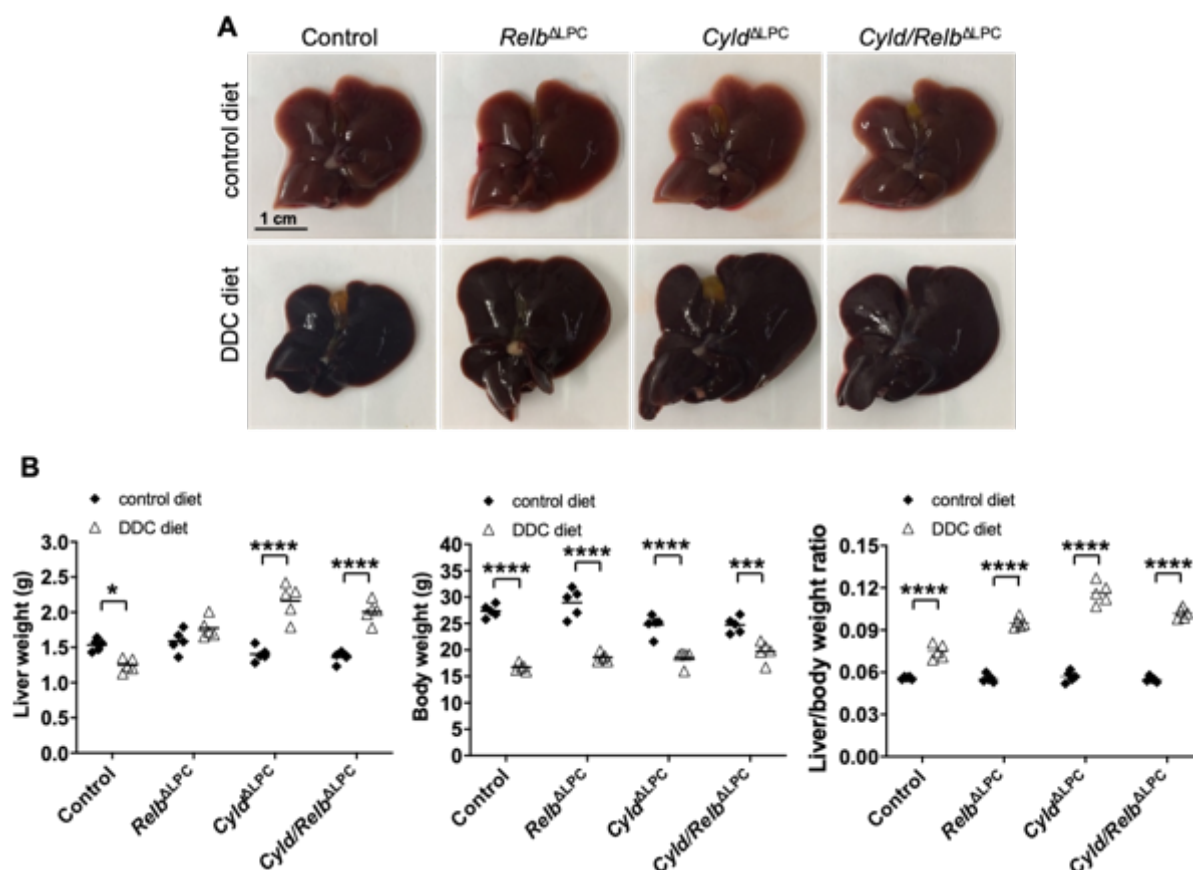


**Figure 21. Robust proliferative/regenerative response in all mice after 4 weeks of chronic exposure to DDC.** (A) Representative macroscopic pictures of livers before (upper panel) and after DDC feeding (lower panel). Scale bar as indicated. (B) Liver weight, body weight, and liver weight/body weight ratios for the indicated genotypes after DDC diet, revealing a significant proliferative/regenerative response *Cyld*<sup>ΔLPC</sup> and *Cyld/Relb*<sup>ΔLPC</sup> mice. Each symbol represents one individual mouse. Data are shown as means, n = 5 mice per group, \*\*\*\*p<0.0001 by one-way ANOVA and Tukey's multiple comparisons test. Adapted from Elßner et al. (2019)<sup>1</sup>.

Histological and immunohistochemical analysis revealed different cholestatic phenotypes after DDC exposure, with different gradings for severity of bile duct proliferation and ductular reactions, ranging from mild (5 to 9 bile ducts per portal tract) to moderate (equal to or greater than 10 bile ducts per portal tract) and severe (equal to or greater than 10 bile ducts per portal tract but the bile ducts are elongated and angulated)<sup>208</sup>.

While cholestasis accompanied by portal fibrosis and mild ductular reaction was induced in DDC-treated control and *Relb*<sup>ΔLPC</sup> mice, *Cyld*<sup>ΔLPC</sup> mice developed the most pronounced liver phenotype with severe ductular reaction and cystic dilatation of the bile ducts as expected after DDC exposure (Fig. 22). DDC-fed *Cyld/Relb*<sup>ΔLPC</sup> mice showed only moderate ductular reaction and were comparable to DDC-fed control mice (Fig. 22).

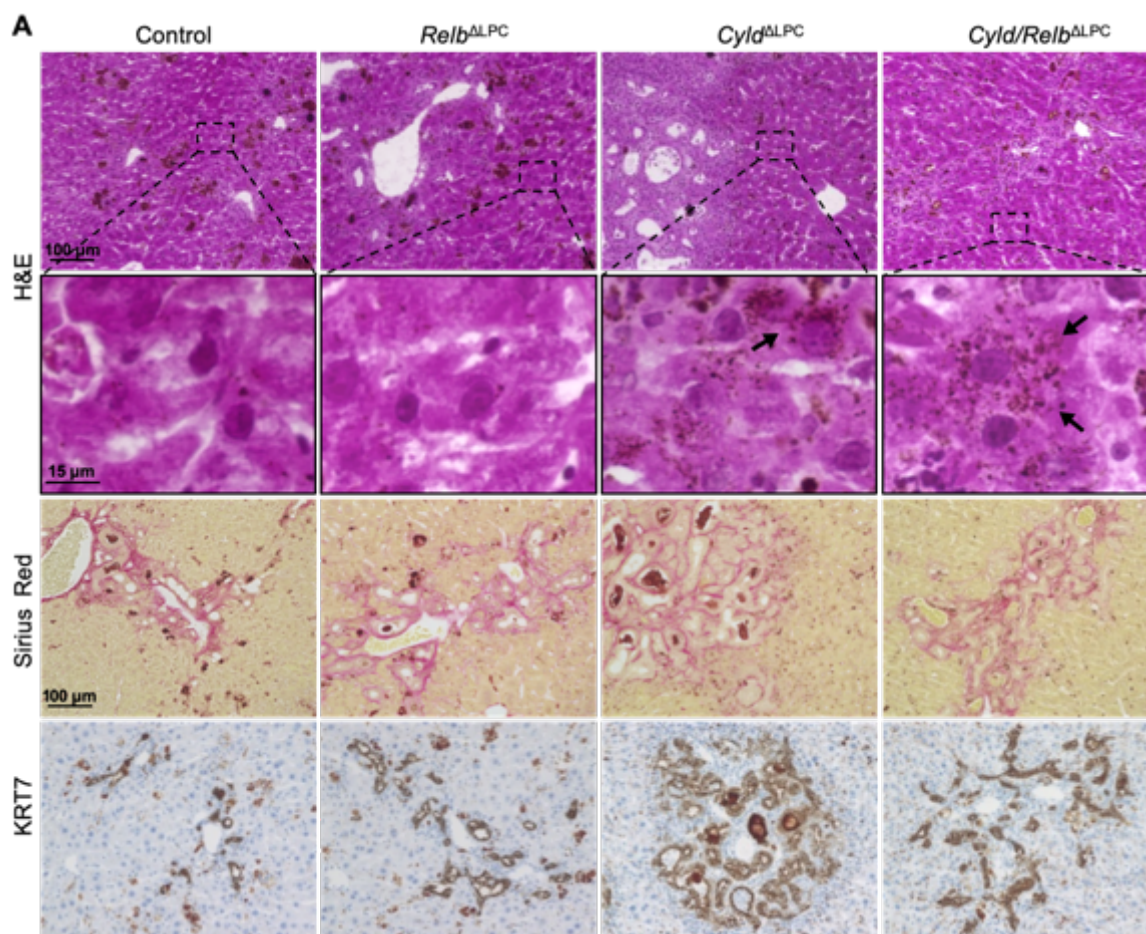


**Figure 22. DDC exposure leads to ductular proliferation and periductal fibrosis.** H&E staining of liver sections from 12-week-old mice fed with a DDC diet for 4 weeks. Dark brown pigments localized in the cytoplasm of some hepatocytes and macrophages indicate porphyrin-loading (arrows). Livers were examined for fibrosis using Sirius Red and biliary epithelial cells (KRT7) with the most prominent phenotype seen in *CYLD*<sup>ALPC</sup> mice. Scale bars as indicated. Adapted from Eißner et al. (2019)<sup>1</sup>.

The observed formation of brown pigment plugs in bile canaliculi after DDC exposure (Fig. 22) is a typical phenomenon of the porphyrinogenic drug and occurs due to increased biliary porphyrin deposition<sup>69</sup>. Here, it is noteworthy that *Cyld*<sup>ALPC</sup> and *Cyld/Relb*<sup>ALPC</sup> mice showed an additional porphyrin sequestration in the cytosol of hepatocytes (Fig. 22, arrows in H&E staining).

To study functional differences potentially leading to the development of the described cholestatic phenotypes, hepatocellular transporters were determined in DDC-treated mice (Fig. 23) since it has been reported that DDC exposure leads to an adaptive hepatic transporter expression in order to reduce bilirubin and hepatocellular accumulation of bile acids<sup>69,209</sup>.

For the visualization of potential changes between untreated and DDC-treated mice, only the untreated control group was depicted in Fig. 23, since the mRNA levels in the untreated mice were similar between all genotypes. Statistical changes were then always calculated between DDC-exposed mice to analyze potential differences between the knockout lines and control mice.

Gene expression analysis of the canalicular bile acid exporter *Bsep* revealed a dramatic repression in all DDC-fed mice with no differences between the strains (Fig. 23, Table 10).

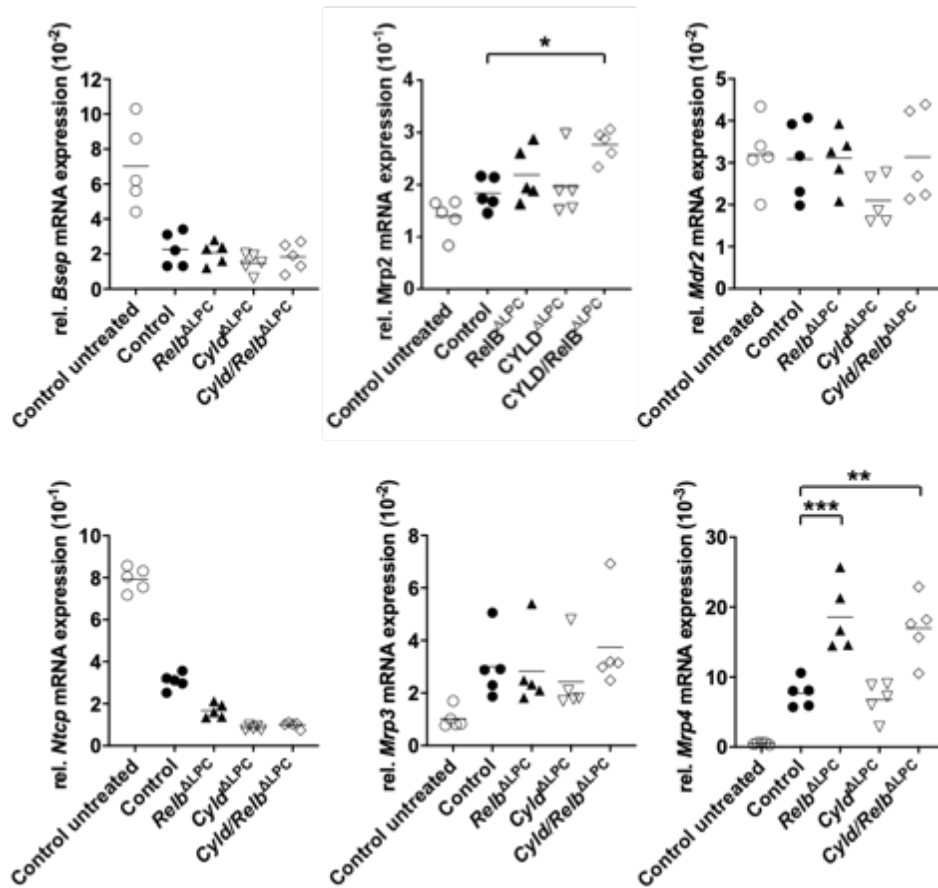


**Fig. 23. Impact of liver-specific full-length CYLD and RELB deficiency on bile acid transporter expression after DDC feeding.** mRNA analysis of different hepatic bile acid transporters in control animals fed with control chow (control untreated) and in mice after DDC feeding ( $n = 5$  male mice per group). Simultaneous repression of basolateral uptake transporter NTCP and canalicular export transporter BSEP in all DDC-fed mice compared with untreated control mice, with the strongest effect seen in *Cyld/Relb<sup>ALPC</sup>* mice. Basolateral exporter Mrp4 is highly upregulated after RELB deletion. NTCP, Na<sup>+</sup>/taurocholate cotransporting polypeptide; Mrp3, multidrug resistance associated protein 3; Mrp4, multidrug resistance associated protein 4; BSEP, bile salt export pump; Mrp2, multidrug resistance associated protein 2; Mdr2, multidrug resistance protein 2. Expression levels are normalized Gapdh and Rps6. Each symbol represents one individual mouse. Data are shown as means ( $n = 5$  mice per group). \*\* $p < 0.01$ , \*\*\* $p < 0.001$  and \*\*\*\* $p < 0.0001$  by one-way ANOVA and Tukey's multiple comparisons test compared with DDC-treated control mice. Adapted from Elßner et al. (2019)<sup>1</sup>.

The expression of *Mrp2*, a canalicular export protein of organic anions, was slightly upregulated in response to DDC with a significantly increase seen in *Cyld/Relb<sup>ALPC</sup>* mice compared with DDC-treated control mice ( $p = 0.0121$ ). No significant changes were detected in the biliary phospholipid exporter *Mdr2*.

**Table 10. Quantitative real-time PCR analysis of bile acid transporter in untreated control livers and DDC-fed livers.** Results are shown as means  $\pm$  SD. \* $p < 0.05$  \*\* $p < 0.01$ , \*\*\* $p < 0.001$  and \*\*\*\* $p < 0.0001$  by one-way ANOVA and Tukey's multiple comparisons test compared with DDC-treated control mice,  $n = 5$  mice per group.

Variables	Control untreated	Control	<i>Relb<sup>ALPC</sup></i>	<i>Cyld<sup>ALPC</sup></i>	<i>Cyld/Relb<sup>ALPC</sup></i>
<i>Bsep</i> ( $10^{-2}$ )	7.0 $\pm$ 2.4	2.3 $\pm$ 1.0	2.1 $\pm$ 0.6	1.5 $\pm$ 0.6	1.8 $\pm$ 0.8
<i>Mrp2</i> ( $10^{-1}$ )	1.4 $\pm$ 0.3	1.8 $\pm$ 0.3	2.2 $\pm$ 0.5	2.0 $\pm$ 0.6	2.8 $\pm$ 0.3*
<i>Mdr2</i> ( $10^{-2}$ )	3.2 $\pm$ 0.8	3.1 $\pm$ 0.9	3.1 $\pm$ 0.7	2.1 $\pm$ 0.6	3.1 $\pm$ 1.1
<i>Ntcp</i> ( $10^{-1}$ )	7.9 $\pm$ 0.6	3.0 $\pm$ 0.4	1.7 $\pm$ 0.3****	0.8 $\pm$ 0.1****	1.0 $\pm$ 0.1****
<i>Mrp3</i> ( $10^{-2}$ )	1.0 $\pm$ 0.4	3.0 $\pm$ 1.2	2.8 $\pm$ 1.5	2.4 $\pm$ 1.3	3.7 $\pm$ 1.8
<i>Mrp4</i> ( $10^{-3}$ )	0.5 $\pm$ 0.1	7.7 $\pm$ 2.0	18.6 $\pm$ 4.9***	6.8 $\pm$ 2.5	17.0 $\pm$ 4.5**

Hepatic transporter regulating the basolateral uptake (*Ntcp*) and export (*Mrp3* and *Mrp4*) were also differentially expressed after DDC exposure (Fig. 23, Table 10). Among them, *Ntcp* was significantly decreased in control mice after DDC feeding. In *Relb*<sup>ΔLPC</sup>, *Cyld*<sup>ΔLPC</sup>, and *Cyld/Relb*<sup>ΔLPC</sup> mice, *Ntcp* levels were even more reduced ( $p < 0.0001$  in all groups), suggesting a reduction in bile acid uptake by hepatocytes in these knockout mice. In contrast, the alternative sinusoidal exporter *Mrp3* and *Mrp4* were both upregulated. While DDC exposure resulted only in a 3-fold enhanced transcription of *Mrp3* in all transgenic mice, *Mrp4* expression was 15-fold upregulated in DDC-treated control mice (Fig. 23, Table 10). Interestingly, RELB deficient mice showed the strongest induction of *Mrp4* expression levels (35-fold increase compared with untreated mice, Fig. 23, Table 10). To confirm these findings on protein level and to investigate MRP4 localization, an immunofluorescent staining for MRP4 was performed (Fig. 24).

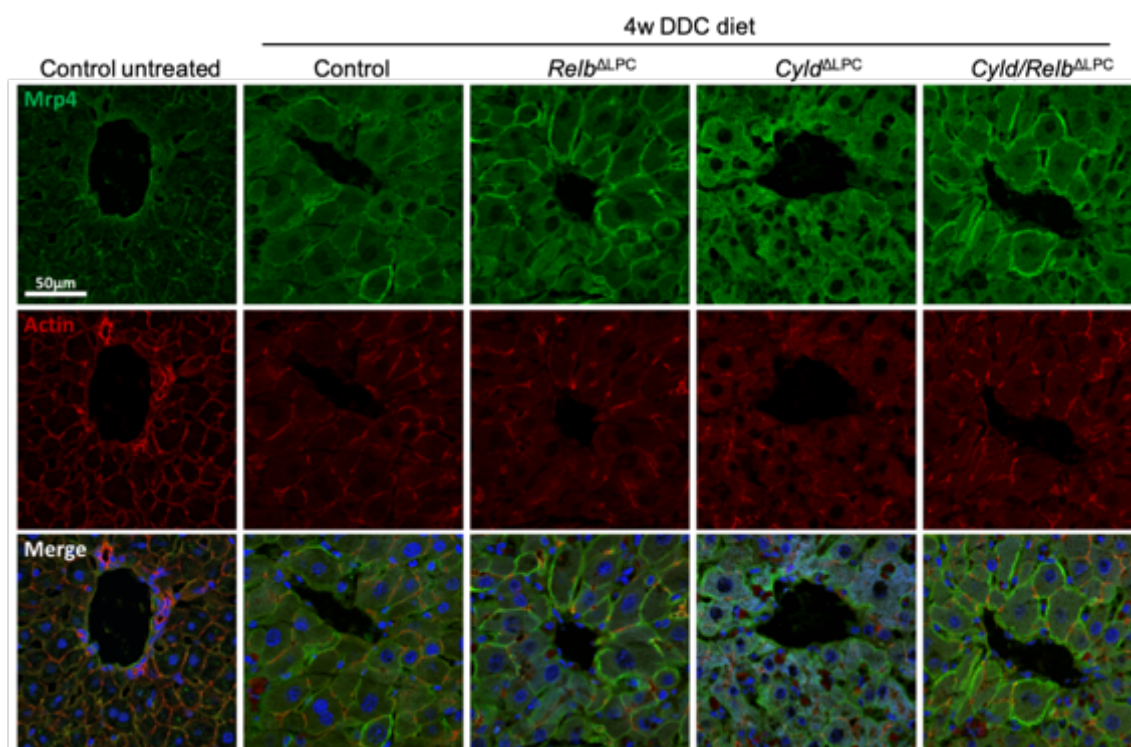


**Figure 24. MRP4 activation is highly upregulated in RELB deficient mice in response to a DDC diet.** Representative immunofluorescent staining in livers from mice fed with a DDC-supplemented diet for 4 weeks. MRP4 is shown in green, ACTIN was stained with Phalloidin in red and cell nuclei were stained blue with DAPI. In response to DDC, specific basolateral MRP4 expression was induced with the highest upregulation in *Relb*<sup>ΔLPC</sup> and *Cyld/Relb*<sup>ΔLPC</sup> mice. Adapted from Eißner et al. (2019)<sup>1</sup>.

As shown in Fig. 24, hepatic MRP4 was expressed at very low levels in untreated mice. Upon DDC feeding, expression and activity of MRP4 was increased, demonstrated by the localization of MRP4 to the basolateral membrane of hepatocytes especially in RELB deficient mice.

These results demonstrate a different modification of the transporter gene expression after DDC feeding, with MRP4 highly induced in RELB deficient mice which may influence the outcome of DDC-induced cholangiopathy.

## 5.2 Non-canonical NF- $\kappa$ B signaling in human chronic liver diseases and liver cancer

### 5.2.1 RELB expression is upregulated in human chronic liver diseases

A specific role of non-canonical NF- $\kappa$ B signaling in the pathogenesis of human chronic liver diseases has not been defined so far. The previous findings that RELB activation drives ductular reaction and biliary fibrosis in *Cyld*<sup>ALPC</sup> mice justified attempt to investigate an involvement of RELB in diseased human livers. Therefore, specimens of patients with HCV (n = 7) and HBV infections (n = 7), AIH (n = 5), NASH (n = 6), and ALD (n = 21) were immunohistochemically analyzed (Fig. 25A). By multiplying the staining quantity by staining intensity, a semi-quantitative immunohistochemical score (IHC score, ranging from 0 to 12) was calculated and evaluated (Fig. 25B).

Compared with healthy, normal liver tissue, nuclear RELB expression was significantly increased in hepatocytes of HCV-induced hepatitis (p = 0.0002), HBV- induced hepatitis (p < 0.0001), AIH (p = 0.0003), and ALD (p = 0.0022), indicating a universal transcriptional activity of RELB independent of the underlying liver disease (Fig. 25A and B).

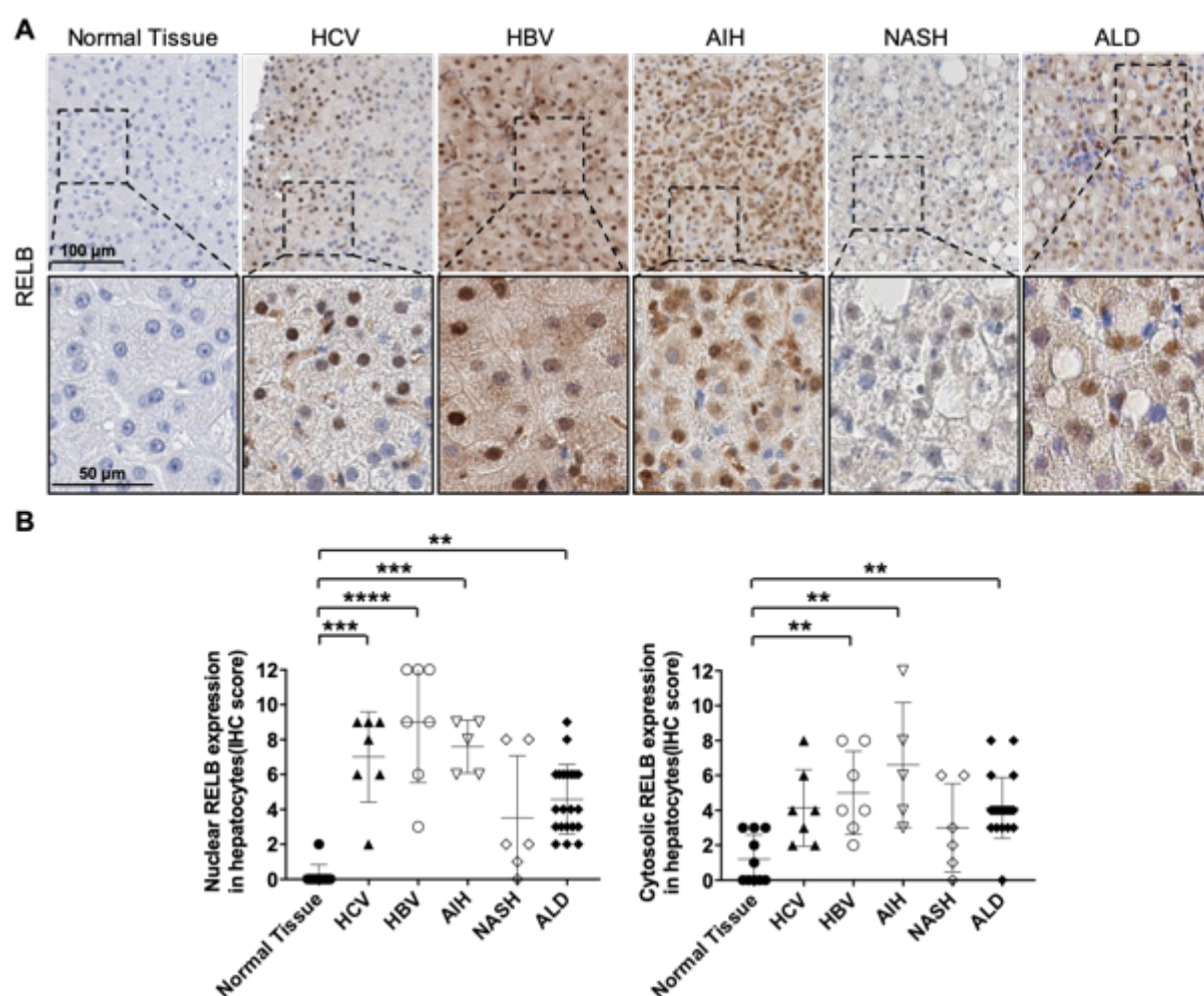


**Figure 25. RELB expression is upregulated in hepatocytes of human chronic liver diseases.** (A) Representative immuno-histochemical staining of RELB in human normal liver (n = 10), HCV (n = 7), HBV (n = 7), AIH (n = 5), NASH (n = 6), and ALD specimens (n = 21). NASH and ALD samples show typical lipid droplets ranging from small- to large-droplet steatosis. The ALD group included samples from patients with mild steatosis to patients with the more advanced form steatohepatitis. Scale bars as indicated. (B) Assessment of staining intensity and quality (IHC score 0-12), demonstrating an increased cytosolic and nuclear RELB expression in viral hepatitis, AIH and ALD. Data are represented as means  $\pm$  SD, \*p < 0.05, \*\*p < 0.01, \*\*\*p < 0.001 \*\*\*\*p < 0.0001 by Kruskal-Wallis and Dunn's comparisons test.

Besides elevated nuclear translocation of RELB, cytosolic fractions of HBV ( $p = 0.0051$ ), AIH ( $p = 0.0015$ ) and ALD specimens ( $p = 0.0014$ ) were also stained positive for RELB, which suggest not only an increased RELB activity but also an increased level of the inactive form in the cytoplasm, indicating overall elevated expression. On the contrary, neither nuclear nor cytosolic RELB expression levels were significantly altered in NASH specimens.

Since ductular reactions often occur in a variety of liver diseases, cholangiocytes in the periportal region were next examined for their RELB expression. As already seen in *Cyld*<sup>ALPC</sup> mice, cholangiocytes of HCV ( $p = 0.0198$ ), HBV ( $p = 0.0020$ ), AIH ( $p = 0.0333$ ), and ALD specimens ( $p < 0.0001$ ) showed significantly upregulated nuclear and cytosolic RELB expression compared with normal liver tissue (Fig. 26A and B, nuclear RELB expression in HCV:  $p = 0.0198$ , HBV:  $p = 0.0020$ , AIH:  $p = 0.0333$ , ALD:  $p < 0.0001$  and cytosolic RELB expression in HCV and HBV:  $p < 0.0001$ , AIH:  $p = 0.0005$ , ALD:  $p = 0.0014$ ). In contrast, NASH specimens were not significantly altered in their RELB expression. Together, these results indicate a potential role of RELB in the pathogenesis of viral hepatitis, AIH and ALD.

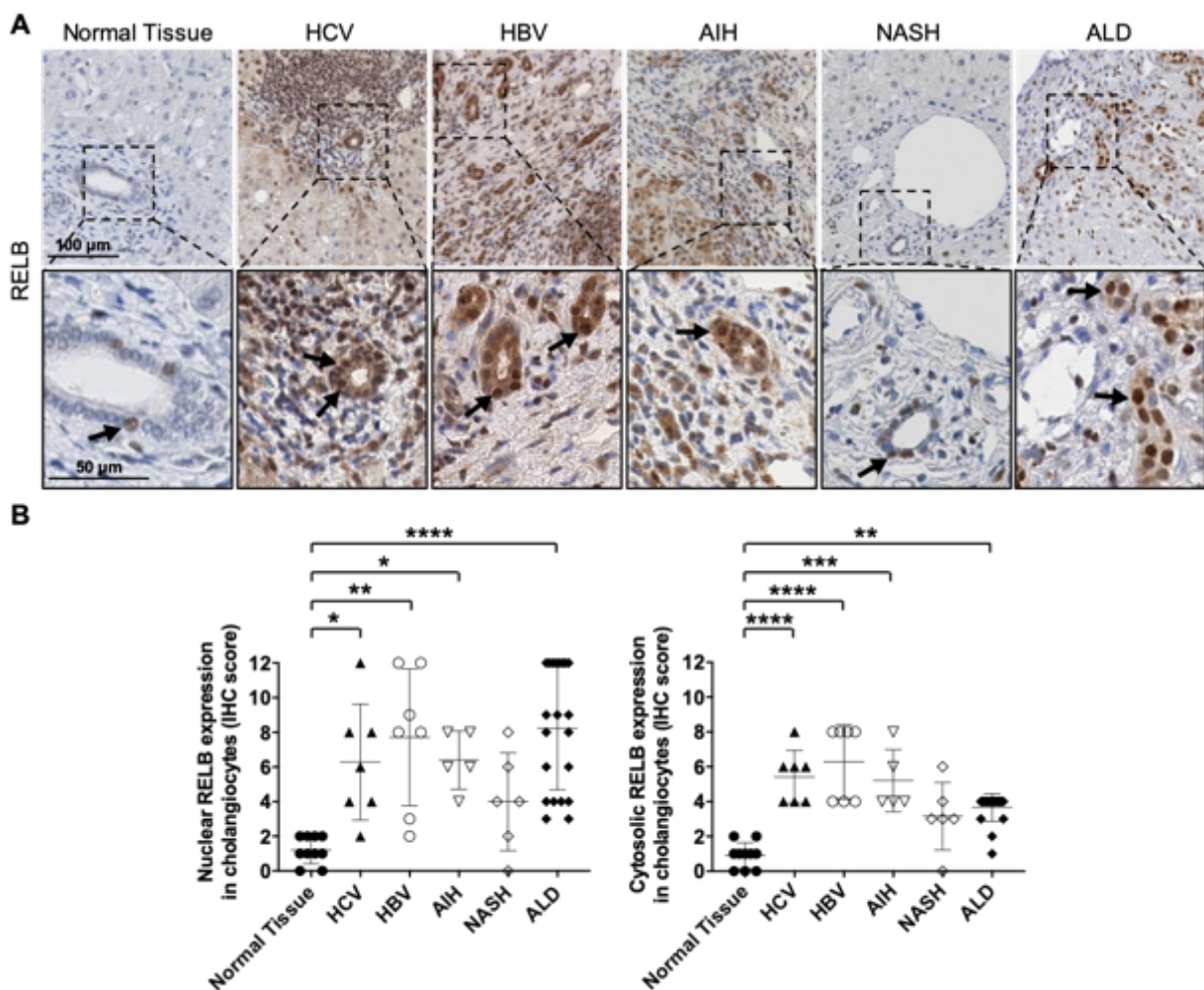


**Figure 26. Increased RELB expression in cholangiocytes of human chronic liver diseases.** (A) Representative immuno-histochemical staining of RELB in human normal liver ( $n = 10$ ), HCV ( $n = 7$ ), HBV ( $n = 7$ ), AIH ( $n = 5$ ), NASH ( $n = 6$ ), and ALD specimens ( $n = 21$ ). Scale bars as indicated. (B) Assessment of staining intensities by multiplying staining quantity and quality (IHC score 0-12). Cytosolic and nuclear RELB expression is significantly upregulated in viral hepatitis, AIH and ALD. Data are represented as means  $\pm$  SD, \* $p < 0.05$ , \*\* $p < 0.01$ , \*\*\* $p < 0.001$ , \*\*\*\* $p < 0.0001$  by Kruskal-Wallis and Dunn's comparisons test. Adapted from Eißner et al. (2019)<sup>1</sup>.

### 5.2.2 Nuclear translocation of RELB is increased in human hepatocellular carcinoma

Patients with chronic liver diseases and cirrhosis are at significant risk for HCC development. In order to investigate whether the expression of RELB is also altered during tumorigenesis of HCC, an HCC tissue microarray (TMA) was stained for RELB (Fig. 27).

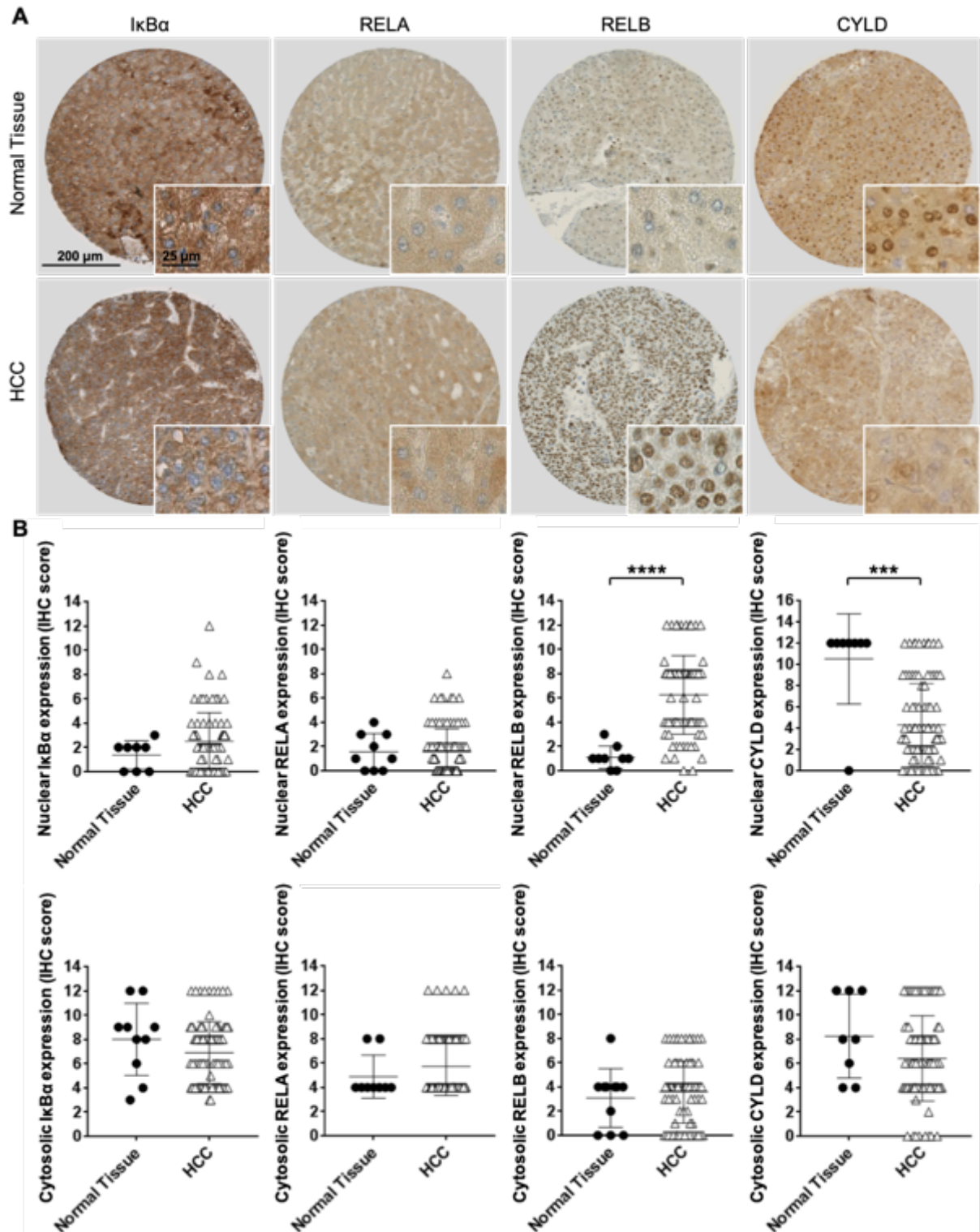


**Figure 27. Expression levels of IκBα, RELA, RELB, CYLD in human HCC.** (A) Representative immunohistochemical staining of IκBα, RELA, RELB, and CYLD on a TMA, containing normal liver (n = 8-10) and HCC specimens (n = 82-92). Scale bars as indicated. (B) Assessment of staining intensities by multiplying staining quantity and quality (IHC score 0-12), showing an increased nuclear RELB expression and decreased nuclear CYLD expression in HCC. Data are represented as means ± SD, \*\*\*p < 0.001 and \*\*\*\*p < 0.0001 by Mann-Whitney U test.

The TMA contained HCC samples of 92 patients with corresponding tumorous liver and normal liver tissue samples. Key regulatory and effector proteins involved in the canonical NF- $\kappa$ B signaling were additionally addressed by analyzing the expression of RELA, the inhibitor I $\kappa$ B $\alpha$ , and the deubiquitinase CYLD (Fig. 27A and B). Assessment of the immunohistochemical staining revealed no differences in the expression levels of I $\kappa$ B $\alpha$  and RELA in HCC specimens compared with normal liver (Fig. 27B). Neither the cytosolic nor the nuclear IHC score was altered. Interestingly, RELB expression was significantly upregulated in the nucleus of HCC specimens ( $p < 0.0001$ ), compared with normal liver tissue (Fig. 27A and B). In contrast to these findings, expression levels of the deubiquitinase CYLD were significantly decreased in HCC samples ( $p = 0.0006$ ). These data indicate that the non-canonical NF- $\kappa$ B pathway via RELB is more involved in HCC development than the canonical pathway via RELA and its inhibitor I $\kappa$ B $\alpha$ .

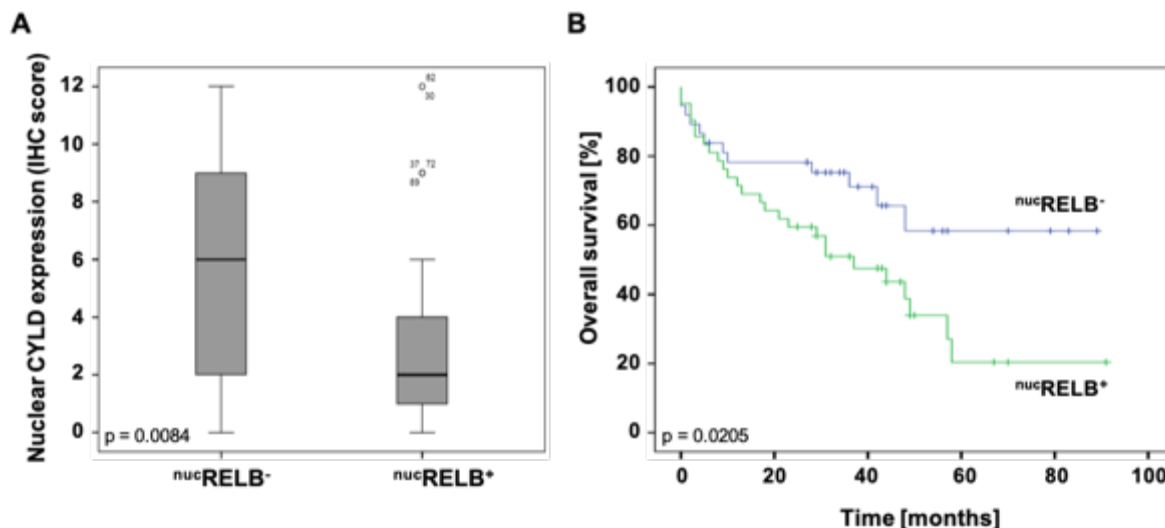
To further examine the effect of increased nuclear RELB expression in HCC patients, patients were grouped into two categories. Patients with an expression level lower the median IHC score of 8 were classified into the negative/low-expression group (<sup>nuc</sup>RELB<sup>-</sup>) and patients with an equal or higher expression level were classified into the positive/high-expression group (<sup>nuc</sup>RELB<sup>+</sup>). Nuclear RELB expression was then correlated with a variety of clinicopathological features. Characteristics of the HCC patients concerning gender, age, tumor stage, tumor size, AFP, bilirubin, Child-Pugh score, etiology, and therapy are listed in Table 11. 45 HCC patients (52 %) showed positive nuclear staining for RELB (<sup>nuc</sup>RELB<sup>+</sup>) and 41 HCC specimens (47 %) were classified as negative for nuclear RELB staining (<sup>nuc</sup>RELB<sup>-</sup>). The median age of HCC patients was 64 years. Gender distribution of cases showed male predominance with a male to female ratio of 3.3:1 (77 %: 23 %). The majority of HCC cases were classified as moderately-differentiated ( $n = 52$ ; 57%), while 25 cases (27 %) were categorized as poorly differentiated and 12 cases (13 %) as well-differentiated. Three cases (3 %) were classified as dedifferentiated. 55 % of the HCC patients had a tumor  $> 5$  cm associated with vascular invasion. 40 % of patients had liver cirrhosis due to viral hepatitis B or C and 24 % of patients due to alcohol abuse. Most patients had Child-Pugh score A (76%, B: 13%, and C: 11 %), 48 % of the total cohort had serum AFP levels  $> 8$  IU/ml and 34% increased bilirubin levels. 89% of patients received no therapy, 1% chemotherapy, and 10% TACE. Within all these clinicopathological features, no significant correlation with nuclear RELB could be observed.

Table 11. Baseline characteristics of HCC patients corresponding to nuclear RELB expression (<sup>nuc</sup>RELB<sup>+/−</sup>).

Variables	N	<sup>nuc</sup> RELB <sup>−</sup>		<sup>nuc</sup> RELB <sup>+</sup>		p value
<b>sex</b>	92	41		45		0.629
men	71 (77 %)	31 (76 %)	36 (80 %)			
women	21 (23 %)	10 (24 %)	9 (20 %)			
<b>age</b>	92	41		45		0.455
< 60 years	34 (37 %)	14 (34 %)	18 (40 %)			
≥ 60 years	58 (63 %)	27 (66 %)	27 (60 %)			
<b>grading</b>	92	41		45		0.081
G1	12 (13 %)	5 (12 %)	6 (13 %)			
G2	52 (57 %)	29 (71 %)	20 (44 %)			
G3	25 (27 %)	5 (12 %)	18 (40 %)			
G4	3 (3 %)	2 (5 %)	1 (2 %)			
<b>tumor size</b>	83	37		41		0.388
< 5 cm	37 (45 %)	19 (51 %)	17 (41 %)			
> 5 cm	46 (55 %)	18 (49 %)	24 (59 %)			
<b>vascular invasion</b>	83	36		41		0.516
negative	37 (45 %)	14 (39 %)	19 (46 %)			
positive	46 (55 %)	22 (61 %)	22 (54 %)			
<b>AFP</b>	80	37		39		0.498
< 8 IU/ml	42 (53 %)	20 (54 %)	18 (46 %)			
> 8 IU/ml	38 (48 %)	17 (46 %)	21 (54 %)			
<b>CHILD</b>	87	38		43		0.896
A	66 (76 %)	29 (76 %)	32 (74 %)			
B	11 (13 %)	4 (11 %)	6 (14 %)			
C	10 (11 %)	5 (13 %)	5 (12 %)			
<b>alcohol consumption</b>	88	39		44		0.580
negative	67 (76 %)	29 (74 %)	35 (80 %)			
positive	21 (24 %)	10 (26 %)	9 (20 %)			
<b>viral hepatitis</b>	88	38		44		0.897
-	51 (58 %)	23 (61 %)	24 (55 %)			
B	13 (15 %)	4 (11 %)	9 (20 %)			
C	19 (22 %)	8 (21 %)	10 (23 %)			
B/C	3 (3 %)	2 (5 %)	0 (0 %)			
B/D	2 (2 %)	1 (3 %)	2 (5 %)			
<b>bilirubin</b>	85	37		42		0.933
normal	56 (66 %)	25 (68 %)	28 (67 %)			
increased	29 (34 %)	12 (32 %)	14 (33 %)			
<b>therapy</b>	88	38		44		0.858
-	78 (89 %)	34 (89 %)	40 (91 %)			
chemotherapy	1 (1 %)	1 (3 %)	0 (0 %)			
TACE	9 (10 %)	3 (8 %)	4 (9 %)			

### 5.2.3 Expression of nuclear RELB is associated with poor overall survival in HCC patients

Next, the question was addressed whether nuclear RELB expression correlates with nuclear expression levels of CYLD, since nuclear CYLD expression levels were significantly reduced in HCC specimens (Fig. 27A and B)<sup>194</sup>. As presented in Fig. 28A, nuclear RELB expression inversely correlated with nuclear CYLD expression ( $p = 0.0084$ ). Patients in the <sup>nuc</sup>RELB<sup>+</sup> group showed a lower nuclear CYLD expression compared with patients in the <sup>nuc</sup>RELB<sup>-</sup> group.



**Figure 28. Nuclear RELB expression in correlation to nuclear CYLD expression and overall survival in human HCC.** (A) Nuclear expression of RELB related to nuclear CYLD expression in HCC (<sup>nuc</sup>RELB<sup>+</sup>,  $n = 45$  and <sup>nuc</sup>RELB<sup>-</sup>,  $n = 41$ ). Spearman correlation coefficient:  $-0.283$ ,  $p = 0.0084$ . (B) Kaplan-Meier analysis of overall survival (OS) in HCC patients with positive (<sup>nuc</sup>RELB<sup>+</sup>,  $n = 42$ ) and negative nuclear RELB expression (<sup>nuc</sup>RELB<sup>-</sup>,  $n = 37$ ,  $p = 0.0205$  by log-rank test), showing shorter OS for <sup>nuc</sup>RELB<sup>+</sup> HCC patients. Positive nuclear RELB staining (<sup>nuc</sup>RELB<sup>+</sup>) was defined as an immunohistochemical score (IHC score)  $\geq 8$ .

Because it has been reported that nuclear CYLD expression is strongly associated with improved overall survival of HCC patients<sup>194</sup>, Kaplan-Meier analysis were performed to assess the relationship between nuclear RELB expression and clinical outcome of HCC patients (Fig. 28B). Strikingly, <sup>nuc</sup>RELB<sup>+</sup> was significantly associated with poor overall survival ( $p = 0.0205$ ). The 1-/3-/5-year overall survival rates were 75/53/21 % for patients with <sup>nuc</sup>RELB<sup>+</sup> compared to 83/75/62 % for the <sup>nuc</sup>RELB<sup>-</sup> group.

The results presented here point to an activation of non-canonical NF- $\kappa$ B signaling via RELB during the tumorigenesis of HCC. Particularly noteworthy is the negative correlation between nuclear RELB translocation and the overall survival of HCC patients.

### 5.2.4 Nuclear RELB expression is elevated in cholangiopathies and intrahepatic cholangiocarcinoma

The previous observation that RELB is involved in the pathogenesis of HCC and chronic liver diseases targeting the hepatocytes raised the question whether RELB plays also a potential role in the development of cholangiopathies. Cholangiopathies refer to a group of chronic liver injuries affecting primarily the cholangiocytes. Therefore, specimens of the two common cholangiopathies PSC and PBC, categorized in early and late stage, were immunohistochemically analyzed for hepatocytic and

cholangiocytic RELB (Fig. 29A). Evaluation of the IHC score (Fig. 29B) revealed an enhanced RELB expression in hepatocytes of cholangiopathies, with the strongest increase detected in early stage PSC (nuclear RELB:  $p = 0.0052$ , cytosolic RELB:  $p = 0.0168$ ) and PBC (nuclear RELB:  $p = 0.0003$ , cytosolic RELB:  $p = 0.0024$ ) compared with normal liver tissue.

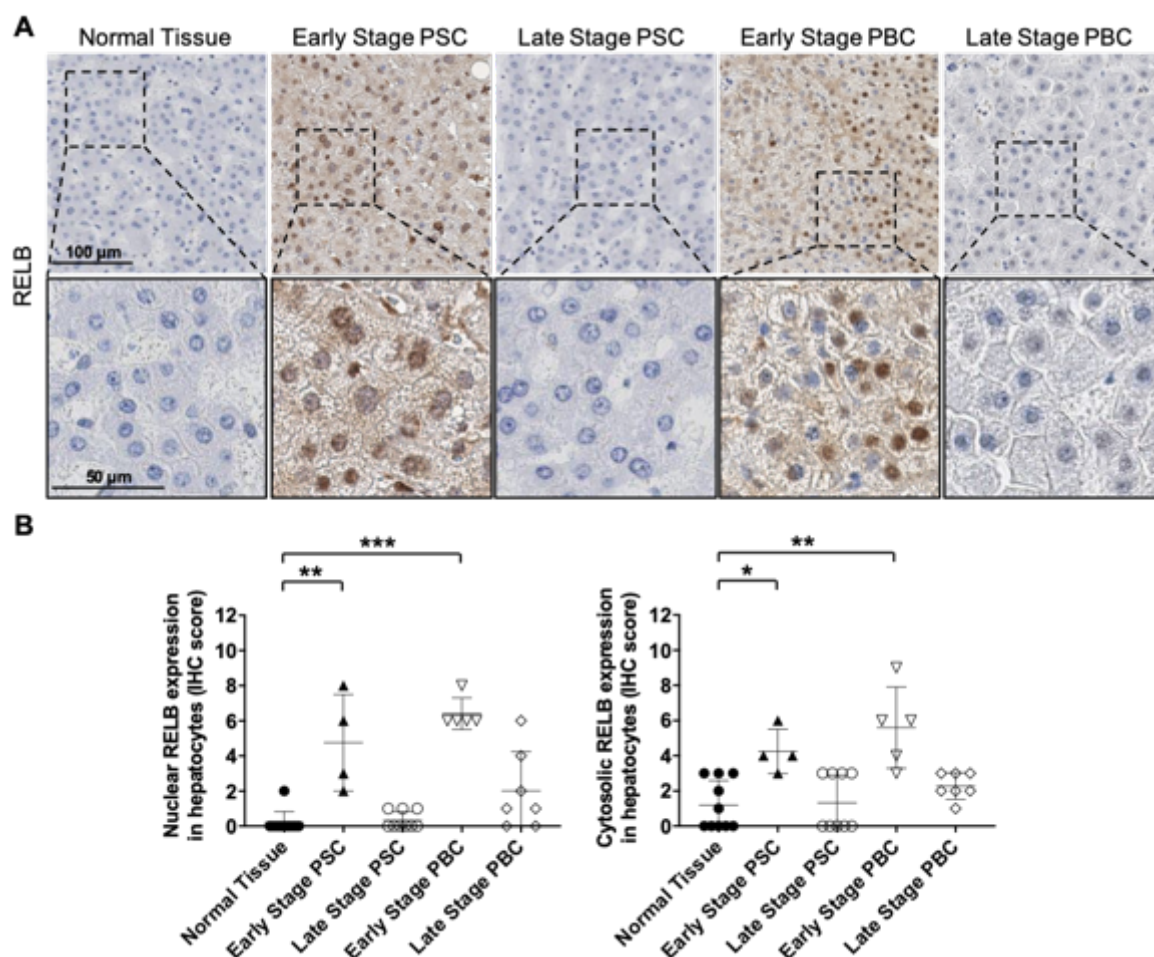


**Figure 29. RELB expression in hepatocytes of human cholangiopathies.** (A) Representative immunohistochemical staining of RELB in human normal liver ( $n = 10$ ), early stage PSC ( $n = 4$ ), late stage PSC ( $n = 9$ ), and early stage PBC ( $n = 5$ ), late stage PBC ( $n = 7$ ). Scale bars as indicated. (B) Assessment of staining intensities by multiplying staining quantity and quality (IHC score 0-12) revealed and increased nuclear RELB expression in early stage PSC, PBC and ICC. Data are represented as means  $\pm$  SD, \* $p < 0.05$ , \*\* $p < 0.01$ , \*\*\* $p < 0.001$  \*\*\*\* $p < 0.0001$  by Kruskal-Wallis and Dunn's comparisons test. Adapted from Elßner et al. (2019)<sup>1</sup>.

Focusing on cholangiocytic RELB expression in cholangiopathies (Fig. 30), assessment of the expression levels resulted in similar findings seen in hepatocytes (Fig. 29). Nuclear and cytosolic RELB expression was significantly upregulated in early stage PSC (nuclear RELB:  $p = 0.0354$ , cytosolic RELB:  $p = 0.0025$ ) and early stage PBC (Fig. 30A and B, nuclear RELB:  $p = 0.0038$ , cytosolic RELB:  $p = 0.0009$ ) compared with normal liver tissue. In addition to PSC and PBC samples, RELB expression was also determined in specimens of patients with intrahepatic cholangiocarcinoma (ICC, Fig. 30A and B) since it has been widely accepted that ICC is a tumor arising from malignant transformation of cholangiocytes. Immunohistochemical staining showed a significant upregulation of RELB in the nucleus of ICC cells ( $p = 0.0206$ ) compared with normal liver (Fig. 30B). In contrast, no significant differences in the expression levels of nuclear or cytosolic RELB between normal liver, late stage PSC, and late stage PBC tissues were found.

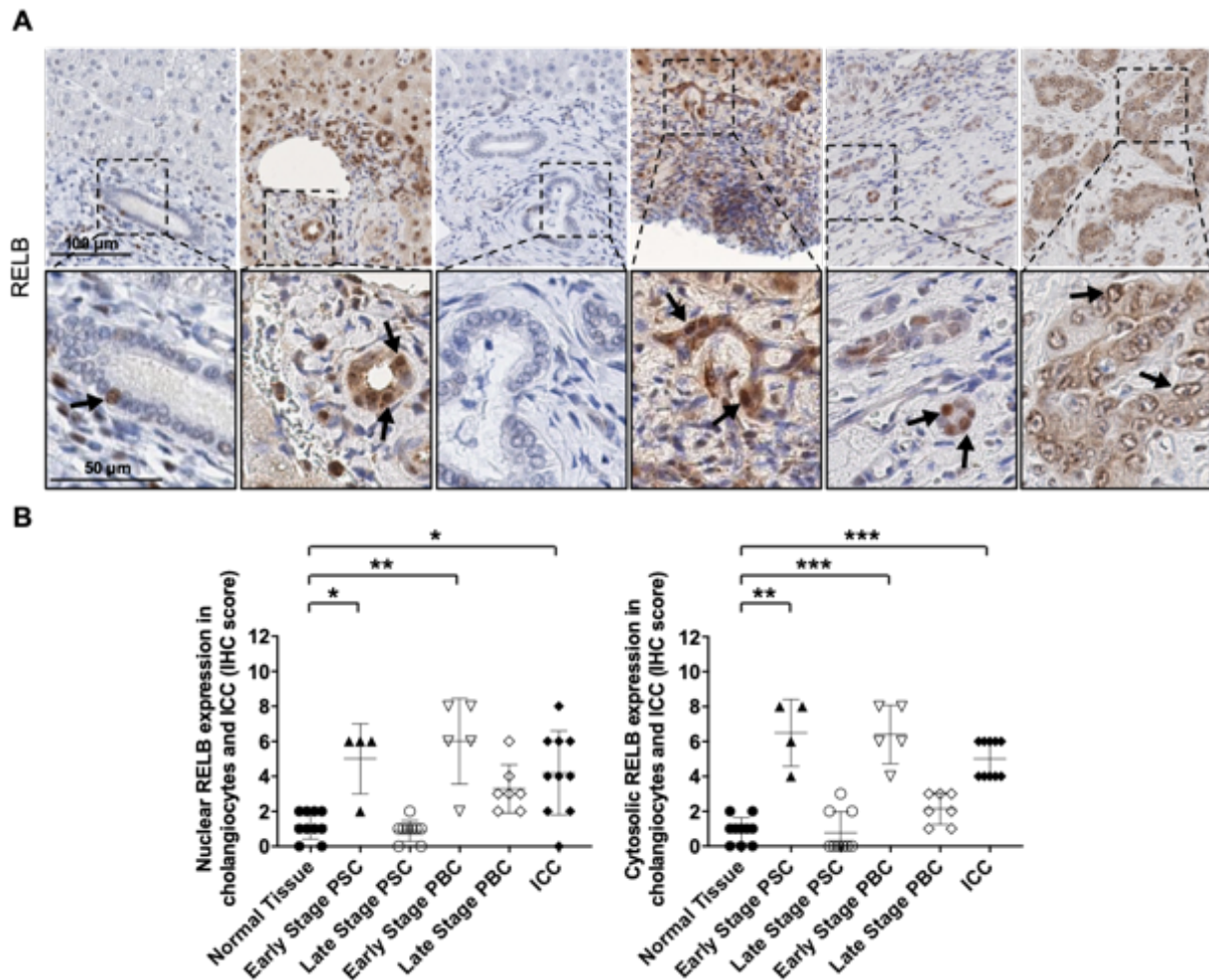


**Figure 30. RELB expression in cholangiocytes of human cholangiopathies.** (A) Representative immunohistochemical staining of RELB in human normal liver (n = 10), early stage PSC (n = 4), late stage PSC (n = 9), early stage PBC (n = 5), late stage PBC (n = 7), and ICC specimens (n = 10). Scale bars as indicated. (B) Assessment of staining intensities by multiplying staining quantity and quality (IHC score 0-12), demonstrating an increased cytosolic and nuclear RELB expression in early stage PSC, PBC, and ICC. Data are represented as means  $\pm$  SD, \* $p < 0.05$ , \*\* $p < 0.01$ , \*\*\* $p < 0.001$  by Kruskal-Wallis and Dunn's comparisons test. Adapted from Elßner et al. (2019)<sup>1</sup>.

### 5.2.5 Hepatic LT $\beta$ expression as a link to sustained RELB activation

Among the cytokines that stimulate the activation of non-canonical NF- $\kappa$ B, LT $\beta$  showed the strongest upregulation in *Cyld*<sup>ALPC</sup> mice. While reactive cholangiocytes represented the cellular source of LT $\beta$  in this mouse model, other studies demonstrated that LT $\beta$  expression by hepatocytes is responsible for chronic liver injury upon HCV and HBV infection<sup>167</sup>. To further assess a possible causal relationship between increased overall RELB activation and LT $\beta$ , human liver specimens with different pathologies were stained for LT $\beta$ . LT $\beta$  was found to be only slightly upregulated in hepatocytes of HBV-induced hepatitis and AIH, but not in HCV-induced liver disease and NASH (Fig. 31A, upper panel, 32B).

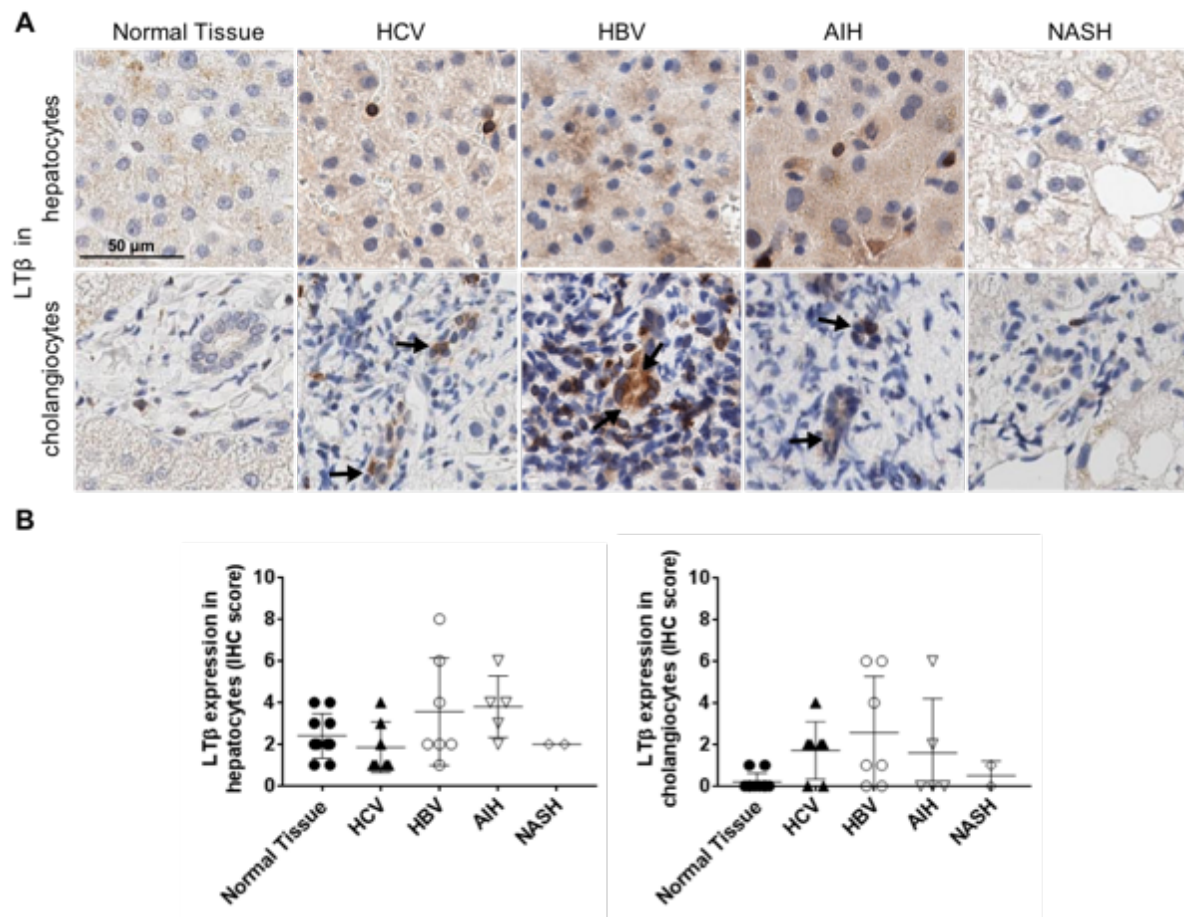


**Figure 31. LTβ expression in human chronic liver diseases.** Representative immunohistochemical staining of LTβ in normal liver (n = 10), HCV (n = 7), HBV (n = 7), AIH (n = 5), and NASH specimens (n = 2). Scale bar as indicated. Arrows indicate LTβ expression in cholangiocytes. (B) Assessment of LTβ expression (IHS 0-12), data are represented as means ± SD. No significant differences were measured by Kruskal-Wallis and Dunn's multiple comparisons test. Adapted from Eißner et al. (2019)<sup>1</sup>.

Evaluation of cholangiocyte LTβ expression revealed LTβ positive cholangiocytes in HBV-, HCV-induced hepatitis and AIH (Fig. 31A, lower panel, 31B), but displayed in total no significant differences compared with normal liver tissue most likely due to the heterogeneous distribution within each group.

To examine whether LTβ signaling might be responsible for the RELB upregulation in cholangiopathies, PSC and PBC samples were additionally analyzed for LTβ. Expression of LTβ was significantly upregulated in cholangiocytes of early but not late stage PSC (p = 0.0428) and PBC (Fig. 32A, lower panel, 32B, p = 0.0110). In hepatocytes, only early stage PBC specimens exhibited a trend towards increased LTβ expression (Fig. 32A, upper panel, 32B).

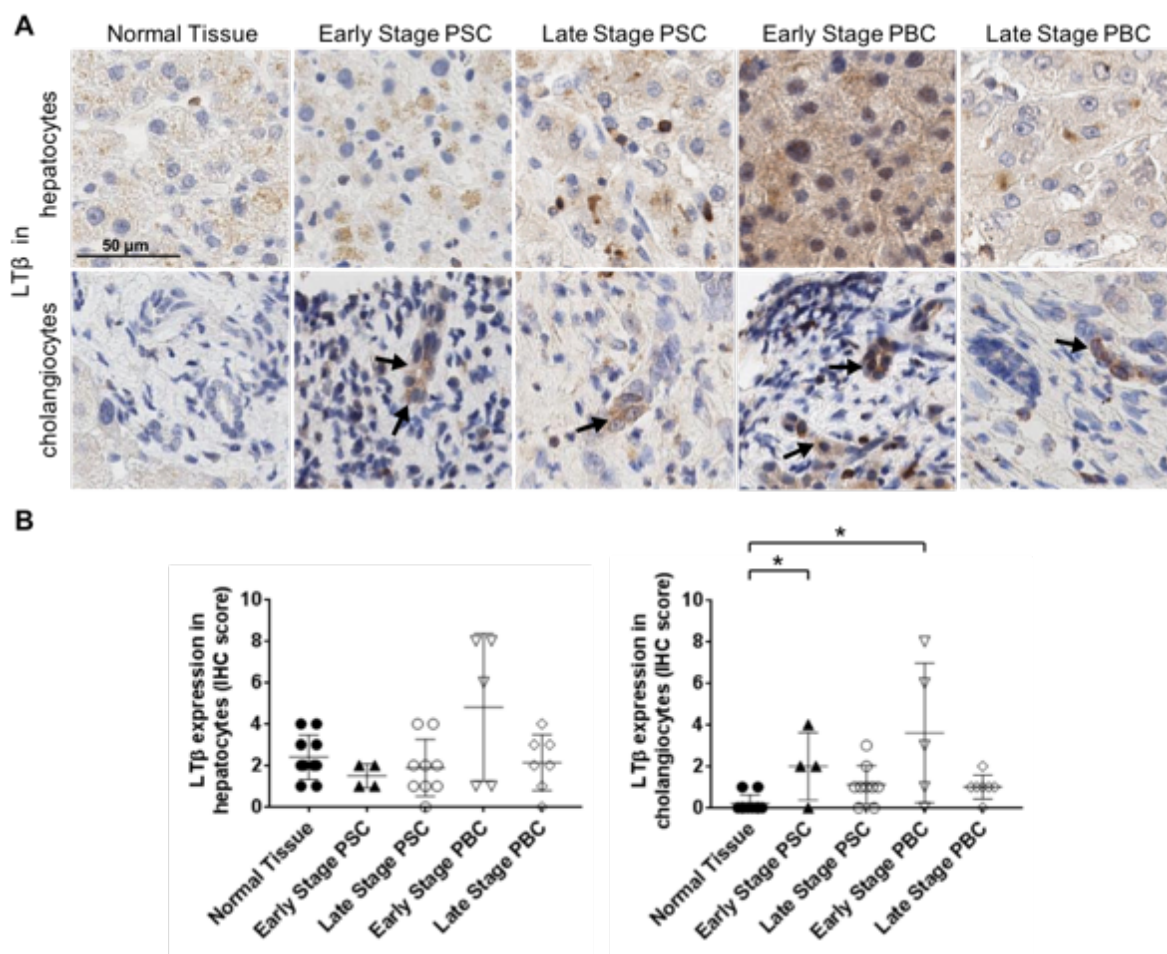


**Figure 32. Increased LT $\beta$  expression in early stage PSC and PBC.** (A) Representative immunohistochemical staining of LT $\beta$  in normal liver (n = 10), early stage PSC (n = 4), late stage PSC (n = 9), early stage PBC (n = 5), and late stage PBC specimens (n = 7) demonstrating an elevated LT $\beta$  expression in cholangiocytes of early stage cholangiopathies. Scale bars as indicated. Arrows indicate LT $\beta$  expression. (B) Assessment of an immunohistochemical score (IHS) for LT $\beta$  by multiplying staining quantity and quality (IHS 0-12), data are represented as means  $\pm$  SD, \*p<0.05 by Kruskal-Wallis and Dunn's multiple comparisons test. Adapted from Elßner et al. (2019)<sup>1</sup>.

In cholangiopathies, cholangiocytes are the primary target cell. During these pathologies, usually quiescent cholangiocytes acquire a reactive phenotype and start to proliferate<sup>210</sup>. The finding that RELB drives cholangiocyte proliferation and ductular reaction in a mouse model, raised the question whether human cholangiocytes show similar dependency on RELB and LT $\beta$ . To elucidate the role of RELB for cholangiocyte proliferation *in vitro*, normal human cholangiocytes were cultured and stimulated with the specific LT $\beta$  receptor ligand LT $\alpha$ 1 $\beta$ 2 (Fig. 33). As shown in Fig. 33C, LT $\beta$  receptor ligation induced significantly the proliferation of normal human cholangiocytes. Indeed, this mechanism was RELB mediated, because knockdown of RELB expression (shown in Fig. 33B) led to significant reduced proliferation of the cholangiocytes.

Together, these findings demonstrate the important role of RELB in regulating cholangiocyte proliferation with LT $\beta$  as possible cytokine triggering RELB activation in cholangiocytes of early stage PBC and PSC.

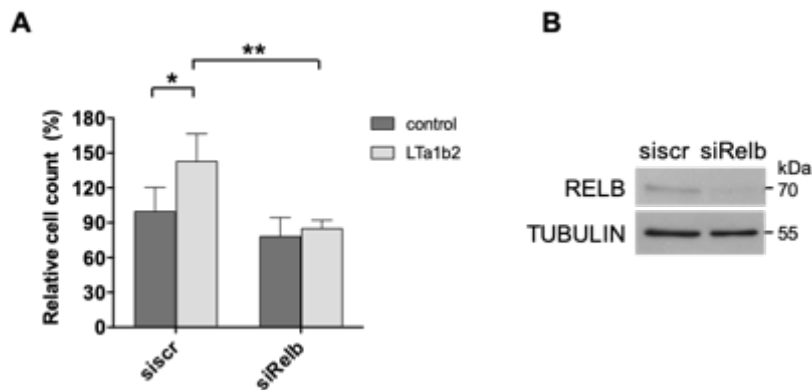


**Figure 33. LT $\beta$  links RELB activation to cholangiocyte proliferation.** Normal human cholangiocytes (NHC) were transfected with scrambled siRNA and siRelb. Relative cell count was determined after 48 hours of incubation with recombinant LTA1b2 (250 ng/mL). Western blot analyses of normal human cholangiocytes confirm siRNA-mediated knockdown of RELB. TUBULIN served as a loading control. Results are shown as mean  $\pm$  standard deviation. \*P<0.05; \*\*P<0.01. Adapted from Eißner et al. (2019)<sup>1</sup>.

In conclusion, the results imply an aberrant RELB overexpression in a variety of human chronic liver diseases, early stage cholangiopathies and primary liver cancer (HCC and ICC) with LT $\beta$  as a possible upstream effector and/or downstream target promoting a perpetuating feedback mechanism of sustained RELB upregulation.

## 6. Discussion

Chronic liver diseases are a major global health problem and a significant source of morbidity and mortality, with cirrhosis, viral hepatitis and HCC representing major causes of death<sup>211</sup>. HCC mostly arises within a background of chronic inflammation and liver fibrosis, but due to the clinically asymptomatic course of HCC, it is often diagnosed at an advanced stage. Therapeutic options are currently still restricted and lacks long-term efficacy so that therapies have only a limited impact on overall survival<sup>188,89</sup>. Therefore, intensive research on the underlying molecular mechanisms that drive the transition from chronic liver diseases to HCC is needed to identify new therapeutic targets and develop new potential strategies for therapy.

The NF- $\kappa$ B signaling pathway plays pivotal roles in immune and inflammatory responses and has been shown to be activated in numerous chronic liver diseases such as ASH, NASH, viral hepatitis, and biliary liver diseases<sup>160,161,163</sup>. In the recent years, crucial functions of NF- $\kappa$ B have been demonstrated not only in mediating chronic inflammation but also in the development of HCC<sup>170</sup>. However, most studies investigated the canonical NF- $\kappa$ B signaling pathway with its inducible transcription factor RELA, whereas relatively little is known about a contribution of non-canonical NF- $\kappa$ B via RELB to chronic liver diseases and liver cancer. Thus, the aim of this study was to characterize the role of RELB for liver homeostasis, chronic liver injury and hepatocarcinogenesis.

### 6.1 The role of RELB in a mouse model with ductular reaction and biliary fibrosis

In unstimulated cells, NF- $\kappa$ B subunits are mostly bound to inhibitory proteins and remain inactive as hetero- or homodimers in the cytoplasm. In the murine liver, RELB expression appears to have dispensable functions during liver development as shown by mice carrying a germline mutation of the RELB gene. RELB deficient animals only developed defects in their immunity associated with a multiorgan inflammation, indicating essential roles in the hematopoietic system but no crucial function for liver development and homeostasis<sup>159</sup>.

To investigate the role of RELB in the development of chronic liver diseases, an established mouse model (*Cyld*<sup>ALPC</sup> mice) with prolonged RELB activation accompanied by ductular reaction and biliary fibrosis was used. The deubiquitinase CYLD acts as a major enzyme negatively regulating NF- $\kappa$ B activation by removing K63-linked polyubiquitin chains from NF- $\kappa$ B signaling components. This process inhibits IKK activation and the following phosphorylation of I $\kappa$ Bs, keeping NF- $\kappa$ B subunits inactive in the cytoplasm<sup>127,212</sup>. However, CYLD mainly deubiquitinates signaling molecules involved in the canonical NF- $\kappa$ B pathway, which is why it was surprising that non-canonical NF- $\kappa$ B signaling components with its key players RELB and p52 showed the strongest induction<sup>179</sup>. To obtain direct evidence whether RELB contributes to the ductular reaction and biliary fibrosis in *Cyld*<sup>ALPC</sup> mice, a double knockout mouse with a liver-specific deletion in full-length CYLD and RELB (*Cyld/Relb*<sup>ALPC</sup>) was generated.

Analysis of *Cyld/Relb*<sup>ALPC</sup> showed that the biliary phenotype of *Cyld*<sup>ALPC</sup> mice strictly depends on the activation of RELB. Increased proliferation of periportal ductules, expansion of the liver progenitor niche and the development of biliary fibrosis in *Cyld*<sup>ALPC</sup> mice were completely prevented in *Cyld/Relb*<sup>ALPC</sup>. To date, only a role of canonical NF- $\kappa$ B signaling through RELA has been described for ductular reaction. Thereby, activation of RELA leads to JAGGED1/NOTCH signaling, which induces cholangiocyte proliferation and the differentiation from liver progenitor cells into cholangiocytes<sup>213</sup>. Strikingly, two other studies already demonstrated an increased non-canonical NF- $\kappa$ B expression in mice lacking full-length CYLD. In 2007, Hövelmeyer et al. described CYLD mutant B cells, which exhibited prolonged B cell survival, massively enlarged secondary lymphoid organs together with a dramatic accumulation of mature B cells. The authors concluded at that time that p100 and RELB or the nuclear Bcl-3 together with p100 induced the expression of Bcl-2, which might lead to elevated B cell survival<sup>178</sup>. Tesio et al. investigated 2015 long-term quiescence of hematopoietic stem cells. Conditional knockout of the catalytic domain of CYLD induced dormant hematopoietic stem cells to exit their quiescence due to increased activation of the p38 pathway. However, the authors stated that loss of functional CYLD did not activate NF- $\kappa$ B signaling although NF- $\kappa$ B2 was significantly changed<sup>202</sup>. Both studies described in different cell entities an upregulation of non-canonical NF- $\kappa$ B signaling after loss of full-length CYLD. The finding that RELB rescued the phenotype of liver-specific CYLD loss led suggest a contribution of non-canonical NF- $\kappa$ B in B cell homeostasis and maintenance of stem cell dormancy as well.

The results presented in this study describe for the first time an essential contribution of RELB to ductular reaction and cholangiocyte proliferation. Hereby, RELB is the central force involved in cholangiocyte homeostasis and responsible for the spontaneous biliary phenotype in *Cyld*<sup>ALPC</sup> mice.

Since ductular reactions are accompanied or driven by the presence of portal inflammation, analysis of inflammatory immune cells and expression of cytokines was addressed next in the mouse models. The strong increase of proinflammatory cytokines such as CCL2, TNF- $\alpha$ , and TGF- $\beta$ 2 and ligands activating non-canonical NF- $\kappa$ B signaling including LT $\beta$ , RANKL, BAFF, CD40LG, and LIGHT was again RELB driven in *Cyld*<sup>ALPC</sup> mice since *Cyld/Relb*<sup>ALPC</sup> mice displayed normal levels compared to control mice. However, in contrast to this strong activation of cytokine components, only few portal T cell infiltrates were detected in *Cyld*<sup>ALPC</sup> mice. By tracing the cellular origin of cytokine transcription, the hypothesis was investigated whether so called reactive cholangiocytes within the ductular reactions are responsible for their secretion<sup>69</sup>. Importantly, it has been shown recently that cholangiocytes represent not only targets for inflammatory cytokines but also actively contribute to the pathogenesis of liver diseases. In response to liver injury, cholangiocytes can become reactive, lose their differentiated epithelial phenotype and acquire the ability to express adhesion molecules such as VCAM<sup>69</sup>, secrete proinflammatory cytokines and chemokines including TNF- $\alpha$ , IL-6, IL-8, CCL2, and growth factors such as TGF- $\beta$ 2<sup>214</sup>. Thus, these molecules and mediators enable an extensive communication between cholangiocytes and other liver cells such as hepatic stellate cells, endothelial and inflammatory cells. In the present study, detection of highly upregulated VCAM expression in biliary epithelial cells of *Cyld*<sup>ALPC</sup> livers indicated a transformation to reactive cholangiocytes. Intriguingly, *in situ* hybridization for LT $\beta$ , one of the strongest upregulated proinflammatory cytokines in *Cyld*<sup>ALPC</sup> mice, revealed the localization of LT $\beta$  exclusively in keratin 7 and A6 positive cells. This is in line with a previous study by Ruddell et al., demonstrating in a dietary model of chronic liver

injury that  $LT\beta$  was expressed by liver progenitor cells. Interaction with adjacent  $LT\beta$  receptor expressing hepatic stellate cells mediated wound healing and regeneration in response to chronic liver injury<sup>215</sup>. Furthermore, autocrine and/or paracrine secretion of cytokines by reactive cholangiocytes would explain the significant discrepancy between the strongly increased cytokine levels and the mild cellular inflammation. Although *Cyld/Relb*<sup>ALPC</sup> livers displayed no ductular reaction, cholangiocytes were still positive for VCAM1 expression and  $LT\beta$ , but in a significantly lower amount. This finding let suggest that *Cyld/Relb*<sup>ALPC</sup> partly maintained their reactive phenotype but RELB deficiency inhibited further proliferation of cholangiocytes and ductular reaction.

Together, loss of full-length CYLD induces the transformation of cholangiocytes to become reactive but sustained RELB activation mediates cholangiocyte proliferation and ductular reaction. Among the elevated cytokines, especially  $LT\beta$  seems to be the main trigger/downstream effector for sustained RELB activation in biliary epithelial cells.

The tumor suppressor CYLD exerts its major role as deubiquitinase in posttranslational modification of NF- $\kappa$ B signaling molecules<sup>126,127,212</sup>. Since CYLD has a predominant role as a negative regulator of NF- $\kappa$ B, suppressed expression of CYLD and persistent NF- $\kappa$ B activation has been observed in several human malignancies such as colon and hepatocellular carcinomas<sup>175</sup>, lung cancer<sup>216</sup>, multiple myeloma<sup>177</sup> and melanoma<sup>176</sup>. The finding that RELB deletion rescued the biliary phenotype of *Cyld*<sup>ALPC</sup> livers histologically, raised the question whether RELB deficiency also affects the NF- $\kappa$ B signaling on protein levels. Expression of TRAF2, RIP1, NEMO, and TAK1 was upregulated in *Cyld*<sup>ALPC</sup> livers due to the inability of truncated CYLD to deconjugate their ubiquitin chains<sup>127,178,179</sup>.

Constitutive activation of TAK1 in livers lacking functional CYLD has also been described in another mouse model, published by the group of Nikolaou et al. in 2012. Liver-specific truncation of CYLD by deletion of exon 9 resulted in a deubiquitinase-deficient form of CYLD. In these mice, JNK mediated hepatocyte death triggered inflammation, progressive fibrosis, and late onset HCC. Additional deletion of TAK1 reduced liver fibrosis and hepatocyte apoptosis of these mice but was not able to rescue the phenotype. Instead, double knockout mice resembled very much TAK1 knockout mice and developed spontaneous liver tumors at 4 months of age<sup>180</sup>. As the results of the present work imply a crucial role of RELB after loss of full-length CYLD, a contribution of RELB to the phenotype of the CYLD mouse model described by Nikolaou et al. would be likely.

With regard to cholangiocytes, ablation of TAK1 caused biliary ductopenia and cholestasis, while increased activation of TAK1 was conversely associated with induced ductular reaction<sup>155</sup>. This indicates a causative link between TAK1 activation and the biliary phenotype.

Astonishingly, increased levels of TRAF2, RIP1, NEMO, and TAK1 were completely diminished in *Cyld/Relb*<sup>ALPC</sup> mice, which let suggest a yet unknown interaction between canonical and non-canonical NF- $\kappa$ B signaling.

Analysis of further downstream NF- $\kappa$ B signaling components such as non-canonical p52 and its precursor p100 revealed increased expression levels in *Cyld*<sup>ALPC</sup> mice, which were completely abolished after RELB deletion. Within the NF- $\kappa$ B signaling cascade, a key function of RELB lies in controlling the balance between unprocessed p100 and its processed form p52. It has been demonstrated that RELB competes with the kinases NIK and IKK $\alpha$  for binding to p100. Changes in the protein concentrations of RELB and NIK/IKK $\alpha$  are critical for the balance between processing and protection of p100<sup>217</sup>. Marked upregulation of p100 expression and processing to p52 in *Cyld*<sup>ALPC</sup> livers might be attributed to increased RELB protein levels and is thereby abrogated in RELB deficient mice. This can be supported by the finding of an unaltered NIK expression, implying a lack of NIK induction during activation of RELB.

Focusing on canonical NF- $\kappa$ B signaling pathway, only proteins levels of C-REL and p105/p50 were found to be elevated. Main signaling molecules such as RELA, IKK $\alpha$ , IKK $\beta$ , and I $\kappa$ B $\alpha$  were surprisingly not altered in its activation. While RELA/p50 represent in general the most abundant NF- $\kappa$ B dimers, p50 also forms dimeric complexes with C-REL. C-REL has been reported to be an important regulator for liver regeneration and fibrogenic response to toxic injury<sup>218</sup>. During the differentiation of B cells, a switch from predominantly cytoplasmic RELA/p50 to nuclear C-REL/p50 heterodimers have been observed<sup>219,220</sup>. C-REL and p50 are also able to homodimerize<sup>221</sup>, in contrast to RELB, which is unique in this and does not homodimerize. Moreover, RELB is unable to heterodimerize with RELA and C-REL and exists only as heterodimers with p100, p52 and p50<sup>103,222</sup>. Recent studies revealed that LT $\beta$  receptor ligation activates not only and RELB/p52 complexes but also RELB/p50<sup>223,224</sup>. In addition, RELB/p52 and RELB/p50 heterodimers strongly induce the expression I $\kappa$ B $\alpha$ , leading to the cytoplasmic retention of canonical NF- $\kappa$ B signaling dimers such as RELA/p50, which have a higher affinity for the inhibitor<sup>222</sup>. Together, this might explain the upregulation of RELB, p52, and p50 in *Cyld*<sup>ALPC</sup> mice in the absence of RELA. However, whether nuclear RELB complexes were formed by heterodimerization with p52 and/or p50 in *Cyld*<sup>ALPC</sup> mice needs further investigations to identify the subunits within the dimers.

The striking finding that RELB deletion results in completely reverted NF- $\kappa$ B protein levels from the canonical branch suggests yet unknown interactions between canonical and non-canonical NF- $\kappa$ B pathways and identifies RELB as an important factor driving the overall increased expression of NF- $\kappa$ B signaling proteins in *Cyld*<sup>ALPC</sup> livers.

To address the question whether additional signaling pathways are involved in the development of the biliary phenotype in *Cyld*<sup>ALPC</sup> mice, signaling pathways leading to apoptosis, proliferation, and biliary differentiation were investigated.

Several studies exist, in which the phenotype of mice due to impaired CYLD function was triggered by other signaling pathways than NF- $\kappa$ B. As already mentioned. Hövelmeyer et al. described the induction of BCL-2 leading to elevated B-cell survival<sup>178</sup>. The group of Tesio et al. demonstrated an increased activation of p38<sup>202</sup>. Nikolaou et al. observed besides dysregulated TAK1 activation a constitutive JNK activation leading to hepatocyte apoptosis<sup>180</sup>.

Addressing first apoptosis and anti-apoptotic BCL-2 proteins, no significant differences were detected. Neither apoptosis induction, shown by cleaved CASPASE 3 and phosphorylated JNK, nor increased proteins levels of BCL-2, BCL-X<sub>L</sub>, MCL-1 were accountable for the biliary phenotype of *Cyld*<sup>ALPC</sup> livers. Levels of mitogen-activated protein kinases such as ERK1/2 and p38 were also unchanged and similar to proteins levels of control mice.

Loss of CYLD has also been shown to be correlated with increased expression of proliferation markers including KI67 and C-MYC<sup>203</sup> and WNT/ $\beta$ -CATENIN<sup>204</sup>. However, *Cyld*<sup>ALPC</sup> livers displayed no significant alterations in the expression levels of CYCLIN D1, C-MYC, and  $\beta$ -CATENIN. However, immunohistochemical staining of KI67 revealed an increased proliferation in the periportal region of *Cyld*<sup>ALPC</sup> livers. Since marked KI67 expression was observed only in a minority of cells, Western Blot analyses on the basis of whole liver lysates might be not sensitive enough to detect such weak overall protein levels. The evaluation of further proliferation marker by additional immunohistochemical staining are needed to gain more insights.

Notch signaling has been implicated in the biliary differentiation of hepatic progenitor cells. Thereby, NOTCH ligand JAGGED1 promotes biliary differentiation, while repressed NOTCH signaling allows hepatocyte differentiation<sup>225,226</sup>. *Cyld*<sup>ALPC</sup> livers exhibited a strong activation of the hepatic progenitor cell compartment and ductular reactions, which is why a contribution of NOTCH signaling to the phenotype of *Cyld*<sup>ALPC</sup> livers was hypothesized. However, no increased protein expression of JAGGED1, Notch receptors (NOTCH1, 2, 3), activated NOTCH and NOTCH target HES1 was seen, indicating no contribution of dysregulated NOTCH signaling to the phenotype of *Cyld*<sup>ALPC</sup> mice. Further immunohistochemical staining for NOTCH receptors, JAGGED1 and target genes should be performed to confirm these results.

Taken all together, the obtained results indicate that besides the activation of the NF- $\kappa$ B signaling pathway via RELB no other signaling pathways were involved in mediating proliferation of cholangiocytes, ductular reaction and biliary fibrosis of *Cyld*<sup>ALPC</sup> livers. A schematic model is presented in Fig. 35. in which the lack of full-length CYLD leads to NF- $\kappa$ B activation, including TAK1, NEMO and especially non-canonical NF- $\kappa$ B signaling components RELB/p52. RELB heterodimers translocate subsequently into the nucleus and activate target gene expression leading to cholangiocyte proliferation and ductular reaction. Among those target genes, LT $\beta$  might play pivotal roles by sustaining RELB activation.

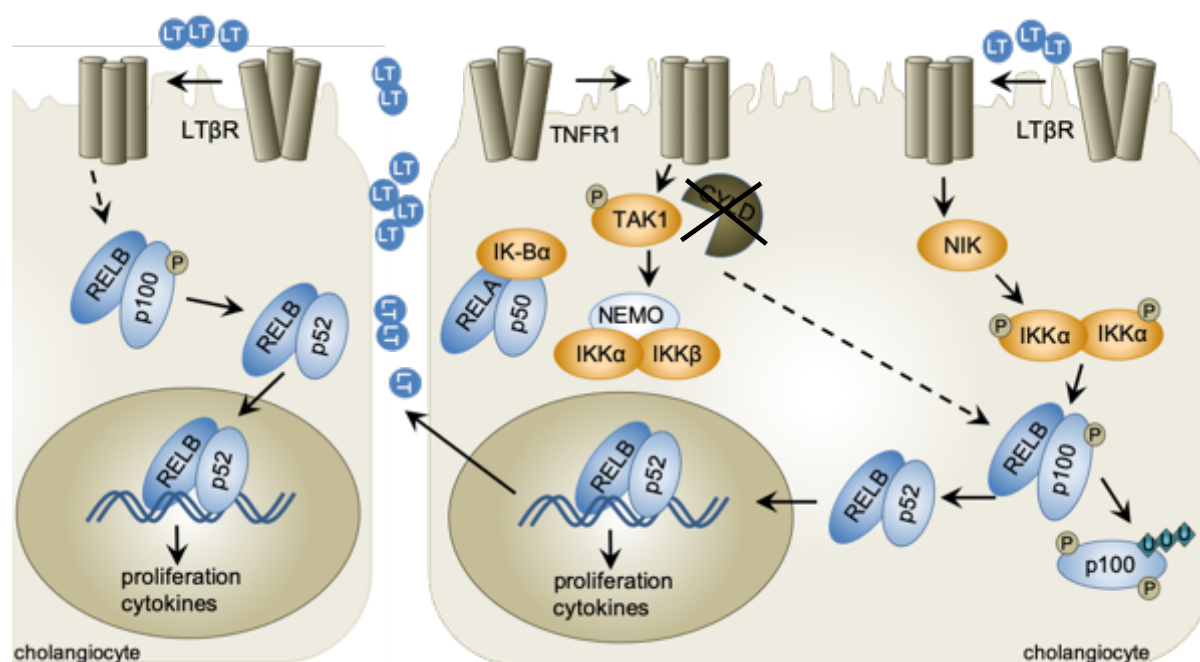


**Fig. 35. Schematic model of sustained RELB activation leading to ductular reaction in *Cyld*<sup>ALPC</sup> mice.** Deletion of full-length CYLD leads to increased expression of canonical NF- $\kappa$ B signaling proteins (phosphorylated TAK1, NEMO) and non-canonical NF- $\kappa$ B subunits RELB and p100. Phosphorylation of p100 results in proteolytically processing to p52. RELB/p52 dimers translocate then into the nucleus and activate target gene expression such as the proinflammatory cytokine LT $\beta$ . Secretion of LT $\beta$  stimulates via auto/paracrine signaling adjacent cholangiocytes, leading to sustained RELB activation which mediates cholangiocyte proliferation and ductular reaction. Adapted from Elßner et al. (2019)<sup>1</sup>.

## 6.2 The role of RELB in chronic liver injury models

So far, the function and role of the non-canonical pathway member RELB for the liver has not yet been described and the current knowledge is insufficient. The observation that additional deletion of RELB can rescue the severe biliary phenotype of *Cyld*<sup>ALPC</sup> mice raised the question whether RELB itself has any functional impact on fibrosis development, biliary injury and hepatocarcinogenesis. Therefore, two different liver damage models mimicking hepatocyte driven fibrosis and cholestasis with biliary fibrosis were performed and analyzed to gain a deeper insight into the functional effect of RELB in injured liver.

### 6.2.1 CCl<sub>4</sub>-induced liver fibrosis

The finding that biliary fibrosis in *Cyld*<sup>ALPC</sup> mice is reverted after additional deletion of RELB indicated a potential role of RELB in the development of liver fibrosis. Since liver fibrosis results as response to persistent injury to both, hepatocytes and cholangiocytes, hepatocyte-driven fibrosis was investigated first in this study. To model non-cholestatic liver fibrosis, long-term CCl<sub>4</sub> intoxication has been commonly used to induce toxin-based liver injury in rodents<sup>187,207</sup>. Thereby, hepatic metabolism of CCl<sub>4</sub> by cytochrome P450 leads to formation of a highly reactive radical that induces lipid peroxidation and consequently lowers the membrane permeability in all cellular compartments (plasma membrane, mitochondria, and endoplasmic reticulum). While injection of a single dose of CCl<sub>4</sub> results in centrilobular necrosis and steatosis, prolonged administration induces liver fibrosis and later on cirrhosis in rodents, mimicking human chronic liver disease associated with toxic damage.<sup>227</sup>

Quantification of the fibrotic area after long-term CCl<sub>4</sub>-intoxication revealed no differences in the fibrosis induction between vehicle and CCl<sub>4</sub>-treated mice of the different knockout mouse models. These findings indicate that neither the lack of RELB nor the lack of full-length CYLD in liver parenchymal cells has an impact on the fibrotic response induced by direct hepatocyte damage and suggests that RELB has its role in biliary fibrosis driven by cholangiocyte damage.

### 6.2.2 DDC-induced cholestatic injury

To test, whether RELB regulates ductular reaction and biliary fibrosis in a xenobiotic-induced cholangiopathy model, mice were fed a DDC-supplemented diet. This model is widely used to study the progenitor cell activation and proliferation<sup>228,229</sup>. Metabolization of DDC by cytochrome P450 results in the inhibition of ferrochelatase, a key enzyme involved in heme synthesis. Decreased activity of the ferrochelatase leads to accumulation of its substrate protoporphyrin and subsequent inhibition of heme synthesis, biliary injury, cholangitis, and ductular reaction<sup>69,230,231</sup>.

DDC exposure caused severe weight loss and hyperbilirubinemia not only in control mice but also in *Relb*<sup>ALPC</sup> mice, indicating a less relevant role of RELB in this model for chemically induced biliary injury. Surprisingly, DDC-fed *Cyld*<sup>ALPC</sup> mice showed only moderate weight loss and low serum bilirubin levels. Since untreated *Cyld*<sup>ALPC</sup> mice displayed already ductular reactions and progenitor cell activation, it was supposed that *Cyld*<sup>ALPC</sup> mice suffer most from the DDC diet. But obviously, existing ductular reaction leading to numerous preformed bile ducts in *Cyld*<sup>ALPC</sup> livers preserve biliary drainage in this chemically induced cholangiopathy model. Strikingly, DDC-fed *Cyld/Relb*<sup>ALPC</sup> mice were protected best against the biliary toxin, maintained their body weight and showed no elevated bilirubin levels. Upon DDC feeding, *Cyld*<sup>ALPC</sup> mice and *Cyld/Relb*<sup>ALPC</sup> mice were the only mice with significantly increased liver weights. In control mice, DDC feeding even led to significantly decreased liver weights after. This robust regenerative response in *Cyld*<sup>ALPC</sup> mice and *Cyld/Relb*<sup>ALPC</sup> might be an explanation for their improved liver functions.

Moreover, high resolution microscopy revealed a cytosolic retention of porphyrin plugs in hepatocytes of *Cyld*<sup>ALPC</sup> livers and *Cyld/Relb*<sup>ALPC</sup> livers. In contrast, DDC-fed control and *Relb*<sup>ALPC</sup> livers showed only larger pigment plugs in bile canaliculi and ductules indicating insufficient efflux. So far, it has been described that accumulation of porphyrin crystals occlude the lumina of bile ducts leading to bile duct obstruction after feeding with DDC<sup>69</sup>. Lyoumi et al. demonstrated that the exceptional porphyrin retention in hepatocytes and Kupffer cells due to lower porphyrin efflux inhibits the formation of less cytotoxic bile acid.<sup>209</sup> Thus, porphyrin sequestration in the cytosol of hepatocytes of *Cyld*<sup>ALPC</sup> mice and *Cyld/Relb*<sup>ALPC</sup> mice might be an additional protective mechanism against DDC exposure.

To gain more mechanistic insights potentially leading to the development of the different cholestatic phenotypes, the adaptive bile acid transporter response was addressed next in this model. Hepatobiliary bile transportation is tightly balanced and regulated to ensure a balance between synthesis, uptake, and excretion<sup>232</sup>. In hepatocytes, mainly NTCP tightly regulates basolateral uptake of bile acids. Upon DDC feeding, a lowered expression of NTCP is reciprocally accompanied by induction of the alternative basolateral exporters MRP3 and MRP4 in order to reduce bilirubin and hepatocellular accumulation of bile acids<sup>69,209</sup>.

Interestingly, *Ntcp* levels were further decreased in DDC-fed knockout mice indicating even more reduced uptake of bile acids by hepatocytes. Levels of *Mrp3* and *Mrp4* were both upregulated. Among them, the bile acid efflux transporter MRP4 was strongly induced in RELB deficient mice after DDC exposure, suggesting a repressive function of RELB. Increased export of toxic bile acids out of hepatocytes back into the circulation decreases hepatotoxicity of bile acids and might be an explanation of the observed effects in DDC-fed *Cyld/Relb*<sup>ALPC</sup> mice. The mechanism by which MRP4 expression is induced in response to cholestasis and repressed by the presence of RELB might be due to possible interactions with the nuclear receptors farnesoid X receptor (FXR) and the constitute-androstane-receptor (CAR), key regulators involved in the bile acid metabolism<sup>233</sup>. Although the role for alternative bile acid transportation remains controversial in this context, regulation of bile acid transporters needs further attention, because they have been identified as possible targets for therapeutic approaches for cholangiopathies<sup>232</sup>.

Together, these data suggest a different interaction between CYLD and RELB, depending on the situation. While under physiological circumstances the spontaneous phenotype of *Cyld*<sup>ALPC</sup> livers completely relies on sustained RELB activation, under challenge, such as a xenobiotic-induced cholestasis model, the phenotype of *Cyld*<sup>ALPC</sup> mice harbors RELB independent features.

### 6.3 The role of RelB for human chronic liver diseases and primary liver cancer

Since NF- $\kappa$ B is a key regulator of immune responses, proliferation, and survival, NF- $\kappa$ B gets activated in virtually every chronic liver disease<sup>170</sup>. Numerous studies described a pivotal role of NF- $\kappa$ B activation in chronic liver diseases. Boya et al. demonstrated the activation of canonical NF- $\kappa$ B signaling in patients with chronic HCV infection. Thereby, RELA expression inversely correlated with apoptosis and accelerated fibrosis progression, suggesting a protective mechanism against hepatocellular damage<sup>162</sup>. Another study identified the NF- $\kappa$ B co-activator BCL-3 being upregulated in sterile inflammations of the biliary tract thereby reducing the inflammatory response<sup>234</sup>. During obstructive cholestasis, NF- $\kappa$ B is activated in hepatocytes in order to reduce liver injury<sup>235</sup>. In liver biopsies of patients with ASH, significantly increased RELA expression in hepatocytes correlated with disease severity and was highly associated with hepatic apoptosis.<sup>160</sup>

Beyond that, a role of non-canonical NF- $\kappa$ B signaling in diseased liver has remained largely elusive. One study links RANK/RANKL axis to the pathogenesis of PBC. Thereby, RANK receptor was strongly expressed by damaged cholangiocytes. Interaction with RANKL expressing lymphocytes might induce cholangiocyte damage. Moreover, hepatic RANKL levels correlated with the disease stage of PBC<sup>163</sup>.

Since the previous obtained *in vivo* results demonstrate, that ductular reaction and biliary fibrosis in *Cyld*<sup>ALPC</sup> mice is driven by sustained RELB expression, a contribution of non-canonical in the pathogenesis of human chronic liver diseases and primary liver cancer was hypothesized. Therefore, liver tissue samples from patients with chronic liver diseases (viral hepatitis, AIH, ALD, NASH), cholangiopathies (PBC, PSC) and primary liver cancer (HCC, ICC) were immunohistological stained for RELB. Strikingly, while RELB is dispensable for healthy liver tissue, nuclear translocation of RELB was significantly increased in hepatocytes and cholangiocytes of HBV- and HCV-induced hepatitis, AIH, and ALD. In cholangiopathies, RELB became activated in liver parenchymal cells of patients with early stage PBC and PSC but was lost at progressed disease stage of PBC and PSC. PBC

and PSC are characterized by the damage to the biliary epithelium<sup>52</sup>. In late stage cholangiopathies, bile duct destruction leading to ductopenia and loss of proliferative cholangiocytes might explain the changes in the expression pattern of RELB.

Among the cytokines that activate non-canonical NF- $\kappa$ B<sup>236</sup>, LT $\beta$  showed the strongest upregulation in *Cyld*<sup>ALPC</sup> mice. In human liver diseases, the only significant upregulation of LT $\beta$  was seen in patients with early stage PSC and PBC. By examining the dependency of cholangiocyte proliferation on RELB and its relation to LT $\beta$ , induced LT $\beta$  receptor ligation triggered the proliferation of normal human whereas knockdown of RELB reduced significantly the proliferation indicating that cholangiocyte proliferation is RELB mediated. These findings unravel a crucial role of RELB in regulating cholangiocyte proliferation, with LT $\beta$  potentially linking sustained RELB activation in early stage PBC and PSC.

Based on the results from diseased liver, the implication of RELB for the primary liver cancer types HCC and ICC was investigated. The finding that RELB is highly activated in diseased liver could be further confirmed by RELB staining demonstrating nuclear translocation of RELB in ICC and HCC tissue. While HCC develops within an established background of chronic injury and inflammation<sup>78</sup>, the true etiology of ICC remains largely unclear and many cases of ICC occur sporadic and in the absence of known etiological factors.<sup>90,91</sup> Since a universal nuclear translocation of RELB was detected independent of the underlying liver disease, the question arises whether RELB activation is increased due to protective mechanism or whether it promotes liver damage. The correlation of nuclear RELB expression and parameter such as fibrosis progression and apoptotic marker would be helpful to address this question.

Strikingly, in HCC patients nuclear RELB expression was significantly associated with poor overall survival. In line with this, nuclear RELB expression inversely correlated with nuclear CYLD expression by meaning patients with highly activated RELB were associated lower nuclear CYLD expression than patients expressing low levels nuclear RELB. In contrast to RELB, it has been shown that nuclear CYLD expression was associated with prolonged overall survival<sup>194</sup>. 5-year overall survival rates were 21% in the group of patients with high nuclear RELB expression whereas vs. 62% in the group of patients with low nuclear RELB expression. Thus, suppression of hepatic RelB expression might be beneficial in liver diseases with chronically activated non-canonical NF- $\kappa$ B signaling pathway.

Together, these results imply that RELB becomes activated in a variety of human chronic liver diseases, early stage cholangiopathies and primary liver cancer. Particularly noteworthy is the negative correlation between nuclear RELB translocation and the overall survival of HCC patients, underlining RELB as a novel prognostic factor to predict the outcome of HCC patients.

## 6.4 Outlook

The results of the present study demonstrate for the first time a crucial role of RELB for biliary damage, chronic liver diseases and hepatocarcinogenesis. Ductular reaction, activation of the oval cell compartment, biliary driven fibrosis, and increased NF- $\kappa$ B activation were completely dependent on sustained RELB activity in a mouse model. Among the potential cytokines triggering RELB hyperactivation, LT $\beta$  showed the strongest upregulation pointing to a perpetuating feedback mechanism causing constitutive RELB expression. In order to confirm whether LT $\beta$ R signaling is

causatively linked to sustained RELB expression *in vivo*, transgenic mice overexpressing liver-specific LT $\alpha$  and LT $\beta$  should be evaluated for their RELB expression. Generation of a double-knockout mouse consisting of additional RELB deletion would help to gain more insight into the function of RELB. The finding that RELB deficiency was able to revert increased activation of TAK1, NEMO, TRAF2, p50, C-REL *Cyld*<sup>ALPC</sup> mice, all components of the canonical NF- $\kappa$ B signaling pathway, point to unknown interactions between canonical and non-canonical NF- $\kappa$ B signaling. To address this, co-immunoprecipitation of RELB for TAK1 or NEMO could provide further details. Potential direct interaction between CYLD and RELB should also be investigated. Furthermore, since direct dimerization partner of nuclear RELB leading to the biliary phenotype of *Cyld*<sup>ALPC</sup> mice remain elusive so far, nuclear and cytosolic fractions of *Cyld*<sup>ALPC</sup> mice should be isolated and investigated for nuclear translocation of the NF- $\kappa$ B subunits.

In a chemically induced cholangiopathy models, it could be shown that pronounced ductular reaction in *Cyld*<sup>ALPC</sup> mice was RELB driven. Moreover, *Cyld/Relb*<sup>ALPC</sup> mice were protected against the DDC induced cholestatic damage. Porphyrin retention in hepatocytes and highly activated basolateral bile acid efflux transporter MRP4 might decrease the hepatotoxicity of bile acid. Since bile acid transporters have been identified already as possible therapeutic target for cholangiopathies, the investigation of the underlying mechanism leading to protection against the biliary toxin in *Cyld/Relb*<sup>ALPC</sup> mice should be addressed<sup>232</sup>. Nuclear receptors such as FXR and CAR are key regulators of bile acid transporters in order to maintain proper bile acid homeostasis<sup>237,238</sup>. Negative crosstalks between RELA and FXR and CAR have already been reported, but the role of RELB in this setting has not been defined<sup>238,239</sup>.

In line with the results obtained from the mice experiments, RELB expression is dispensable for human healthy liver but becomes activated in diseased liver including liver tissue samples from patients with viral hepatitis, AIH, ALD, early-stage PBC and PSC. However, the observation of the overall elevated RELB levels in diseased livers raises the question of the functional significance. To answer this question, correlation with further parameter including fibrosis progression, ductular reaction and apoptosis rate would be a good approach. Aberrant RELB activation was also shown in tissue specimens of HCC and ICC patients. Intriguingly, nuclear RELB expression was associated with poor overall survival of HCC patients. To confirm these data and to obtain direct evidence for the role of RELB in the development of HCC and ICC, different chemically induced hepatocarcinogenesis models such as DEN in combination with CCl<sub>4</sub> to induce HCC should be applied. Another suitable approach in order to induce hepatocarcinogenesis is the procedure of hydrodynamic transfection together with the Sleeping Beauty transposase. In this way, somatic integration results in long term gene expression<sup>240,241</sup>. Transfection of different oncogenes, which are frequently amplified in HCC such as *c-Myc* or constitutively activated AKT (myr-AKT) could be used to investigate the role of RELB in HCC development<sup>242,243</sup>. To study ICC development, hydrodynamic transfection of activated AKT and the intracellular domain of NOTCH1 receptor (NICD) would lead to ICC formation within 5 weeks<sup>244</sup>. Given that hyperactivated RELB drives ductular reaction in a mouse model and that diseased liver displayed aberrant RELB activation, stable overexpression of RELB itself might induce liver damage and hepatocarcinogenesis.

## 7. References

- 1 Elßner C, Goeppert B, Longerich T, Scherr A-L, Stindt J, Nanduri LK *et al.* Nuclear Translocation of RELB Is Increased in Diseased Human Liver and Promotes Ductular Reaction and Biliary Fibrosis in Mice. *Gastroenterology* 2019; **156**: 1190-1205.e14.
- 2 Tanimizu N, Miyajima A. Notch signaling controls hepatoblast differentiation by altering the expression of liver-enriched transcription factors. *J Cell Sci* 2004; **117**: 3165–3174.
- 3 Daoust R, Cantero A. The numerical proportions of cell types in rat liver during carcinogenesis by 4-dimethylaminoazobenzene (DAB). *Cancer Res* 1959; **19**: 757–762.
- 4 Rui L. Energy metabolism in the liver. *Compr Physiol* 2014; **4**: 177–197.
- 5 Gissen P, Arias IM. Structural and functional hepatocyte polarity and liver disease. *J Hepatol* 2015; **63**: 1023–1037.
- 6 Boyer JL. Bile Formation and Secretion. *Compr Physiol* 2013; **3**: 1035–1078.
- 7 Tabibian JH, Masyuk AI, Masyuk TV, O’Hara SP, LaRusso NF. Physiology of cholangiocytes. *Compr Physiol* 2013; **3**: 541–565.
- 8 Roskams TA, Theise ND, Balabaud C, Bhagat G, Bhathal PS, Bioulac-Sage P *et al.* Nomenclature of the finer branches of the biliary tree: canals, ductules, and ductular reactions in human livers. *Hepatology* 2004; **39**: 1739–1745.
- 9 Schruppf E, Tan C, Karlsten TH, Sponheim J, Björkström NK, Sundnes O *et al.* The biliary epithelium presents antigens to and activates natural killer T cells. *Hepatology* 2015; **62**: 1249–1259.
- 10 Reynoso-Paz S, Coppel RL, Mackay IR, Bass NM, Ansari AA, Gershwin ME. The immunobiology of bile and biliary epithelium. *Hepatology* 1999; **30**: 351–357.
- 11 Wisse E, De Zanger RB, Charels K, Van Der Smissen P, McCuskey RS. The liver sieve: considerations concerning the structure and function of endothelial fenestrae, the sinusoidal wall and the space of Disse. *Hepatology* 1985; **5**: 683–692.
- 12 Miyata E, Masuya M, Yoshida S, Nakamura S, Kato K, Sugimoto Y *et al.* Hematopoietic origin of hepatic stellate cells in the adult liver. *Blood* 2008; **111**: 2427–2435.
- 13 Kluwe J, Wongsiriroj N, Troeger JS, Gwak G-Y, Dapito DH, Pradere J-P *et al.* Absence of hepatic stellate cell retinoid lipid droplets does not enhance hepatic fibrosis but decreases hepatic carcinogenesis. *Gut* 2011; **60**: 1260–1268.
- 14 Carpino G, Morini S, Ginanni Corradini S, Franchitto A, Merli M, Siciliano M *et al.* Alpha-SMA expression in hepatic stellate cells and quantitative analysis of hepatic fibrosis in cirrhosis and in recurrent chronic hepatitis after liver transplantation. *Dig Liver Dis Off J Ital Soc Gastroenterol Ital Assoc Study Liver* 2005; **37**: 349–356.

- 15 Testerink N, Ajat M, Houweling M, Brouwers JF, Pully VV, van Manen H-J *et al.* Replacement of Retinyl Esters by Polyunsaturated Triacylglycerol Species in Lipid Droplets of Hepatic Stellate Cells during Activation. *PLoS ONE* 2012; **7**. doi:10.1371/journal.pone.0034945.
- 16 Venturi C, Reding R, Quinones JA, Sokal E, Rahier J, Bueno J *et al.* Relevance of activated hepatic stellate cells in predicting the development of pediatric liver allograft fibrosis. *Liver Transplant Off Publ Am Assoc Study Liver Dis Int Liver Transplant Soc* 2016; **22**: 822–829.
- 17 Adams DH, Eksteen B. Aberrant homing of mucosal T cells and extra-intestinal manifestations of inflammatory bowel disease. *Nat Rev Immunol* 2006; **6**: 244–251.
- 18 Mönkemöller V, Øie C, Hübner W, Huser T, McCourt P. Multimodal super-resolution optical microscopy visualizes the close connection between membrane and the cytoskeleton in liver sinusoidal endothelial cell fenestrations. *Sci Rep* 2015; **5**: 16279.
- 19 Zapotoczny B, Szafranska K, Owczarczyk K, Kus E, Chlopicki S, Szymonski M. Atomic Force Microscopy Reveals the Dynamic Morphology of Fenestrations in Live Liver Sinusoidal Endothelial Cells. *Sci Rep* 2017; **7**. doi:10.1038/s41598-017-08555-0.
- 20 Seternes T, Sørensen K, Smedsrød B. Scavenger endothelial cells of vertebrates: a nonperipheral leukocyte system for high-capacity elimination of waste macromolecules. *Proc Natl Acad Sci U S A* 2002; **99**: 7594–7597.
- 21 Gomez Perdiguero E, Klapproth K, Schulz C, Busch K, Azzoni E, Crozet L *et al.* Tissue-resident macrophages originate from yolk-sac-derived erythro-myeloid progenitors. *Nature* 2015; **518**: 547–551.
- 22 Hagemeyer N, Kierdorf K, Frenzel K, Xue J, Ringelhan M, Abdullah Z *et al.* Transcriptome-based profiling of yolk sac-derived macrophages reveals a role for Irf8 in macrophage maturation. *EMBO J* 2016; **35**: 1730–1744.
- 23 Beattie L, Sawtell A, Mann J, Frame TCM, Teal B, de Labastida Rivera F *et al.* Bone marrow-derived and resident liver macrophages display unique transcriptomic signatures but similar biological functions. *J Hepatol* 2016; **65**: 758–768.
- 24 Gale RP, Sparkes RS, Golde DW. Bone marrow origin of hepatic macrophages (Kupffer cells) in humans. *Science* 1978; **201**: 937–938.
- 25 Zhou W, McCollum MO, Levine BA, Olson MS. Inflammation and platelet-activating factor production during hepatic ischemia/reperfusion. *Hepatology Baltim Md* 1992; **16**: 1236–1240.
- 26 Luckey SW, Petersen DR. Activation of Kupffer cells during the course of carbon tetrachloride-induced liver injury and fibrosis in rats. *Exp Mol Pathol* 2001; **71**: 226–240.
- 27 Wammers M, Schupp A-K, Bode JG, Ehling C, Wolf S, Deenen R *et al.* Reprogramming of pro-inflammatory human macrophages to an anti-inflammatory phenotype by bile acids. *Sci Rep* 2018; **8**: 255.

- 28 Norris S, Collins C, Doherty DG, Smith F, McEntee G, Traynor O *et al.* Resident human hepatic lymphocytes are phenotypically different from circulating lymphocytes. *J Hepatol* 1998; **28**: 84–90.
- 29 Schrage A, Wechsung K, Neumann K, Schumann M, Schulzke J-D, Engelhardt B *et al.* Enhanced T cell transmigration across the murine liver sinusoidal endothelium is mediated by transcytosis and surface presentation of chemokines. *Hepatol Baltim Md* 2008; **48**: 1262–1272.
- 30 Vollmar B, Menger MD. The Hepatic Microcirculation: Mechanistic Contributions and Therapeutic Targets in Liver Injury and Repair. *Physiol Rev* 2009; **89**: 1269–1339.
- 31 Marcellin P, Kutala BK. Liver diseases: A major, neglected global public health problem requiring urgent actions and large-scale screening. *Liver Int Off J Int Assoc Study Liver* 2018; **38 Suppl 1**: 2–6.
- 32 Pellicoro A, Ramachandran P, Iredale JP, Fallowfield JA. Liver fibrosis and repair: immune regulation of wound healing in a solid organ. *Nat Rev Immunol* 2014; **14**: 181–194.
- 33 Marra F, DeFranco R, Grappone C, Milani S, Pastacaldi S, Pinzani M *et al.* Increased expression of monocyte chemoattractant protein-1 during active hepatic fibrogenesis: correlation with monocyte infiltration. *Am J Pathol* 1998; **152**: 423–430.
- 34 Seki E, de Minicis S, Inokuchi S, Taura K, Miyai K, van Rooijen N *et al.* CCR2 promotes hepatic fibrosis in mice. *Hepatol Baltim Md* 2009; **50**: 185–197.
- 35 Gressner AM. Transdifferentiation of hepatic stellate cells (Ito cells) to myofibroblasts: a key event in hepatic fibrogenesis. *Kidney Int Suppl* 1996; **54**: S39–45.
- 36 Hellerbrand C, Stefanovic B, Giordano F, Burchardt ER, Brenner DA. The role of TGFbeta1 in initiating hepatic stellate cell activation in vivo. *J Hepatol* 1999; **30**: 77–87.
- 37 Shouval DS, Biswas A, Goettel JA, McCann K, Conaway E, Redhu NS *et al.* Interleukin-10 receptor signaling in innate immune cells regulates mucosal immune tolerance and anti-inflammatory macrophage function. *Immunity* 2014; **40**: 706–719.
- 38 Petrasek J, Bala S, Csak T, Lippai D, Kodys K, Menashy V *et al.* IL-1 receptor antagonist ameliorates inflammasome-dependent alcoholic steatohepatitis in mice. *J Clin Invest* 2012; **122**: 3476–3489.
- 39 Fiore E, Malvicini M, Bayo J, Peixoto E, Atorrasagasti C, Sierra R *et al.* Involvement of hepatic macrophages in the antifibrotic effect of IGF-I-overexpressing mesenchymal stromal cells. *Stem Cell Res Ther* 2016; **7**: 172.
- 40 Iredale JP, Benyon RC, Pickering J, McCullen M, Northrop M, Pawley S *et al.* Mechanisms of spontaneous resolution of rat liver fibrosis. Hepatic stellate cell apoptosis and reduced hepatic expression of metalloproteinase inhibitors. *J Clin Invest* 1998; **102**: 538–549.
- 41 Ramachandran P, Pellicoro A, Vernon MA, Boulter L, Aucott RL, Ali A *et al.* Differential Ly-6C expression identifies the recruited macrophage phenotype, which orchestrates the regression of

- murine liver fibrosis. *Proc Natl Acad Sci U S A* 2012; **109**: E3186-3195.
- 42 Cui X, Shimizu I, Lu G, Itonaga M, Inoue H, Shono M *et al*. Inhibitory effect of a soluble transforming growth factor beta type II receptor on the activation of rat hepatic stellate cells in primary culture. *J Hepatol* 2003; **39**: 731–737.
- 43 Okada H, Honda M, Campbell JS, Takegoshi K, Sakai Y, Yamashita T *et al*. Inhibition of microRNA-214 ameliorates hepatic fibrosis and tumor incidence in platelet-derived growth factor C transgenic mice. *Cancer Sci* 2015; **106**: 1143–1152.
- 44 Anthony PP, Ishak KG, Nayak NC, Poulsen HE, Scheuer PJ, Sobin LH. The morphology of cirrhosis. Recommendations on definition, nomenclature, and classification by a working group sponsored by the World Health Organization. *J Clin Pathol* 1978; **31**: 395–414.
- 45 Schuppan D, Afdhal NH. Liver cirrhosis. *Lancet Lond Engl* 2008; **371**: 838–851.
- 46 Nakamoto Y, Kaneko S. Mechanisms of viral hepatitis induced liver injury. *Curr Mol Med* 2003; **3**: 537–544.
- 47 Singal AK, Bataller R, Ahn J, Kamath PS, Shah VH. ACG Clinical Guideline: Alcoholic Liver Disease. *Am J Gastroenterol* 2018; **113**: 175–194.
- 48 European Association for the Study of Liver. EASL clinical practical guidelines: management of alcoholic liver disease. *J Hepatol* 2012; **57**: 399–420.
- 49 Chalasani N, Younossi Z, Lavine JE, Diehl AM, Brunt EM, Cusi K *et al*. The diagnosis and management of non-alcoholic fatty liver disease: practice Guideline by the American Association for the Study of Liver Diseases, American College of Gastroenterology, and the American Gastroenterological Association. *Hepatol Baltim Md* 2012; **55**: 2005–2023.
- 50 Hoyles L, Fernández-Real J-M, Federici M, Serino M, Abbott J, Charpentier J *et al*. Molecular phenomics and metagenomics of hepatic steatosis in non-diabetic obese women. *Nat Med* 2018; **24**: 1070–1080.
- 51 Oo YH, Hubscher SG, Adams DH. Autoimmune hepatitis: new paradigms in the pathogenesis, diagnosis, and management. *Hepatol Int* 2010; **4**: 475–493.
- 52 Desmet VJ. Histopathology of cholestasis. *Verh Dtsch Ges Pathol* 1995; **79**: 233–240.
- 53 Murray KF, Carithers RL. AASLD practice guidelines: Evaluation of the patient for liver transplantation. *Hepatology* 2005; **41**: 1407–1432.
- 54 Selmi C, Bowlus CL, Gershwin ME, Coppel RL. Primary biliary cirrhosis. *The Lancet* 2011; **377**: 1600–1609.
- 55 Eaton JE, Talwalkar JA, Lazaridis KN, Gores GJ, Lindor KD. Pathogenesis of Primary Sclerosing Cholangitis and Advances in Diagnosis and Management. *Gastroenterology* 2013; **145**: 521–536.

- 56 Marshall A, Rushbrook S, Davies SE, Morris LS, Scott IS, Vowler SL *et al.* Relation between hepatocyte G1 arrest, impaired hepatic regeneration, and fibrosis in chronic hepatitis C virus infection. *Gastroenterology* 2005; **128**: 33–42.
- 57 Tachtatzis PM, Marshall A, Arvinthan A, Aravinthan A, Verma S, Penrhyn-Lowe S *et al.* Chronic Hepatitis B Virus Infection: The Relation between Hepatitis B Antigen Expression, Telomere Length, Senescence, Inflammation and Fibrosis. *PloS One* 2015; **10**: e0127511.
- 58 Aravinthan A, Scarpini C, Tachtatzis P, Verma S, Penrhyn-Lowe S, Harvey R *et al.* Hepatocyte senescence predicts progression in non-alcohol-related fatty liver disease. *J Hepatol* 2013; **58**: 549–556.
- 59 Richardson MM, Jonsson JR, Powell EE, Brunt EM, Neuschwander-Tetri BA, Bhathal PS *et al.* Progressive fibrosis in nonalcoholic steatohepatitis: association with altered regeneration and a ductular reaction. *Gastroenterology* 2007; **133**: 80–90.
- 60 Wiemann SU, Satyanarayana A, Tshuridu M, Tillmann HL, Zender L, Klempnauer J *et al.* Hepatocyte telomere shortening and senescence are general markers of human liver cirrhosis. *FASEB J Off Publ Fed Am Soc Exp Biol* 2002; **16**: 935–942.
- 61 Sasaki M, Ikeda H, Yamaguchi J, Nakada S, Nakanuma Y. Telomere shortening in the damaged small bile ducts in primary biliary cirrhosis reflects ongoing cellular senescence. *Hepatol Baltim Md* 2008; **48**: 186–195.
- 62 Tabibian JH, O'Hara SP, Splinter PL, Trussoni CE, LaRusso NF. Cholangiocyte senescence by way of N-ras activation is a characteristic of primary sclerosing cholangitis. *Hepatol Baltim Md* 2014; **59**: 2263–2275.
- 63 Thung SN. The development of proliferating ductular structures in liver disease. An immunohistochemical study. *Arch Pathol Lab Med* 1990; **114**: 407–411.
- 64 Alison MR, Golding M, Sarraf CE, Edwards RJ, Lalani EN. Liver damage in the rat induces hepatocyte stem cells from biliary epithelial cells. *Gastroenterology* 1996; **110**: 1182–1190.
- 65 Paku S, Schnur J, Nagy P, Thorgeirsson SS. Origin and structural evolution of the early proliferating oval cells in rat liver. *Am J Pathol* 2001; **158**: 1313–1323.
- 66 Roskams T, Desmet V. Ductular reaction and its diagnostic significance. *Semin Diagn Pathol* 1998; **15**: 259–269.
- 67 Pinzani M, Milani S, Herbst H, DeFranco R, Grappone C, Gentilini A *et al.* Expression of platelet-derived growth factor and its receptors in normal human liver and during active hepatic fibrogenesis. *Am J Pathol* 1996; **148**: 785–800.
- 68 Kruglov EA, Nathanson RA, Nguyen T, Dranoff JA. Secretion of MCP-1/CCL2 by bile duct epithelia induces myofibroblastic transdifferentiation of portal fibroblasts. *Am J Physiol Gastrointest Liver Physiol* 2006; **290**: G765–771.

- 69 Fickert P, Stöger U, Fuchsbichler A, Moustafa T, Marschall H-U, Weiglein AH *et al.* A new xenobiotic-induced mouse model of sclerosing cholangitis and biliary fibrosis. *Am J Pathol* 2007; **171**: 525–536.
- 70 Lowes KN, Brennan BA, Yeoh GC, Olynyk JK. Oval cell numbers in human chronic liver diseases are directly related to disease severity. *Am J Pathol* 1999; **154**: 537–541.
- 71 Libbrecht L, Desmet V, Van Damme B, Roskams T. Deep intralobular extension of human hepatic ‘progenitor cells’ correlates with parenchymal inflammation in chronic viral hepatitis: can ‘progenitor cells’ migrate? *J Pathol* 2000; **192**: 373–378.
- 72 Clouston AD, Powell EE, Walsh MJ, Richardson MM, Demetris AJ, Jonsson JR. Fibrosis correlates with a ductular reaction in hepatitis C: roles of impaired replication, progenitor cells and steatosis. *Hepatology* 2005; **41**: 809–818.
- 73 Knight B, Lim R, Yeoh GC, Olynyk JK. Interferon-gamma exacerbates liver damage, the hepatic progenitor cell response and fibrosis in a mouse model of chronic liver injury. *J Hepatology* 2007; **47**: 826–833.
- 74 Kuramitsu K, Sverdlov DY, Liu SB, Csizmadia E, Burkly L, Schuppan D *et al.* Failure of fibrotic liver regeneration in mice is linked to a severe fibrogenic response driven by hepatic progenitor cell activation. *Am J Pathol* 2013; **183**: 182–194.
- 75 Verhulst S, Best J, Syn W-K, Reynaert H, Hellemans KH, Canbay A *et al.* Infliximab and Dexamethasone Attenuate the Ductular Reaction in Mice. *Sci Rep* 2016; **6**: 36586.
- 76 Torre LA, Bray F, Siegel RL, Ferlay J, Lortet-Tieulent J, Jemal A. Global cancer statistics, 2012. *CA Cancer J Clin* 2015; **65**: 87–108.
- 77 GBD 2015 Mortality and Causes of Death Collaborators. Global, regional, and national life expectancy, all-cause mortality, and cause-specific mortality for 249 causes of death, 1980–2015: a systematic analysis for the Global Burden of Disease Study 2015. *Lancet Lond Engl* 2016; **388**: 1459–1544.
- 78 Global Burden of Disease Liver Cancer Collaboration, Akinyemiju T, Abera S, Ahmed M, Alam N, Alemayohu MA *et al.* The Burden of Primary Liver Cancer and Underlying Etiologies From 1990 to 2015 at the Global, Regional, and National Level: Results From the Global Burden of Disease Study 2015. *JAMA Oncol* 2017; **3**: 1683–1691.
- 79 Altekruse SF, Devesa SS, Dickie LA, McGlynn KA, Kleiner DE. Histological classification of liver and intrahepatic bile duct cancers in SEER registries. *J Regist Manag* 2011; **38**: 201–205.
- 80 Rahib L, Smith BD, Aizenberg R, Rosenzweig AB, Fleshman JM, Matrisian LM. Projecting cancer incidence and deaths to 2030: the unexpected burden of thyroid, liver, and pancreas cancers in the United States. *Cancer Res* 2014; **74**: 2913–2921.
- 81 El-Serag HB. Epidemiology of Viral Hepatitis and Hepatocellular Carcinoma. *Gastroenterology* 2012; **142**: 1264–1273.e1.

- 82 Center MM, Jemal A. International trends in liver cancer incidence rates. *Cancer Epidemiol Biomark Prev Publ Am Assoc Cancer Res Cosponsored Am Soc Prev Oncol* 2011; **20**: 2362–2368.
- 83 Finucane MM, Stevens GA, Cowan MJ, Danaei G, Lin JK, Paciorek CJ *et al*. National, regional, and global trends in body-mass index since 1980: systematic analysis of health examination surveys and epidemiological studies with 960 country-years and 9·1 million participants. *Lancet Lond Engl* 2011; **377**: 557–567.
- 84 Bosch FX, Ribes J, Díaz M, Cléries R. Primary liver cancer: worldwide incidence and trends. *Gastroenterology* 2004; **127**: S5–S16.
- 85 Tabrizian P, Jibara G, Shrager B, Schwartz M, Roayaie S. Recurrence of hepatocellular cancer after resection: patterns, treatments, and prognosis. *Ann Surg* 2015; **261**: 947–955.
- 86 Kulik L. Criteria for liver transplantation in hepatocellular carcinoma: Criteria for Transplant in HCC. *Clin Liver Dis* 2015; **6**: 100–102.
- 87 Bruix J, Sherman M, American Association for the Study of Liver Diseases. Management of hepatocellular carcinoma: an update. *Hepatology Baltim Md* 2011; **53**: 1020–1022.
- 88 Llovet JM, Montal R, Sia D, Finn RS. Molecular therapies and precision medicine for hepatocellular carcinoma. *Nat Rev Clin Oncol* 2018. doi:10.1038/s41571-018-0073-4.
- 89 Greten TF, Papendorf F, Bleck JS, Kirchoff T, Wohlberedt T, Kubicka S *et al*. Survival rate in patients with hepatocellular carcinoma: a retrospective analysis of 389 patients. *Br J Cancer* 2005; **92**: 1862–1868.
- 90 Palmer WC, Patel T. Are common factors involved in the pathogenesis of primary liver cancers? A meta-analysis of risk factors for intrahepatic cholangiocarcinoma. *J Hepatol* 2012; **57**: 69–76.
- 91 Banales JM, Cardinale V, Carpino G, Marzioni M, Andersen JB, Invernizzi P *et al*. Expert consensus document: Cholangiocarcinoma: current knowledge and future perspectives consensus statement from the European Network for the Study of Cholangiocarcinoma (ENS-CCA). *Nat Rev Gastroenterol Hepatol* 2016; **13**: 261–280.
- 92 Haswell-Elkins MR, Mairiang E, Mairiang P, Chaiyakum J, Chamadol N, Loapaiboon V *et al*. Cross-sectional study of *Opisthorchis viverrini* infection and cholangiocarcinoma in communities within a high-risk area in northeast Thailand. *Int J Cancer* 1994; **59**: 505–509.
- 93 Patel T. Worldwide trends in mortality from biliary tract malignancies. *BMC Cancer* 2002; **2**: 10.
- 94 Valverde A, Bonhomme N, Farges O, Sauvanet A, Flejou JF, Belghiti J. Resection of intrahepatic cholangiocarcinoma: a Western experience. *J Hepatobiliary Pancreat Surg* 1999; **6**: 122–127.
- 95 Shaib YH, Davila JA, McGlynn K, El-Serag HB. Rising incidence of intrahepatic cholangiocarcinoma in the United States: a true increase? *J Hepatol* 2004; **40**: 472–477.

- 96 Bridgewater J, Galle PR, Khan SA, Llovet JM, Park J-W, Patel T *et al.* Guidelines for the diagnosis and management of intrahepatic cholangiocarcinoma. *J Hepatol* 2014; **60**: 1268–1289.
- 97 Dhanasekaran R, Hemming AW, Zendejas I, George T, Nelson DR, Soldevila-Pico C *et al.* Treatment outcomes and prognostic factors of intrahepatic cholangiocarcinoma. *Oncol Rep* 2013; **29**: 1259–1267.
- 98 Sen R, Baltimore D. Multiple nuclear factors interact with the immunoglobulin enhancer sequences. *Cell* 1986; **46**: 705–716.
- 99 Pahl HL. Activators and target genes of Rel/NF-kappaB transcription factors. *Oncogene* 1999; **18**: 6853–6866.
- 100 Karin M. Nuclear factor-kappaB in cancer development and progression. *Nature* 2006; **441**: 431–436.
- 101 Ghosh S, Gifford AM, Riviere LR, Tempst P, Nolan GP, Baltimore D. Cloning of the p50 DNA binding subunit of NF-kappa B: homology to rel and dorsal. *Cell* 1990; **62**: 1019–1029.
- 102 Ruben SM, Dillon PJ, Schreck R, Henkel T, Chen CH, Maher M *et al.* Isolation of a rel-related human cDNA that potentially encodes the 65-kD subunit of NF-kappa B. *Science* 1991; **251**: 1490–1493.
- 103 Ryseck RP, Bull P, Takamiya M, Bours V, Siebenlist U, Dobrzanski P *et al.* RelB, a new Rel family transcription activator that can interact with p50-NF-kappa B. *Mol Cell Biol* 1992; **12**: 674–684.
- 104 Schmid RM, Perkins ND, Duckett CS, Andrews PC, Nabel GJ. Cloning of an NF-kappa B subunit which stimulates HIV transcription in synergy with p65. *Nature* 1991; **352**: 733–736.
- 105 Latimer M, Ernst MK, Dunn LL, Drutskaya M, Rice NR. The N-terminal domain of IkappaB alpha masks the nuclear localization signal(s) of p50 and c-Rel homodimers. *Mol Cell Biol* 1998; **18**: 2640–2649.
- 106 Jost PJ, Ruland J. Aberrant NF-kappaB signaling in lymphoma: mechanisms, consequences, and therapeutic implications. *Blood* 2007; **109**: 2700–2707.
- 107 Schmitz ML, Stelzer G, Altmann H, Meisterernst M, Baeuerle PA. Interaction of the COOH-terminal transactivation domain of p65 NF-kappa B with TATA-binding protein, transcription factor IIB, and coactivators. *J Biol Chem* 1995; **270**: 7219–7226.
- 108 Bull P, Morley KL, Hoekstra MF, Hunter T, Verma IM. The mouse c-rel protein has an N-terminal regulatory domain and a C-terminal transcriptional transactivation domain. *Mol Cell Biol* 1990; **10**: 5473–5485.
- 109 Dobrzanski P, Ryseck RP, Bravo R. Both N- and C-terminal domains of RelB are required for full transactivation: role of the N-terminal leucine zipper-like motif. *Mol Cell Biol* 1993; **13**: 1572–1582.

- 110 Rice NR, MacKichan ML, Israël A. The precursor of NF-kappa B p50 has I kappa B-like functions. *Cell* 1992; **71**: 243–253.
- 111 Dobrzanski P, Ryseck RP, Bravo R. Specific inhibition of RelB/p52 transcriptional activity by the C-terminal domain of p100. *Oncogene* 1995; **10**: 1003–1007.
- 112 Orian A, Gonen H, Bercovich B, Fajerman I, Eytan E, Israël A *et al.* SCF(beta)(-TrCP) ubiquitin ligase-mediated processing of NF-kappaB p105 requires phosphorylation of its C-terminus by IkappaB kinase. *EMBO J* 2000; **19**: 2580–2591.
- 113 Fong A, Sun S-C. Genetic evidence for the essential role of beta-transducin repeat-containing protein in the inducible processing of NF-kappa B2/p100. *J Biol Chem* 2002; **277**: 22111–22114.
- 114 Schmitz ML, Baeuerle PA. The p65 subunit is responsible for the strong transcription activating potential of NF-kappa B. *EMBO J* 1991; **10**: 3805–3817.
- 115 Nolan GP, Fujita T, Bhatia K, Huppi C, Liou HC, Scott ML *et al.* The bcl-3 proto-oncogene encodes a nuclear I kappa B-like molecule that preferentially interacts with NF-kappa B p50 and p52 in a phosphorylation-dependent manner. *Mol Cell Biol* 1993; **13**: 3557–3566.
- 116 Huxford T, Huang D-B, Malek S, Ghosh G. The Crystal Structure of the IkB $\alpha$ /NF- $\kappa$ B Complex Reveals Mechanisms of NF- $\kappa$ B Inactivation. *Cell* 1998; **95**: 759–770.
- 117 Thompson JE, Phillips RJ, Erdjument-Bromage H, Tempst P, Ghosh S. IkB- $\beta$  regulates the persistent response in a biphasic activation of NF- $\kappa$ B. *Cell* 1995; **80**: 573–582.
- 118 Whiteside ST, Epinat J-C, Rice NR, Israël A. I kappa B epsilon, a novel member of the IkB family, controls RelA and cRel NF- $\kappa$ B activity. *EMBO J* 1997; **16**: 1413–1426.
- 119 Inoue J, Kerr LD, Kakizuka A, Verma IM. IkB $\gamma$ , a 70 kd protein identical to the C-terminal half of p110 NF- $\kappa$ B: A new member of the IkB family. *Cell* 1992; **68**: 1109–1120.
- 120 Kwak YT, Guo J, Shen J, Gaynor RB. Analysis of Domains in the IKK $\alpha$  and IKK $\beta$  Proteins That Regulate Their Kinase Activity. *J Biol Chem* 2000; **275**: 14752–14759.
- 121 May MJ, Marienfeld RB, Ghosh S. Characterization of the Ikappa B-kinase NEMO binding domain. *J Biol Chem* 2002; **277**: 45992–46000.
- 122 Varfolomeev E, Goncharov T, Fedorova AV, Dynek JN, Zobel K, Deshayes K *et al.* c-IAP1 and c-IAP2 are critical mediators of tumor necrosis factor alpha (TNFalpha)-induced NF-kappaB activation. *J Biol Chem* 2008; **283**: 24295–24299.
- 123 Gerondakis S, Fulford TS, Messina NL, Grumont RJ. NF- $\kappa$ B control of T cell development. *Nat Immunol* 2014; **15**: 15–25.
- 124 Wang C, Deng L, Hong M, Akkaraju GR, Inoue J, Chen ZJ. TAK1 is a ubiquitin-dependent kinase of MKK and IKK. *Nature* 2001; **412**: 346–351.
- 125 Chen ZJ. Ubiquitin signalling in the NF-kappaB pathway. *Nat Cell Biol* 2005; **7**: 758–765.

- 126 Kovalenko A, Chable-Bessia C, Cantarella G, Israël A, Wallach D, Courtois G. The tumour suppressor CYLD negatively regulates NF-kappaB signalling by deubiquitination. *Nature* 2003; **424**: 801–805.
- 127 Reiley WW, Jin W, Lee AJ, Wright A, Wu X, Tewalt EF *et al.* Deubiquitinating enzyme CYLD negatively regulates the ubiquitin-dependent kinase Tak1 and prevents abnormal T cell responses. *J Exp Med* 2007; **204**: 1475–1485.
- 128 Wright A, Reiley WW, Chang M, Jin W, Lee AJ, Zhang M *et al.* Regulation of early wave of germ cell apoptosis and spermatogenesis by deubiquitinating enzyme CYLD. *Dev Cell* 2007; **13**: 705–716.
- 129 Chen Z, Hagler J, Palombella VJ, Melandri F, Scherer D, Ballard D *et al.* Signal-induced site-specific phosphorylation targets I kappa B alpha to the ubiquitin-proteasome pathway. *Genes Dev* 1995; **9**: 1586–1597.
- 130 Taniguchi K, Karin M. NF-κB, inflammation, immunity and cancer: coming of age. *Nat Rev Immunol* 2018; **18**: 309–324.
- 131 Solan NJ, Miyoshi H, Carmona EM, Bren GD, Paya CV. RelB cellular regulation and transcriptional activity are regulated by p100. *J Biol Chem* 2002; **277**: 1405–1418.
- 132 Dejardin E, Droin NM, Delhase M, Haas E, Cao Y, Makris C *et al.* The lymphotoxin-beta receptor induces different patterns of gene expression via two NF-kappaB pathways. *Immunity* 2002; **17**: 525–535.
- 133 Novack DV, Yin L, Hagen-Stapleton A, Schreiber RD, Goeddel DV, Ross FP *et al.* The IkappaB function of NF-kappaB2 p100 controls stimulated osteoclastogenesis. *J Exp Med* 2003; **198**: 771–781.
- 134 Claudio E, Brown K, Park S, Wang H, Siebenlist U. BAFF-induced NEMO-independent processing of NF-kappa B2 in maturing B cells. *Nat Immunol* 2002; **3**: 958–965.
- 135 Saitoh T, Nakayama M, Nakano H, Yagita H, Yamamoto N, Yamaoka S. TWEAK induces NF-kappaB2 p100 processing and long lasting NF-kappaB activation. *J Biol Chem* 2003; **278**: 36005–36012.
- 136 Coope HJ, Atkinson PGP, Huhse B, Belich M, Janzen J, Holman MJ *et al.* CD40 regulates the processing of NF-kappaB2 p100 to p52. *EMBO J* 2002; **21**: 5375–5385.
- 137 Zarnegar BJ, Wang Y, Mahoney DJ, Dempsey PW, Cheung HH, He J *et al.* Noncanonical NF-κB activation requires coordinated assembly of a regulatory complex of the adaptors cIAP1, cIAP2, TRAF2 and TRAF3 and the kinase NIK. *Nat Immunol* 2008; **9**: 1371–1378.
- 138 Senftleben U, Cao Y, Xiao G, Greten FR, Krähn G, Bonizzi G *et al.* Activation by IKKalpha of a second, evolutionary conserved, NF-kappa B signaling pathway. *Science* 2001; **293**: 1495–1499.
- 139 Dejardin E. The alternative NF-κB pathway from biochemistry to biology: Pitfalls and promises for future drug development. *Biochem Pharmacol* 2006; **72**: 1161–1179.

- 140 Frelin C, Imbert V, Griessinger E, Peyron A-C, Rochet N, Philip P *et al.* Targeting NF-kappaB activation via pharmacologic inhibition of IKK2-induced apoptosis of human acute myeloid leukemia cells. *Blood* 2005; **105**: 804–811.
- 141 Nakanishi C, Toi M. Nuclear factor-kappaB inhibitors as sensitizers to anticancer drugs. *Nat Rev Cancer* 2005; **5**: 297–309.
- 142 Ahmed KM, Li JJ. NF-kappa B-mediated adaptive resistance to ionizing radiation. *Free Radic Biol Med* 2008; **44**: 1–13.
- 143 Godwin P, Baird AM, Heavey S, Barr MP, O’Byrne KJ, Gately K. Targeting nuclear factor-kappa B to overcome resistance to chemotherapy. *Front Oncol* 2013; **3**: 120.
- 144 Yamamoto Y, Gaynor RB. Therapeutic potential of inhibition of the NF-kappaB pathway in the treatment of inflammation and cancer. *J Clin Invest* 2001; **107**: 135–142.
- 145 Luedde T, Trautwein C. Intracellular survival pathways in the liver. *Liver Int Off J Int Assoc Study Liver* 2006; **26**: 1163–1174.
- 146 Beg AA, Sha WC, Bronson RT, Ghosh S, Baltimore D. Embryonic lethality and liver degeneration in mice lacking the RelA component of NF-kappa B. *Nature* 1995; **376**: 167–170.
- 147 Doi TS, Marino MW, Takahashi T, Yoshida T, Sakakura T, Old LJ *et al.* Absence of tumor necrosis factor rescues RelA-deficient mice from embryonic lethality. *Proc Natl Acad Sci U S A* 1999; **96**: 2994–2999.
- 148 Alcamo E, Mizgerd JP, Horwitz BH, Bronson R, Beg AA, Scott M *et al.* Targeted mutation of TNF receptor I rescues the RelA-deficient mouse and reveals a critical role for NF-kappa B in leukocyte recruitment. *J Immunol Baltim Md 1950* 2001; **167**: 1592–1600.
- 149 Li Q, Van Antwerp D, Mercurio F, Lee KF, Verma IM. Severe liver degeneration in mice lacking the IkappaB kinase 2 gene. *Science* 1999; **284**: 321–325.
- 150 Rudolph D, Yeh WC, Wakeham A, Rudolph B, Nallainathan D, Potter J *et al.* Severe liver degeneration and lack of NF-kappaB activation in NEMO/IKKgamma-deficient mice. *Genes Dev* 2000; **14**: 854–862.
- 151 Geisler F, Algül H, Paxian S, Schmid RM. Genetic inactivation of RelA/p65 sensitizes adult mouse hepatocytes to TNF-induced apoptosis in vivo and in vitro. *Gastroenterology* 2007; **132**: 2489–2503.
- 152 Luedde T, Assmus U, Wüstefeld T, Meyer zu Vilsendorf A, Roskams T, Schmidt-Supprian M *et al.* Deletion of IKK2 in hepatocytes does not sensitize these cells to TNF-induced apoptosis but protects from ischemia/reperfusion injury. *J Clin Invest* 2005; **115**: 849–859.
- 153 Lavon I, Goldberg I, Amit S, Landsman L, Jung S, Tsuberi BZ *et al.* High susceptibility to bacterial infection, but no liver dysfunction, in mice compromised for hepatocyte NF-kappaB activation. *Nat Med* 2000; **6**: 573–577.

- 154 Luedde T, Beraza N, Kotsikoris V, van Loo G, Nenci A, De Vos R *et al.* Deletion of NEMO/IKKgamma in liver parenchymal cells causes steatohepatitis and hepatocellular carcinoma. *Cancer Cell* 2007; **11**: 119–132.
- 155 Bettermann K, Vucur M, Haybaeck J, Koppe C, Janssen J, Heymann F *et al.* TAK1 suppresses a NEMO-dependent but NF-kappaB-independent pathway to liver cancer. *Cancer Cell* 2010; **17**: 481–496.
- 156 Sunami Y, Leithäuser F, Gul S, Fiedler K, Güldiken N, Espenlaub S *et al.* Hepatic activation of IKK/NFκB signaling induces liver fibrosis via macrophage-mediated chronic inflammation. *Hepatology Baltim Md* 2012; **56**: 1117–1128.
- 157 Sha WC, Liou HC, Tuomanen EI, Baltimore D. Targeted disruption of the p50 subunit of NF-kappa B leads to multifocal defects in immune responses. *Cell* 1995; **80**: 321–330.
- 158 Caamaño JH, Rizzo CA, Durham SK, Barton DS, Raventós-Suárez C, Snapper CM *et al.* Nuclear factor (NF)-kappa B2 (p100/p52) is required for normal splenic microarchitecture and B cell-mediated immune responses. *J Exp Med* 1998; **187**: 185–196.
- 159 Weih F, Carrasco D, Durham SK, Barton DS, Rizzo CA, Ryseck RP *et al.* Multiorgan inflammation and hematopoietic abnormalities in mice with a targeted disruption of RelB, a member of the NF-kappa B/Rel family. *Cell* 1995; **80**: 331–340.
- 160 Ribeiro PS, Cortez-Pinto H, Solá S, Castro RE, Ramalho RM, Baptista A *et al.* Hepatocyte apoptosis, expression of death receptors, and activation of NF-kappaB in the liver of nonalcoholic and alcoholic steatohepatitis patients. *Am J Gastroenterol* 2004; **99**: 1708–1717.
- 161 Tai DI, Tsai SL, Chen YM, Chuang YL, Peng CY, Sheen IS *et al.* Activation of nuclear factor kappaB in hepatitis C virus infection: implications for pathogenesis and hepatocarcinogenesis. *Hepatology Baltim Md* 2000; **31**: 656–664.
- 162 Boya P, Larrea E, Sola I, Majano PL, Jiménez C, Civeira MP *et al.* Nuclear factor-kappa B in the liver of patients with chronic hepatitis C: decreased RelA expression is associated with enhanced fibrosis progression. *Hepatology Baltim Md* 2001; **34**: 1041–1048.
- 163 Lleo A, Bian Z, Zhang H, Miao Q, Yang F, Peng Y *et al.* Quantitation of the Rank-Rankl Axis in Primary Biliary Cholangitis. *PLoS One* 2016; **11**: e0159612.
- 164 Maeda S, Kamata H, Luo J-L, Leffert H, Karin M. IKKbeta couples hepatocyte death to cytokine-driven compensatory proliferation that promotes chemical hepatocarcinogenesis. *Cell* 2005; **121**: 977–990.
- 165 Mauad TH, van Nieuwkerk CM, Dingemans KP, Smit JJ, Schinkel AH, Notenboom RG *et al.* Mice with homozygous disruption of the mdr2 P-glycoprotein gene. A novel animal model for studies of nonsuppurative inflammatory cholangitis and hepatocarcinogenesis. *Am J Pathol* 1994; **145**: 1237–1245.
- 166 Pikarsky E, Porat RM, Stein I, Abramovitch R, Amit S, Kasem S *et al.* NF-kappaB functions as

- a tumour promoter in inflammation-associated cancer. *Nature* 2004; **431**: 461–466.
- 167 Haybaeck J, Zeller N, Wolf MJ, Weber A, Wagner U, Kurrer MO *et al.* A lymphotoxin-driven pathway to hepatocellular carcinoma. *Cancer Cell* 2009; **16**: 295–308.
- 168 Jiang R, Xia Y, Li J, Deng L, Zhao L, Shi J *et al.* High expression levels of IKKalpha and IKKbeta are necessary for the malignant properties of liver cancer. *Int J Cancer* 2010; **126**: 1263–1274.
- 169 Yuan D, Huang S, Berger E, Liu L, Gross N, Heinzmann F *et al.* Kupffer Cell-Derived Tnf Triggers Cholangiocellular Tumorigenesis through JNK due to Chronic Mitochondrial Dysfunction and ROS. *Cancer Cell* 2017; **31**: 771-789.e6.
- 170 Luedde T, Schwabe RF. NF- $\kappa$ B in the liver--linking injury, fibrosis and hepatocellular carcinoma. *Nat Rev Gastroenterol Hepatol* 2011; **8**: 108–118.
- 171 Chau V, Tobias JW, Bachmair A, Marriott D, Ecker DJ, Gonda DK *et al.* A multiubiquitin chain is confined to specific lysine in a targeted short-lived protein. *Science* 1989; **243**: 1576–1583.
- 172 Sun L, Chen ZJ. The novel functions of ubiquitination in signaling. *Curr Opin Cell Biol* 2004; **16**: 119–126.
- 173 Biggs PJ, Wooster R, Ford D, Chapman P, Mangion J, Quirk Y *et al.* Familial cylindromatosis (turban tumour syndrome) gene localised to chromosome 16q12-q13: evidence for its role as a tumour suppressor gene. *Nat Genet* 1995; **11**: 441–443.
- 174 Bignell GR, Warren W, Seal S, Takahashi M, Rapley E, Barfoot R *et al.* Identification of the familial cylindromatosis tumour-suppressor gene. *Nat Genet* 2000; **25**: 160–165.
- 175 Hellerbrand C, Bumès E, Bataille F, Dietmaier W, Massoumi R, Bosserhoff AK. Reduced expression of CYLD in human colon and hepatocellular carcinomas. *Carcinogenesis* 2007; **28**: 21–27.
- 176 Massoumi R, Kuphal S, Hellerbrand C, Haas B, Wild P, Spruss T *et al.* Down-regulation of CYLD expression by Snail promotes tumor progression in malignant melanoma. *J Exp Med* 2009; **206**: 221–232.
- 177 Keats JJ, Fonseca R, Chesi M, Schop R, Baker A, Chng W-J *et al.* Promiscuous mutations activate the noncanonical NF-kappaB pathway in multiple myeloma. *Cancer Cell* 2007; **12**: 131–144.
- 178 Hövelmeyer N, Wunderlich FT, Massoumi R, Jakobsen CG, Song J, Wörns MA *et al.* Regulation of B cell homeostasis and activation by the tumor suppressor gene CYLD. *J Exp Med* 2007; **204**: 2615–2627.
- 179 Urbanik T, Boger RJ, Longerich T, Becker K, Ehrenberg KR, Hövelmeyer N *et al.* Liver specific deletion of CYLDexon7/8 induces severe biliary damage, fibrosis and increases hepatocarcinogenesis in mice. *J Hepatol* 2012; **57**: 995–1003.
- 180 Nikolaou K, Tsagaratou A, Eftychi C, Kollias G, Mosialos G, Talianidis I. Inactivation of the

deubiquitinase CYLD in hepatocytes causes apoptosis, inflammation, fibrosis, and cancer. *Cancer Cell* 2012; **21**: 738–750.

181 Postic C, Shiota M, Niswender KD, Jetton TL, Chen Y, Moates JM *et al.* Dual roles for glucokinase in glucose homeostasis as determined by liver and pancreatic beta cell-specific gene knock-outs using Cre recombinase. *J Biol Chem* 1999; **274**: 305–315.

182 Postic C, Magnuson MA. DNA excision in liver by an albumin-Cre transgene occurs progressively with age. *Genes N Y N* 2000; **26**: 149–150.

183 Huh WJ, Mysorekar IU, Mills JC. Inducible activation of Cre recombinase in adult mice causes gastric epithelial atrophy, metaplasia, and regenerative changes in the absence of ‘floxed’ alleles. *Am J Physiol Gastrointest Liver Physiol* 2010; **299**: G368-380.

184 Berry MN, Friend DS. High-yield preparation of isolated rat liver parenchymal cells: a biochemical and fine structural study. *J Cell Biol* 1969; **43**: 506–520.

185 Troyanovsky S. Cadherin dimers in cell-cell adhesion. *Eur J Cell Biol* 2005; **84**: 225–233.

186 Bataller R, Brenner DA. Liver fibrosis. *J Clin Invest* 2005; **115**: 209–218.

187 Constandinou C, Henderson N, Iredale JP. Modeling liver fibrosis in rodents. *Methods Mol Med* 2005; **117**: 237–250.

188 Banales JM, Sáez E, Uriz M, Sarvide S, Urribarri AD, Splinter P *et al.* Up-regulation of microRNA 506 leads to decreased Cl<sup>-</sup>/HCO<sub>3</sub><sup>-</sup> anion exchanger 2 expression in biliary epithelium of patients with primary biliary cirrhosis. *Hepatology* 2012; **56**: 687–697.

189 Bruix J, Sherman M, Llovet JM, Beaugrand M, Lencioni R, Burroughs AK *et al.* Clinical management of hepatocellular carcinoma. Conclusions of the Barcelona-2000 EASL conference. European Association for the Study of the Liver. *J Hepatology* 2001; **35**: 421–430.

190 Ludwig J, Barham SS, LaRusso NF, Elveback LR, Wiesner RH, McCall JT. Morphologic features of chronic hepatitis associated with primary sclerosing cholangitis and chronic ulcerative colitis. *Hepatology* 1981; **1**: 632–640.

191 Desmet VJ, Gerber M, Hoofnagle JH, Manns M, Scheuer PJ. Classification of chronic hepatitis: diagnosis, grading and staging. *Hepatology* 1994; **19**: 1513–1520.

192 Scheuer PJ. Pathologic Features and Evolution of Primary Biliary Cirrhosis and Primary Sclerosing Cholangitis. *Mayo Clin Proc* 1998; **73**: 179–183.

193 Kleiner DE, Brunt EM, Van Natta M, Behling C, Contos MJ, Cummings OW *et al.* Design and validation of a histological scoring system for nonalcoholic fatty liver disease. *Hepatology* 2005; **41**: 1313–1321.

194 Welte S, Urbanik T, Elßner C, Kautz N, Koehler BC, Waldburger N *et al.* Nuclear expression of the deubiquitinase CYLD is associated with improved survival in human hepatocellular carcinoma.

*PloS One* 2014; **9**: e110591.

195 Edmondson HA, Steiner PE. Primary carcinoma of the liver: a study of 100 cases among 48,900 necropsies. *Cancer* 1954; **7**: 462–503.

196 Junqueira LC, Bignolas G, Brentani RR. Picrosirius staining plus polarization microscopy, a specific method for collagen detection in tissue sections. *Histochem J* 1979; **11**: 447–455.

197 Bankhead P, Loughrey MB, Fernández JA, Dombrowski Y, McArt DG, Dunne PD *et al.* QuPath: Open source software for digital pathology image analysis. *Sci Rep* 2017; **7**: 16878.

198 Macher-Goeppinger S, Bermejo JL, Wagener N, Hohenfellner M, Haferkamp A, Schirmacher P *et al.* Expression and prognostic relevance of the death receptor CD95 (Fas/APO1) in renal cell carcinomas. *Cancer Lett* 2011; **301**: 203–211.

199 Lazaridis KN, Strazzabosco M, Larusso NF. The cholangiopathies: disorders of biliary epithelia. *Gastroenterology* 2004; **127**: 1565–1577.

200 Hengartner MO. The biochemistry of apoptosis. *Nature* 2000; **407**: 770–776.

201 Wang H, Lai Y, Mathis BJ, Wang W, Li S, Qu C *et al.* Deubiquitinating enzyme CYLD mediates pressure overload-induced cardiac maladaptive remodeling and dysfunction via downregulating Nrf2. *J Mol Cell Cardiol* 2015; **84**: 143–153.

202 Tesio M, Tang Y, Müdder K, Saini M, von Paleske L, Macintyre E *et al.* Hematopoietic stem cell quiescence and function are controlled by the CYLD-TRAF2-p38MAPK pathway. *J Exp Med* 2015; **212**: 525–538.

203 Pannem RR, Dorn C, Ahlqvist K, Bosserhoff AK, Hellerbrand C, Massoumi R. CYLD controls c-MYC expression through the JNK-dependent signaling pathway in hepatocellular carcinoma. *Carcinogenesis* 2014; **35**: 461–468.

204 Tauriello DVF, Haegerbarth A, Kuper I, Edelmann MJ, Henraat M, Canninga-van Dijk MR *et al.* Loss of the tumor suppressor CYLD enhances Wnt/beta-catenin signaling through K63-linked ubiquitination of Dvl. *Mol Cell* 2010; **37**: 607–619.

205 Fiorotto R, Raizner A, Morell CM, Torsello B, Scirpo R, Fabris L *et al.* Notch signaling regulates tubular morphogenesis during repair from biliary damage in mice. *J Hepatol* 2013; **59**: 124–130.

206 Flynn DM, Nijjar S, Hubscher SG, de Goyet J de V, Kelly DA, Strain AJ *et al.* The role of Notch receptor expression in bile duct development and disease. *J Pathol* 2004; **204**: 55–64.

207 Martínez AK, Maroni L, Marzioni M, Ahmed ST, Milad M, Ray D *et al.* Mouse models of liver fibrosis mimic human liver fibrosis of different etiologies. *Curr Pathobiol Rep* 2014; **2**: 143–153.

208 Muthukanagarajan SJ, Karnan I, Srinivasan P, Sadagopan P, Manickam S. Diagnostic and Prognostic Significance of Various Histopathological Features in Extrahepatic Biliary Atresia. *J Clin*

*Diagn Res JCDR* 2016; **10**: EC23-27.

209 Lyoumi S, Abitbol M, Rainteau D, Karim Z, Bernex F, Oustric V *et al*. Protoporphyrin retention in hepatocytes and Kupffer cells prevents sclerosing cholangitis in erythropoietic protoporphyria mouse model. *Gastroenterology* 2011; **141**: 1509–1519, 1519.e1–3.

210 Franchitto A, Onori P, Renzi A, Carpino G, Mancinelli R, Alvaro D *et al*. Recent advances on the mechanisms regulating cholangiocyte proliferation and the significance of the neuroendocrine regulation of cholangiocyte pathophysiology. *Ann Transl Med* 2013; **1**: 27.

211 Asrani SK, Devarbhavi H, Eaton J, Kamath PS. Burden of liver diseases in the world. *J Hepatol* 2019; **70**: 151–171.

212 Trompouki E, Hatzivassiliou E, Tschritzis T, Farmer H, Ashworth A, Mosialos G. CYLD is a deubiquitinating enzyme that negatively regulates NF-kappaB activation by TNFR family members. *Nature* 2003; **424**: 793–796.

213 Kim K-H, Chen C-C, Alpini G, Lau LF. CCN1 induces hepatic ductular reaction through integrin  $\alpha\beta_5$ -mediated activation of NF- $\kappa$ B. *J Clin Invest* 2015; **125**: 1886–1900.

214 Park SM. The crucial role of cholangiocytes in cholangiopathies. *Gut Liver* 2012; **6**: 295–304.

215 Ruddell RG, Knight B, Tirnitz-Parker JEE, Akhurst B, Summerville L, Subramaniam VN *et al*. Lymphotoxin-beta receptor signaling regulates hepatic stellate cell function and wound healing in a murine model of chronic liver injury. *Hepatology* 2009; **49**: 227–239.

216 Zhong S, Fields CR, Su N, Pan Y-X, Robertson KD. Pharmacologic inhibition of epigenetic modifications, coupled with gene expression profiling, reveals novel targets of aberrant DNA methylation and histone deacetylation in lung cancer. *Oncogene* 2007; **26**: 2621–2634.

217 Fusco AJ, Mazumder A, Wang VY-F, Tao Z, Ware C, Ghosh G. The NF- $\kappa$ B subunit RelB controls p100 processing by competing with the kinases NIK and IKK1 for binding to p100. *Sci Signal* 2016; **9**: ra96.

218 Gieling RG, Elsharkawy AM, Caamaño JH, Cowie DE, Wright MC, Ebrahimkhani MR *et al*. The c-Rel subunit of nuclear factor-kappaB regulates murine liver inflammation, wound-healing, and hepatocyte proliferation. *Hepatology* 2010; **51**: 922–931.

219 Grumont RJ, Gerondakis S. The subunit composition of NF-kappa B complexes changes during B-cell development. *Cell Growth Differ Mol Biol J Am Assoc Cancer Res* 1994; **5**: 1321–1331.

220 Miyamoto S, Schmitt MJ, Verma IM. Qualitative changes in the subunit composition of kappa B-binding complexes during murine B-cell differentiation. *Proc Natl Acad Sci U S A* 1994; **91**: 5056–5060.

221 Kunsch C, Ruben SM, Rosen CA. Selection of optimal kappa B/Rel DNA-binding motifs: interaction of both subunits of NF-kappa B with DNA is required for transcriptional activation. *Mol Cell Biol* 1992; **12**: 4412–4421.

- 222 Dobrzanski P, Ryseck RP, Bravo R. Differential interactions of Rel-NF-kappa B complexes with I kappa B alpha determine pools of constitutive and inducible NF-kappa B activity. *EMBO J* 1994; **13**: 4608–4616.
- 223 Derudder E, Dejardin E, Pritchard LL, Green DR, Korner M, Baud V. RelB/p50 dimers are differentially regulated by tumor necrosis factor-alpha and lymphotoxin-beta receptor activation: critical roles for p100. *J Biol Chem* 2003; **278**: 23278–23284.
- 224 Lo JC, Basak S, James ES, Quiambo RS, Kinsella MC, Alegre M-L *et al*. Coordination between NF-kappaB family members p50 and p52 is essential for mediating LTbetaR signals in the development and organization of secondary lymphoid tissues. *Blood* 2006; **107**: 1048–1055.
- 225 Spee B, Carpino G, Schotanus BA, Katoonizadeh A, Vander Borgh S, Gaudio E *et al*. Characterisation of the liver progenitor cell niche in liver diseases: potential involvement of Wnt and Notch signalling. *Gut* 2010; **59**: 247–257.
- 226 Boulter L, Govaere O, Bird TG, Radulescu S, Ramachandran P, Pellicoro A *et al*. Macrophage-derived Wnt opposes Notch signaling to specify hepatic progenitor cell fate in chronic liver disease. *Nat Med* 2012; **18**: 572–579.
- 227 Coleman JB, Condie LW, Lamb RG. The role of CCl4 biotransformation in the activation of hepatocyte phospholipase C in vivo and in vitro. *Toxicol Appl Pharmacol* 1988; **95**: 208–219.
- 228 Jakubowski A, Ambrose C, Parr M, Lincecum JM, Wang MZ, Zheng TS *et al*. TWEAK induces liver progenitor cell proliferation. *J Clin Invest* 2005; **115**: 2330–2340.
- 229 Wang X, Foster M, Al-Dhalimy M, Lagasse E, Finegold M, Grompe M. The origin and liver repopulating capacity of murine oval cells. *Proc Natl Acad Sci U S A* 2003; **100 Suppl 1**: 11881–11888.
- 230 McCluskey SA, Marks GS, Sutherland EP, Jacobsen N, Ortiz de Montellano PR. Ferrochelatase-inhibitory activity and N-alkylprotoporphyrin formation with analogues of 3,5-diethoxycarbonyl-1,4-dihydro-2,4,6-trimethylpyridine (DDC) containing extended 4-alkyl groups: implications for the active site of ferrochelatase. *Mol Pharmacol* 1986; **30**: 352–357.
- 231 Brady AM, Lock EA. Inhibition of ferrochelatase and accumulation of porphyrins in mouse hepatocyte cultures exposed to porphyrinogenic chemicals. *Arch Toxicol* 1992; **66**: 175–181.
- 232 Halilbasic E, Claudel T, Trauner M. Bile acid transporters and regulatory nuclear receptors in the liver and beyond. *J Hepatol* 2013; **58**: 155–168.
- 233 Renga B, Migliorati M, Mencarelli A, Cipriani S, D'Amore C, Distrutti E *et al*. Farnesoid X receptor suppresses constitutive androstane receptor activity at the multidrug resistance protein-4 promoter. *Biochim Biophys Acta* 2011; **1809**: 157–165.
- 234 Song L, Wörmann S, Ai J, Neuhöfer P, Lesina M, Diakopoulos KN *et al*. BCL3 Reduces the Sterile Inflammatory Response in Pancreatic and Biliary Tissues. *Gastroenterology* 2016; **150**: 499-512.e20.

- 235 Miyoshi H, Rust C, Guicciardi ME, Gores GJ. NF-kappaB is activated in cholestasis and functions to reduce liver injury. *Am J Pathol* 2001; **158**: 967–975.
- 236 Müller JR, Siebenlist U. Lymphotoxin beta receptor induces sequential activation of distinct NF-kappa B factors via separate signaling pathways. *J Biol Chem* 2003; **278**: 12006–12012.
- 237 Kim I, Ahn S-H, Inagaki T, Choi M, Ito S, Guo GL *et al*. Differential regulation of bile acid homeostasis by the farnesoid X receptor in liver and intestine. *J Lipid Res* 2007; **48**: 2664–2672.
- 238 Gabbia D, Pozzo L, Zigiotta G, Roverso M, Sacchi D, Dalla Pozza A *et al*. Dexamethasone counteracts hepatic inflammation and oxidative stress in cholestatic rats via CAR activation. *PLoS One* 2018; **13**: e0204336.
- 239 Wang Y-D, Chen W-D, Wang M, Yu D, Forman BM, Huang W. Farnesoid X receptor antagonizes nuclear factor kappaB in hepatic inflammatory response. *Hepatology* 2008; **48**: 1632–1643.
- 240 Strömberg I, Björklund H, Melander T, Rökaeus A, Hökfelt T, Olson L. Galanin-immunoreactive nerves in the rat iris: alterations induced by denervations. *Cell Tissue Res* 1987; **250**: 267–275.
- 241 Ivics Z, Hackett PB, Plasterk RH, Izsvák Z. Molecular reconstruction of Sleeping Beauty, a Tc1-like transposon from fish, and its transposition in human cells. *Cell* 1997; **91**: 501–510.
- 242 Abou-Ellella A, Gramlich T, Fritsch C, Gansler T. c-myc amplification in hepatocellular carcinoma predicts unfavorable prognosis. *Mod Pathol Off J U S Can Acad Pathol Inc* 1996; **9**: 95–98.
- 243 Calvisi DF, Wang C, Ho C, Ladu S, Lee SA, Mattu S *et al*. Increased lipogenesis, induced by AKT-mTORC1-RPS6 signaling, promotes development of human hepatocellular carcinoma. *Gastroenterology* 2011; **140**: 1071–1083.
- 244 Fan B, Malato Y, Calvisi DF, Naqvi S, Razumilava N, Ribback S *et al*. Cholangiocarcinomas can originate from hepatocytes in mice. *J Clin Invest* 2012; **122**: 2911–2915.

## 8. List of Figures

Figure 1: Illustration showing a three-dimensional structure of a portion of a liver lobule.....	7
Figure 2: Natural history of chronic liver disease.....	9
Figure 3: Structure of NF- $\kappa$ B, I $\kappa$ B, and IKK family members.....	13
Figure 4: Canonical and non-canonical NF- $\kappa$ B signaling pathway.....	15
Figure 5. Increased RELB expression in <i>Cyld</i> <sup>ALPC</sup> mice.....	41
Figure 6. Generation of liver-specific RELB and CYLD/RELB knockout mice.....	42
Figure 7. Basal characterization of <i>Cyld/Relb</i> <sup>ALPC</sup> mice.....	44
Figure 8. Sustained activation of RELB is required for the biliary phenotype in <i>Cyld</i> <sup>ALPC</sup> mice.....	45
Figure 9. Increased proliferation and oval cell activation in <i>Cyld</i> <sup>ALPC</sup> mice can be abolished by additional RELB deletion.....	46
Figure 10. Deletion of RELB reduces infiltration of CD3 positive cells in <i>Cyld</i> <sup>ALPC</sup> mice.....	47
Figure 11. Deletion of RELB dampens the elevated cytokine milieu in <i>Cyld</i> <sup>ALPC</sup> mice.....	48
Figure 12. Increased expression of cytokines targeting the non-canonical NF- $\kappa$ B pathway in <i>Cyld</i> <sup>ALPC</sup> mice is RELB dependent.....	49
Figure 13. Reactive biliary epithelial phenotype in <i>Cyld</i> <sup>ALPC</sup> mice depends on sustained RELB activation.....	50
Figure 14. Increased NF- $\kappa$ B activation in <i>Cyld</i> <sup>ALPC</sup> mice is rescued by RELB deletion.....	51
Figure 15. Increased expression of NF- $\kappa$ B regulating factors in <i>Cyld</i> <sup>ALPC</sup> mice is rescued by RELB deletion.....	52
Figure 16. Analysis of cell death and anti-apoptotic BCL-2 proteins.....	53
Figure 17. Analysis of proliferation and mitogen-activated protein kinases.....	54
Figure 18. Analysis of NOTCH signaling pathway.....	54
Figure 19. CCl <sub>4</sub> -induced liver fibrosis.....	55
Figure 20. Combined ablation of full-length CYLD and RELB protects from chemically induced biliary damage.....	56
Figure 21. Robust proliferative/regenerative response in all mice after 4 weeks of chronic exposure to DDC.....	58
Figure 22. DDC exposure leads to ductular proliferation and periductal fibrosis.....	59
Figure 23. Impact of liver-specific full-length CYLD and RELB deficiency on bile acid transporter expression after DDC feeding.....	60
Figure 24. MRP4 activation is highly upregulated in RELB deficient mice in response to a DDC diet.....	61
Figure 25. RELB expression is upregulated in hepatocytes of human chronic liver diseases.....	62
Figure 26. Increased RELB expression in cholangiocytes of human chronic liver diseases.....	63
Figure 27. Expression levels of I $\kappa$ B $\alpha$ , RELA, RELB, CYLD in human HCC.....	64
Figure 28. Nuclear RELB expression in correlation to nuclear CYLD expression and overall survival in human HCC.....	67
Figure 29. RELB expression in hepatocytes of human cholangiopathies.....	68
Figure 30. RELB expression in cholangiocytes of human cholangiopathies.....	69
Figure 31. LT $\beta$ expression in human chronic liver diseases.....	70
Figure 32. Increased LT $\beta$ expression in early stage PSC and PBC.....	71
Figure 33. LT $\beta$ links RELB activation to cholangiocyte proliferation.....	72

---

## 9. List of Tables

<b>Table 1. Components for the preparation of the indicated PCR master mixes</b> .....	22
<b>Table 2. PCR primer sequences for mouse genotyping</b> .....	22
<b>Table 3. PCR programs</b> .....	22
<b>Table 4. Components for the preparation of two 12 % polyacrylamide gels</b> .....	29
<b>Table 5. Antibodies used for Western blot analyses</b> .....	31
<b>Table 6. Components for the Reverse Transcriptase Master Mix</b> .....	33
<b>Table 7. qRT-PCR primers</b> .....	34
<b>Table 8. Antibodies used for immunohistochemical staining</b> .....	38
<b>Table 9. Serum analyses of untreated control mice and DDC-fed mice</b> .....	57
<b>Table 10. Quantitative real-time PCR analysis of bile acid transporter in untreated control livers and DDC-fed livers</b> .....	60
<b>Table 11. Baseline characteristics of HCC patients corresponding to nuclear RELB expression (<sup>nuc</sup>RELB<sup>+/-</sup>)</b> .....	68

## 10. Abbreviations

A	Adenine
AIH	Autoimmune hepatitis
AlbCre	Albumin-Cre
ALD	Alcoholic liver disease
ALT	Alanine transaminase
AP	Alkaline phosphatase
APS	Ammonium persulfate
$\alpha$ -SMA	Alpha-smooth muscle actin
AST	Aspartate transaminase
BAFF	B-cell activating factor
Bcl-2, Bcl-xL, Bcl-3	B-cell lymphoma-leukemia-2, -xL, -3
bp	Base pair
BSA	Bovine serum albumin
BSEP	Bile salt export pump
C	Cytosine
CaCl <sub>2</sub>	Calcium chloride
CCL2	C-C motif chemokine ligand 2 (also known as MCP1)
CCl <sub>4</sub>	Carbon tetrachloride
CCR2	C-C motif chemokine receptor 2
CD	Cluster of differentiation
CD40LG	CD40 ligand
cDNA	Complementary DNA
c-IAP1/2	Cellular inhibitor of apoptosis protein 1/2
KRT7	Keratin 7
CO <sub>2</sub>	Carbon dioxide
Colla1	Collagen type 1
Cp	Crossing point
C-terminal	Carboxy-terminal
CYLD	Cylindromatosis
DAB	Diaminobenzidine
DAPI	4',6-Diamidin-2-phenylindol
DDC	3,5-diethoxycarbonyl-1,4-dihydrocollidine
ddH <sub>2</sub> O	Double distilled water
DIG	Digoxygenin
DMEM	Dulbecco's Modified Eagle's Medium
DNA	Deoxyribonucleic acid
dNTPs	Deoxynucleotides
DTT	1,4 dithiothreitol
E.coli	Escherichia coli
ECL	Enhanced chemiluminescence
EDTA	Ethylenediaminetetraacetic acid

---

Erk1/2	Extracellular signal-regulated kinase 1/2
FCS	Fetal calf serum
fl	floxed
for	Forward
G	Guanine
GAPDH	Glycerinaldehyde-3-phosphate-dehydrogenase
GFP	Green fluorescent protein
H	Hour
H <sub>2</sub> O	Water
HBV	Hepatitis B virus
HCC	Hepatocellular carcinoma
HCl	Hydrochloric acid
HCV	Hepatitis C virus
HE	hematoxylin and eosin
HRP	Horseradish peroxidase
ICC	Intrahepatic cholangiocarcinoma
IHC	Immunohistochemistry
HIS	immunohistochemical score
I $\kappa$ B	Inhibitor of NF- $\kappa$ B
IKK	I $\kappa$ B kinase
IL	Interleukin
i.p.	intraperitoneal
JNK	c-Jun N-terminal kinase
K	Lysine
KCl	Potassium chloride
kDa	Kilodalton
LIGHT	Lymphotoxin-like inducible protein that competes with glycoprotein D for herpesvirus entry on T cells
loxP	Locus of crossover in P1
LPS	Lipopolysaccharide
LPC	Liver parenchymal cell
LT $\alpha$ / $\beta$	Lymphotoxin alpha/beta
M	Molar
MAPK	Mitogen-activated protein kinase
Mcl-1	Myeloid cell leukemia-1
Mdr2	Multidrug resistance protein 2
MgCl <sub>2</sub>	Magnesium chloride
min	Minute
mRNA	Messenger RNA
Mrp	Multidrug resistance-associated protein
NaCl	Sodium chloride
NaF	Sodium fluoride
NAFL	Nonalcoholic fatty liver

NAFLD	Nonalcoholic fatty liver disease
NASH	Nonalcoholic steatohepatitis
NEMO	NF- $\kappa$ B essential modulator
NF- $\kappa$ B	Nuclear factor kappa-light-chain-enhancer of activated B cells
NIK	NF- $\kappa$ B inducing kinase
NP-40	Nonylphenylpolyethylenglycol
NTCP	Na <sup>+</sup> -dependent taurocholate co-transport protein
N-terminal	Amino-terminal
nuc	Nuclear
OS	Overall survival
PAGE	Polyacrylamide gel electrophoresis
Pen/Strep	Penicillin/Streptomycin
PB	Phenobarbital
PBC	Primary biliary cholangitis
PBS	Phosphate-buffered saline
PBS-T	PBS-Tween
PCR	Polymerase chain reaction
PDGF	Platelet derived growth factor
PFA	Paraformaldehyde
PI	Protease inhibitor
PMSF	Phenylmethanesulfonyl fluoride
PSC	Primary sclerosing cholangitis
PVDF	Polyvinylidene fluoride
qRT-PCR	Quantitative real-time polymerase chain reaction
RANKL	Receptor activator for nuclear factor $\kappa$ B ligand
rev	Reverse
RIP1	Receptor-interacting protein 1
RIPA	Radioimmunoprecipitation Assay
RNA	Ribonucleic Acid
ROS	Reactive oxygen species
Rps6	Ribosomal protein S6
RT	Room temperature
SD	Standard deviation
SDS	Sodium dodecyl sulfate
sec	Seconds
T	Thymine
TACE	Transarterial chemoembolization
TAE	Tris-acetate-EDTA
TAK1	TGF- $\beta$ activated kinase 1
Taq	Thermus aquaticus (bacterium)
TARE	Transarterial radioembolization
TBS	Tris-buffered saline
TEMED	Tetramethylethylenediamine

TGF- $\beta$	Transforming growth factor beta
TMA	Tissue microarray
TNF- $\alpha$	Tumor necrosis factor alpha
TNFR	Tumor necrosis factor receptor
TRAF	TNF receptor-associated factor
TWEAK	TNF-like weak inducer of apoptosis
UV	Ultra-violet
v/v	Volume per volume
VCAM1	Vascular cell adhesion molecule
w/v	Weight per volume
wt	Wild type

## 11. Contributions

Knockdown experiments, LT $\beta$  incubation and Western blot analyses shown in Fig. 34 were performed by Dr. Anna-Lena Scherr (Department of Medical Oncology, National Center for Tumor Diseases (NCT), Heidelberg). Fibrotic area of the Sirius Red staining (Fig. 8B and 19B) and KI67, A6, CD3, CD11B, and CD68 positive cells (Fig. 9B and 10B) were quantified by Jakob Kather (Department of Medicine III, University Hospital RWTH Aachen) using the open-source software QuPath. LT $\beta$  *in situ* hybridization (Fig. 13) and immunohistochemistry for RELA (Fig. 5), A6 (Fig. 9), and LT $\beta$  (Fig. 32 and 33) was done by our cooperation partners, the group of Prof. Dr. Mathias Heikenwalder (Division of Chronic Inflammation and Cancer, German Cancer Research Center (DKFZ), Heidelberg). Mrp4 staining, shown in Fig. 24, was performed by our cooperation partners Jan Stindt from the group of Prof. Dr. Verena Keitel (Department of Gastroenterology, Hepatology and Infectious Diseases, Medical Faculty, Heinrich Heine University, Dusseldorf).

## 12. Acknowledgements

Zunächst möchte ich mich bei Prof. Dr. Henning Schulze-Bergkamen dafür bedanken, dass er mir die Möglichkeit gegeben hat meine Doktorarbeit in seiner Gruppe am Nationalen Centrum für Tumorerkrankungen in Heidelberg anfertigen zu können. Trotz anfänglicher Tiefschläge, die letztlich (glücklicherweise) zum Themenwechsel geführt haben, bin ich ihm sehr dankbar für seine Unterstützung und die wertvollen Diskussionen. Ein besonderer Dank geht an Prof. Dr. Ralf Bartenschlager, der sich freundlicherweise dazu bereit erklärt hat, mein Erstgutachter zu sein und den Prüfungsvorsitz zu übernehmen. Ebenso danke ich Frau PD Dr. Karin Müller-Decker und Dr. Darjus Tschaharganeh für ihre Bereitschaft als weitere Mitglieder meines Prüfungskomitees zu fungieren.

In ganz besonderer Weise möchte ich Dr. Bruno Köhler für die hervorragende Betreuung danken, für das in mich (und in das Projekt) gesetzte Vertrauen, für die Möglichkeit eigene Ideen zu generieren und umzusetzen und die stete Unterstützung, auch über die Doktorandenzeit hinaus. Die Publikation wäre ohne ihn so nicht möglich gewesen. Ein riesen großes Dankeschön vor allem auch für das so Korrekturlesen und seine Flexibilität dabei. Bedanken möchte ich mich auch bei meinen Laborkollegen Anna-Lena Scherr, Adam Jassowicz, Nathalie Schmitt, Dr. Toni Urbanik, Dr. med Stefan Welte, Umut Yildiz, Stephan Lorenz und Laura Wolpert, mit denen ich in den letzten Jahren zusammenarbeiten konnte. Danke euch für das tolle Umfeld, das den Arbeitsalltag um einige erleichtert hat. Nicole Kautz danke ich insbesondere für die Unterstützung bei den vielem Tierversuchen, qPCRs und dafür, dass sie immer ein offenes Ohr für meine Hoch und Tiefs hatte. Bedanken möchte ich mich auch bei allen Mitgliedern der AG Jäger und AG Podar für ein sehr angenehmes Arbeitsklima, die stete Hilfsbereitschaft und Auskunft bei auftretenden Fragen. Ein weiterer Dank gilt all unseren Kooperationspartnern Prof. Dr. Mathias Heikenwälder, Prof. Dr. Thomas Longerich, PD Dr. Benjamin Goeppert, Jakob Kather, PD Dr. Kai Breuhahn und Jan Stindt, für ihre Hilfe, Anregungen und Unterstützung bei der Veröffentlichung der Daten.

Außerdem möchte ich Moritz, Sajo, Tine, Felix, Caro P. Lisa, Anja, Marius, Romolo und die Italiener Clique, Caro S., Daniel, Jonas, Sebastian (und vielen weiteren BioContactlern) für die vielen gemeinsame Erlebnisse, Parties und sonstigen Unternehmungen außerhalb des Laboralltags danken. Ich würde keine dieser Erinnerungen missen wollen.

Mein größter Dank gilt abschließend meiner Familie, die mich zu jeder Zeit unterstützt haben und ohne die das Ganze nicht möglich gewesen wäre.